Special Technical Report 25

FULL-SCALE PATTERN MEASUREMENTS OF SIMPLE HF FIELD ANTENNAS IN A US CONIFER FOREST

By: WILLIAM A. RAY GARY E. BARKER SANDRA S. MARTENSEN

Prepared for:

U.S. ARMY ELECTRONICS COMMAND
FORT MONMOUTH, NEW JERSEY

CONTRACT DA-36-039 AMC-00040(E)
ORDER NO. 5384-PM-63-91

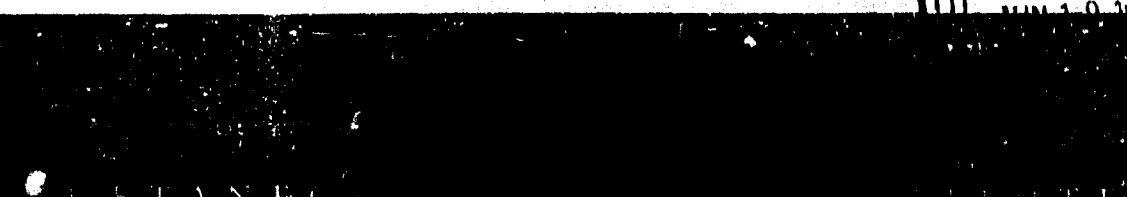

STANFORD RESEARCH INSTITUTE
MENLO PARK, CALIFORNIA

February 1967

Special Technical Report 25

FULL-SCALE PATTERN MEASUREMENTS OF SIMPLE HF FIELD ANTENNAS IN A US CONIFER FOREST

By: WILLIAM A. RAY GARY E. BARKER SANDRA S. MARTENSEN

Prepared for:

U.S. ARMY ELECTRONICS COMMAND
FORT MONMOUTH, NEW JERSEY

037,500

CONTRACT DA-36-039 AMC-00040(E)
ORDER NO. 5384-PM-63-91

SRI Project 4240

Approved: W. R. VINCENT, MANAGER
COMMUNICATION LABORATORY

D. R. SCHEUCH, EXECUTIVE DIRECTOR
ELECTRONICS AND RADIO SCIENCES

SPONSORED BY
ADVANCED RESEARCH PROJECTS AGENCY
ARPA ORDER 371

Copy No. 130

PREFACE

This work was conducted under Contract DA 36-039 AMC-00040(E) sponsored by the Advanced Research Projects Agency in support of Research Engineering for Tropical Communications. It is part of a continuing effort in the investigation of antenna environment and antenna systems now classified under Task A of the contract. One of the goals of this effort is to correlate the effects of various environments in the United States and in Thailand, with emphasis on simple field-expedient antennas. This report discusses the CONUS phase of the measurement of HF antennas in a forested area.

ABSTRACT

During May and June of 1965, measurements of field-expedient antenna impedance and radiation patterns were conducted in a conifer forest. The antennas measured included dipoles, slant wires, and inverted L's.

The pattern measurements were conducted with an aircraft-towed transmitter. The results are presented on contour maps showing individual polarization response for elevation angles from 5 to 60° from the horizon and power response from 5° above the horizon to the zenith for several frequencies between 2 and 15 Mc/s.

Input impedances are presented on Smith charts for each antenna over the frequency range that the above pattern data are presented. In addition, curves of resonant frequency and input impedance as a function of antenna height are presented for selected dipoles.

The results demonstrate that the trees surrounding the antennas begin to cause perturbations to the vertical polarization response of antennas at approximately 8 Mc/s.

CONTENTS

ILLUSTRATIONS

ILLUSTRATIONS (continued)

ILLUSTRATIONS (continued)

ILLUSTRATIONS (concluded)

TABLES

I INTRODUCTION

The characteristics of conventional field-expedient antennas used under ideal conditions are reasonably well known and documented. However, when these "simple" antennas are placed in a situation removed from the ideal case--unbalanced feed lines, poor ground, and foliage--little information is available on their characteristics and performance. The importance of measuring similar sets of HF field-expedient antennas in various situations was stressed in a previous report,[1]* describing the first set of measurements of these antennas, made over open, flat terrain near Lodi, California. The set of measurements presented here was made in a conifer forest near Lake Almanor, California.

Radiation patterns of the antennas were measured on several frequencies between 2 and 15 Mc/s in both horizontal and vertical polarizations. Patterns are presented for both horizontally and vertically polarized incident waves for elevation angles from approximately 3° to 50°; power patterns are presented for a full hemisphere from 3° to the zenith.

Section II describes the site and antennas used for these measurements. Most of the antennas duplicated those measured over open, flat terrain; however, for the measurements discussed here, the antennas were immersed in a pine forest.

Section III describes the changes made in the measurement technique between the measurements over open, flat terrain and in a conifer forest. Basically, these changes were:

---

*References are listed at the end of the report.

(1) Full hemispherical power pattern measurements were made (Sec. III-C).

(2) Visual checkpoints were needed to fly patterns because the weather balloon beacon tracker (AN/GMD-1) could not always track through the trees near the site.

(3) Wavemeter measurements of the multi-frequency transmitter (Xeledop) used for these measurements were conducted daily to ensure constant output.

Section IV describes the impedance measurements made of each antenna and presents limited data of impedance as a function of height above ground at the resonant frequency, and resonant frequency as a function of height above ground for half-wave dipoles.

II SITE AND ANTENNA DESCRIPTIONS

A. General

Measurements in a conifer forest were conducted during May and June 1965. The forest was a pine farm located near Lake Almanor in northern California. The trees varied in height from 50 to 100 ft and in diameter from 1 to 3 ft. They were randomly spaced on the order of 10 ft apart. Undergrowth consisted primarily of pine saplings. The density of the trees can be seen in photographs showing typical antenna installations (Figs. 1 and 2). The field site consisted of a small clearing near a highway and small lake, where the receiving and recording equipment van and tracking unit were placed. Most of the antennas duplicated those measured at Lodi, California over open, flat terrain[1] so that a comparison could be made of the antennas in and out of foliage. The number of antennas to be measured necessitated measurement as two separate sets, as indicated in Figs. 3 and 4. Note that the forest extends to the west of the indicated tree line. The experimental antennas were placed in the forest at least 200 ft from the edge of the clearing used for the receiving van and were erected in open spaces among the trees.

The antennas tested, with the exceptions of the sleeve dipole, the monopole and the balanced dipole, were designed to conform as closely as possible to those in a tactical situation. This was easy in the case of the dipoles, since they are normally fed through a coaxial line. However, the slant wires and inverted L's are normally used with the radio set and the operator located at the feed point. This was not possible here, because the receivers and recorders were located at some distance. For the inverted L's, the coaxial line was led in at right angles, and the

FIG. 7 PHOTOGRAPH OF FIELD SITE SHOWING 2-FOOT-HIGH UNBALANCED DIPOLE ANTENNA

FIG. 2 PHOTOGRAPH OF FIELD SITE SHOWING MONOPOLE ANTENNA

shield was simply connected to an 18-inch grounding rod at the feed point. In all cases, the shield of the coaxial lines was continuous from the antenna to the cable connection at the equipment van. Grounding rods were used at various places (uncommon in normal communication practics) to control currents on the coaxial lines, particularly to help define the limits of the coax counterpoise. It should be noted that these rods changed the current distributions in the ground system to some extent, principally affecting the antenna impedances.

The radiating elements of all antennas were made of No. 12 solid copper wire, unless otherwise noted.

B. 30° Slant-Wire Antenna

The 4-Mc/s 30° slant-wire antenna consisted of a 58.4-ft-long elevated radiator and a 25-ft counterpoise. The counterpoise was located 135° in azimuth from the horizontal projection of the elevated radiator and was laid directly on the ground. The remote end of the counterpoise was lamped to a copper grounding rod. The transmission line was RG-8 coaxial line with the shield grounded 25 ft from the feed point. The elevated radiator was tied, with dielectric rope, approximately 2 ft from the trunk of a pine tree. The other trees in the vicinity of the antenna were about 15 ft from the elevated radiator.

C. 2:1 Inverted L Antenna

The 2:1 inverted L, so named because of the ratio of the horizontal wire length to the vertical wire length, was designed for resonance at 8 Mc/s. At this frequency, the total elevated wire length is 95 percent of three quarters of a wavelength. The horizontal element was 58.4 ft long and was suspended between two pine trees by dielectric rope with approximately 4 ft of clearance between the trunks and either end of the antenna. The vertical

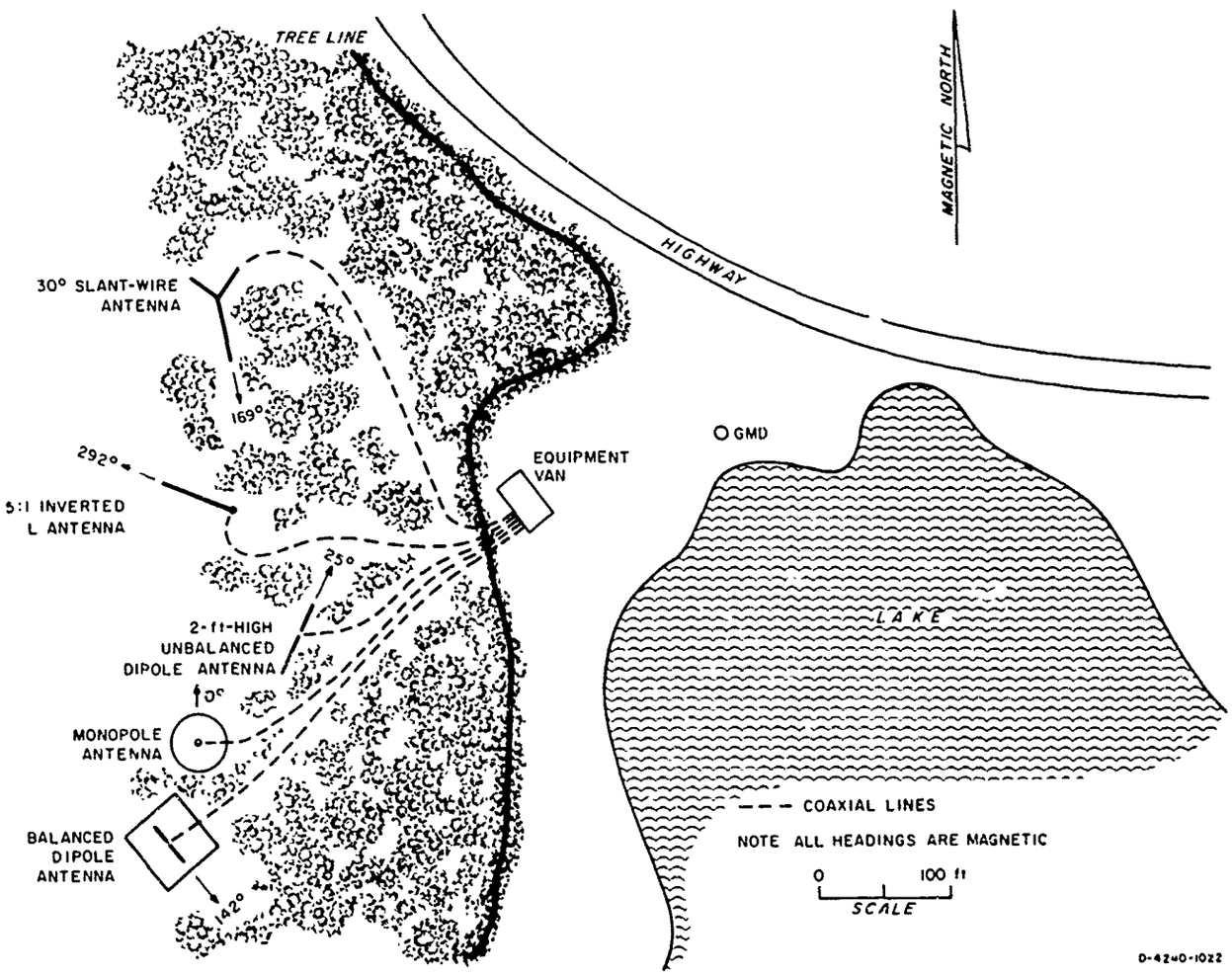

FIG. 3 SITE MAP FOR ANTENNA SET 1

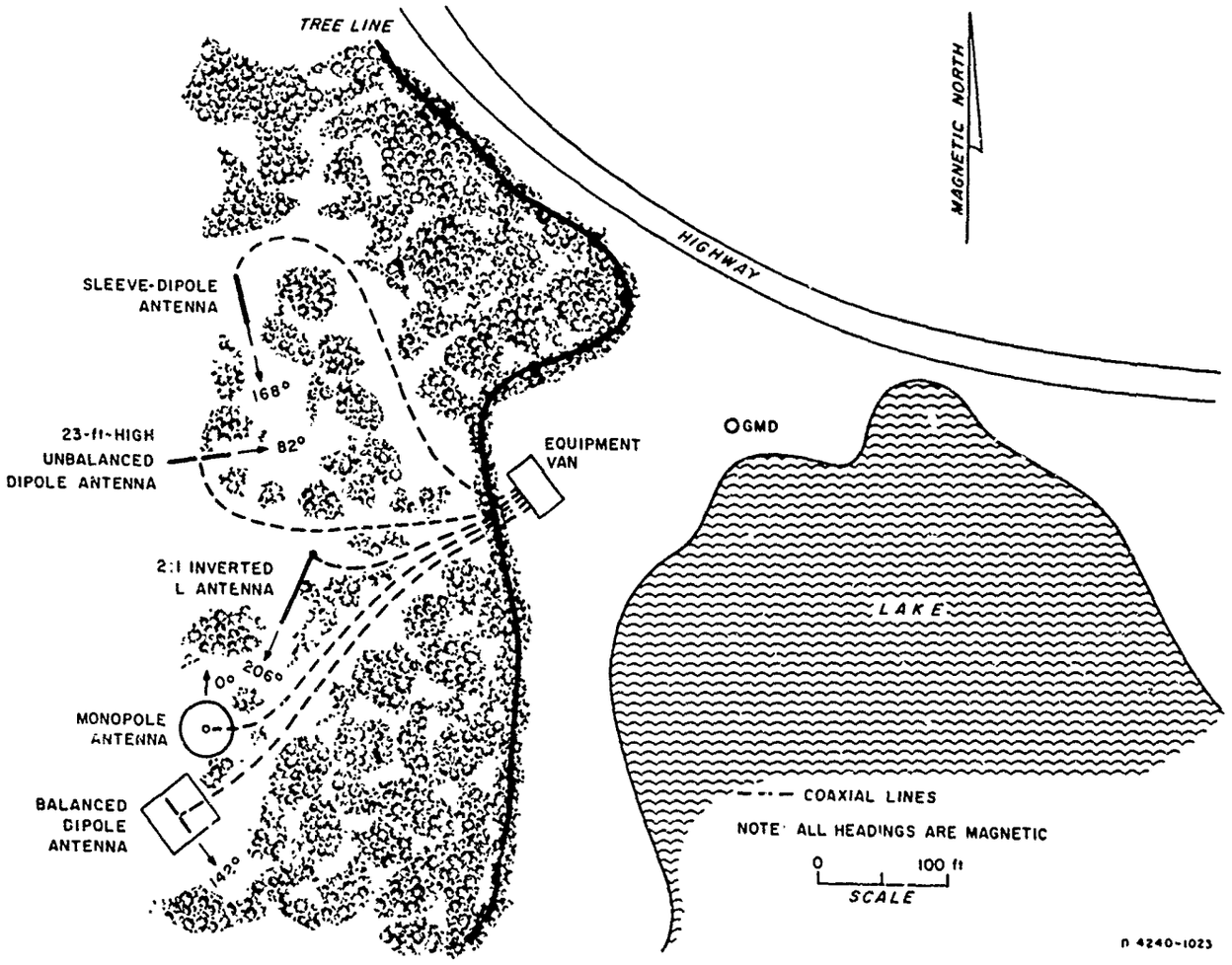

FIG. 1 SITE MAP FOR ANTENNA SET 2

element was 29.2 ft long, soldered to one end of the horizontal element and was suspended between its connection with the horizontal element and the feed point on the ground, thus determining the height above ground of the horizontal element. The antenna transmission line was RG-8 coaxial line with the braid connected to a copper grounding rod at the feed point. The closest trees to the antenna were the ones used for supporting the ends of the antenna; all others were approximately 10 ft away.

D. 5:1 Inverted L Antenna

The construction of the 10-Mc/s 5:1 inverted L was the same as that of the 2:1 inverted L except the vertical element was 11.7 ft long; the horizontal element was again 58.4 ft long. This antenna was suspended with approximately 6 ft of clearance between the tree trunks and the elements. Other trees in the vicinity were about 8 to 10 ft fron the antenna.

E. 23-Foot-High Unbalanced Dipole Antenna

The elements of the 8-Mc/s 23-ft-high unbalanced dipole were 29.2 ft long and were suspended by dielectric rope from tree trunks, approximately 18 feet from the ends of the radiators. The 23 ft of RG-58 coaxial line was perpendicular to the antenna and the ground with the braid connected to a copper grounding rod. RG-8 coaxial line was used from the ground to the receiver van. There were trees on either side of this antenna within 5 ft of the antenna.

F. 2-Foot-High Unbalanced Dipole Antenna

The 6-Mc/s 2-ft-high unbalanced dipole consisted of two radiators 38.9 ft long supported by four wooden stakes driven into the ground approximately 20 ft apart. The transmission line consisted of a 2-ft piece of RG-58 coaxial line with the braid connected to a copper grounding rod. This line was then connected to the RG-8 coaxial line leading to the receiver van. The antenna

was about 5 ft from the trees. The installation of this antenna is shown in Fig. 1.

G. Sleeve Dipole Antenna

The 5-Mc/s sleeve dipole consisted of 46.7 ft of solid copper wire and 46.7 ft of tinned copper tubular braid over the insulation of RG-8 coaxial lead line; and the braid was soldered to the shield of the coaxial line at the feed point, and the center conductor of the coaxial line was soldered to the solid copper wire. This antenna was laid, in a straight line, directly on the ground with no direct connections made to the ground. It was placed about 2 ft from the trees.

H. Monopole Antenna

The monopole antenna was constructed from a one-inch-diameter copper tubing cut to 15.6 ft (95 percent of a quarter wavelength at 15 Mc/s) and capped at both ends. The ground screen for this antenna was constructed from rolls of "chicken wire," laced together (with approximately 6 inches of overlap) with No. 12 copper wire. The lacings were not soldered to the netting. This screen was cut to form a 50-ft-diameter circle. The screen was laid in a clearing directly on the ground, except pine needles and such were left beneath the screen. The screen was then clamped to four copper grounding rods driven into the ground about 1 ft, approximately equidistant around the circumference, and soldered to one copper grounding rod in the center to which the shield of the RG-8 coaxial line was also soldered. The closest tree was at the edge of the ground screen, 25 ft from the monopole element (see Fig. 2).

I. Balance Dipole Antenna

The 15-Mc/s balanced dipole antenna consisted of two 15.6-ft elements, 16.4 ft from the ground. The antenna was supported by dielectric rope from trees 10 ft from either end of the antenna.

The ground screen for this antenna was constructed similar to that for the monopole antenna except it was cut to form a 50-ft square instead of a circle (note that the monopole and the balanced dipole were the only antennas that used metal ground screens). The closest trees were on the perimeter of the ground screen. A North Hills Model 0501 BB balun was used with the antenna; this device is a true ferrite core transformer, nominally matching 50 Ω unbalanced to 300 Ω balanced. This high turns ratio was chosen to minimize the VSWR over the entire band of test frequencies rather than match the 72 Ω resonant value exactly. RG-58 coaxial line was used for the elevated portion of the feed line while RG-8 coaxial line was used for the portion leading to the van.

Drawings of the antennas are shown in Figs. 5 to 12.

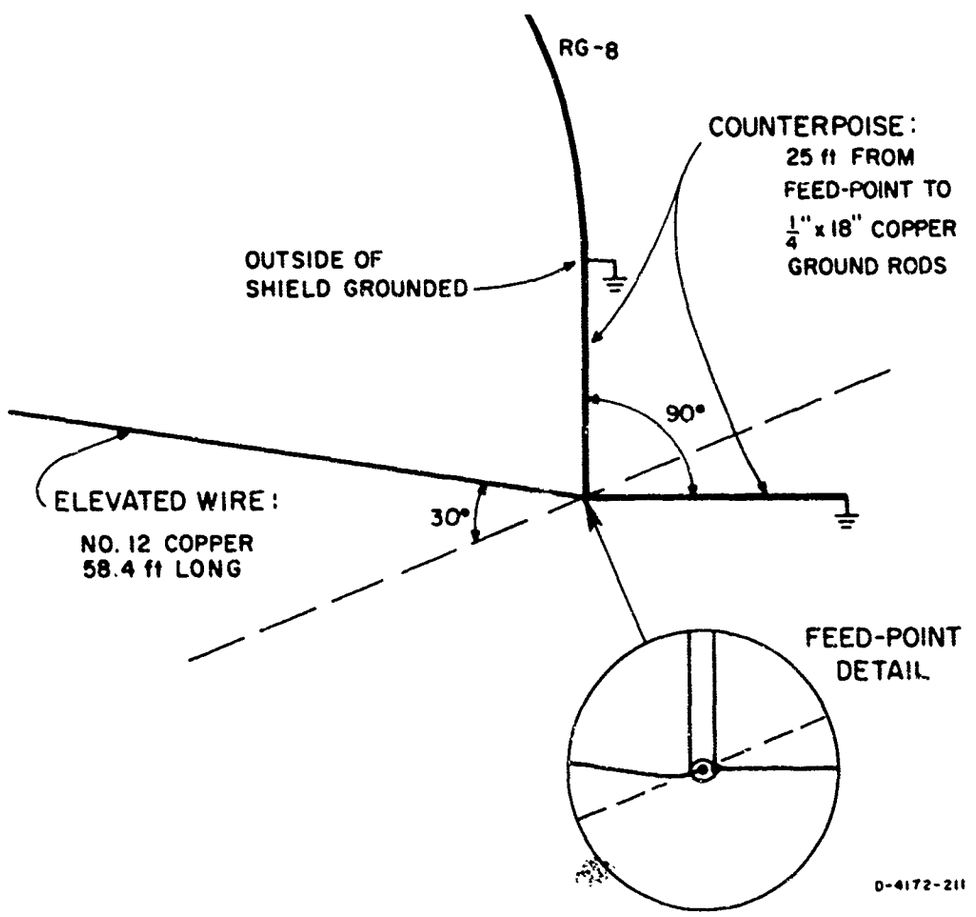

FIG. 5 ISOMETRIC VIEW OF 30° SLANT-WIRE ANTENNA

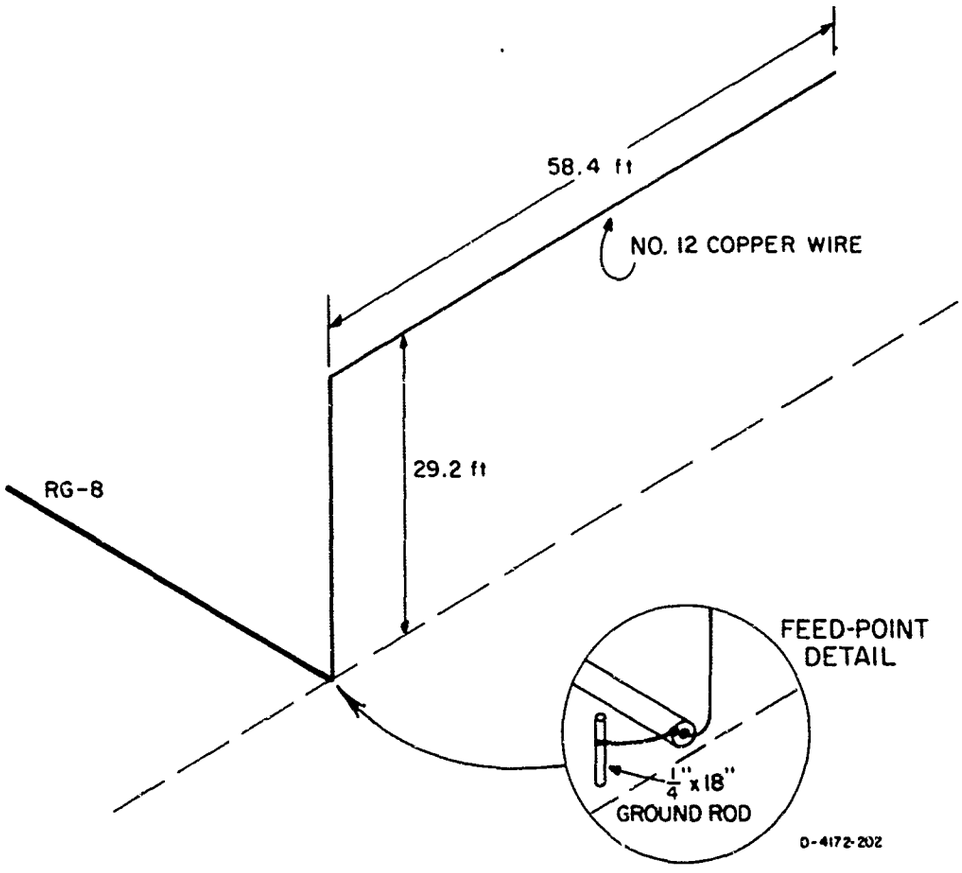

FIG. 6 ISOMETRIC VIEW OF 2:1 INVERTED L ANTENNA

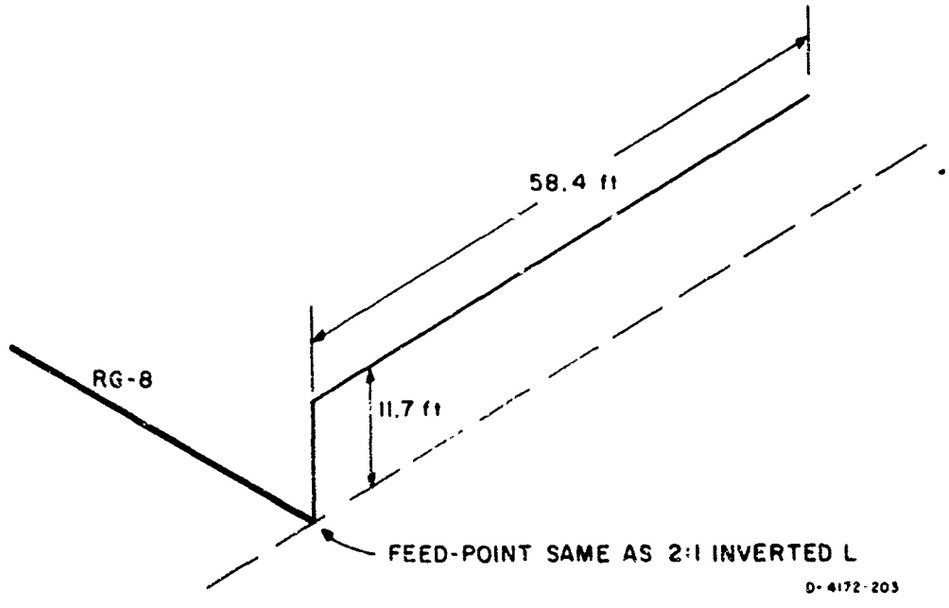

FIG. 7 ISOMETRIC VIEW OF 5:1 INVERTED L ANTENNA

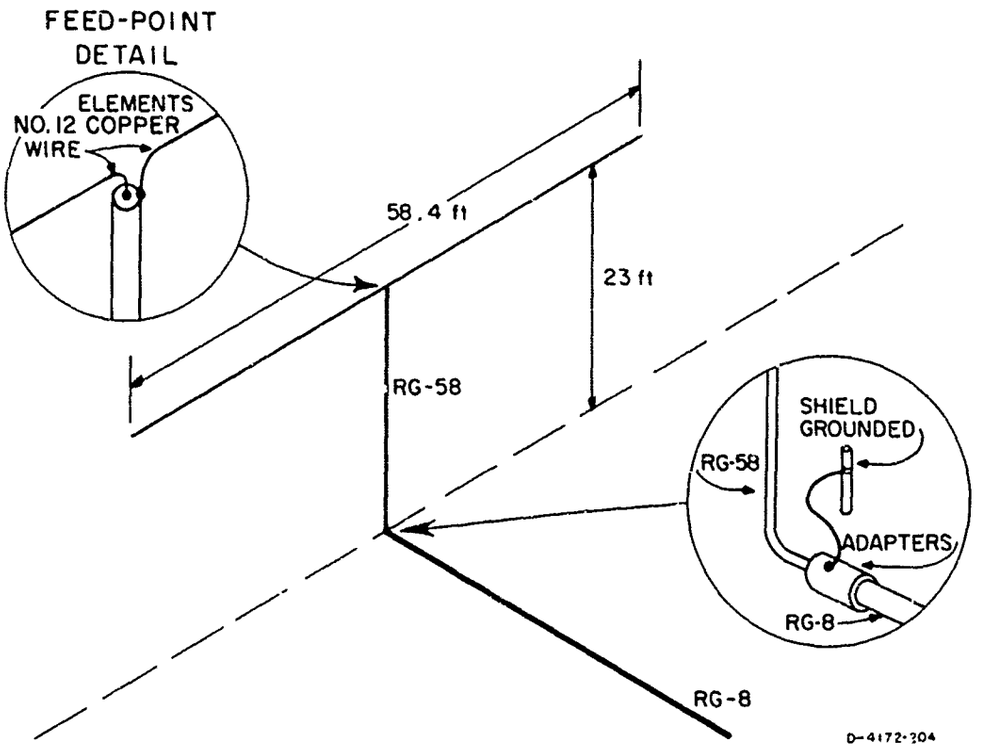

FIG. 8 ISOMETRIC VIEW OF 23-FOOT-HIGH UNBALANCED DIPOLE ANTENNA

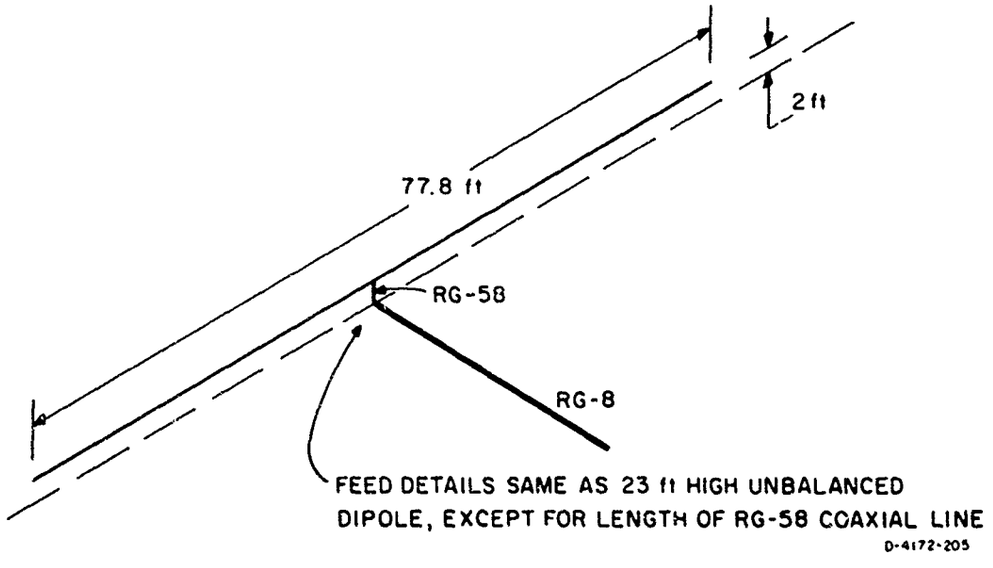

FIG. 9 ISOMETRIC VIEW OF 2-FOOT-HIGH UNBALANCED DIPOLE ANTENNA

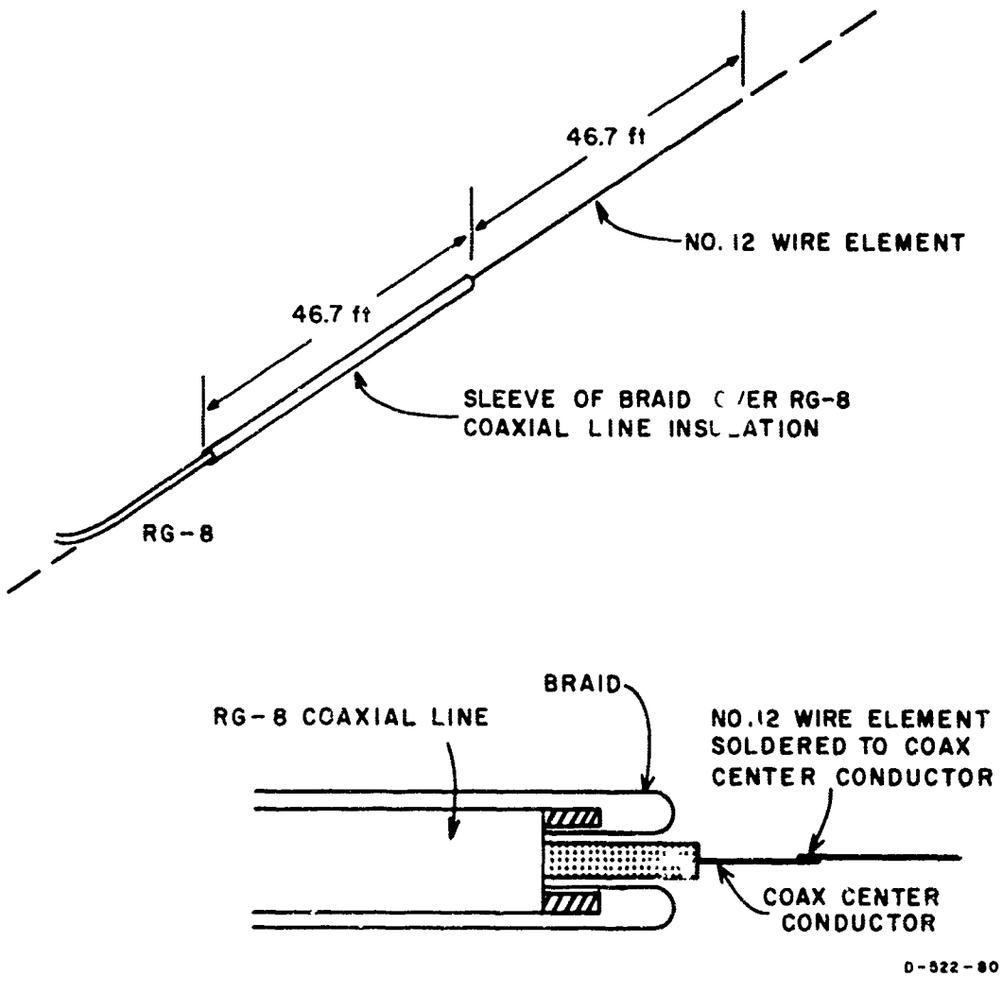

FIG. 10 ISOMETRIC VIEW OF SLEEVE DIPOLE ANTENNA

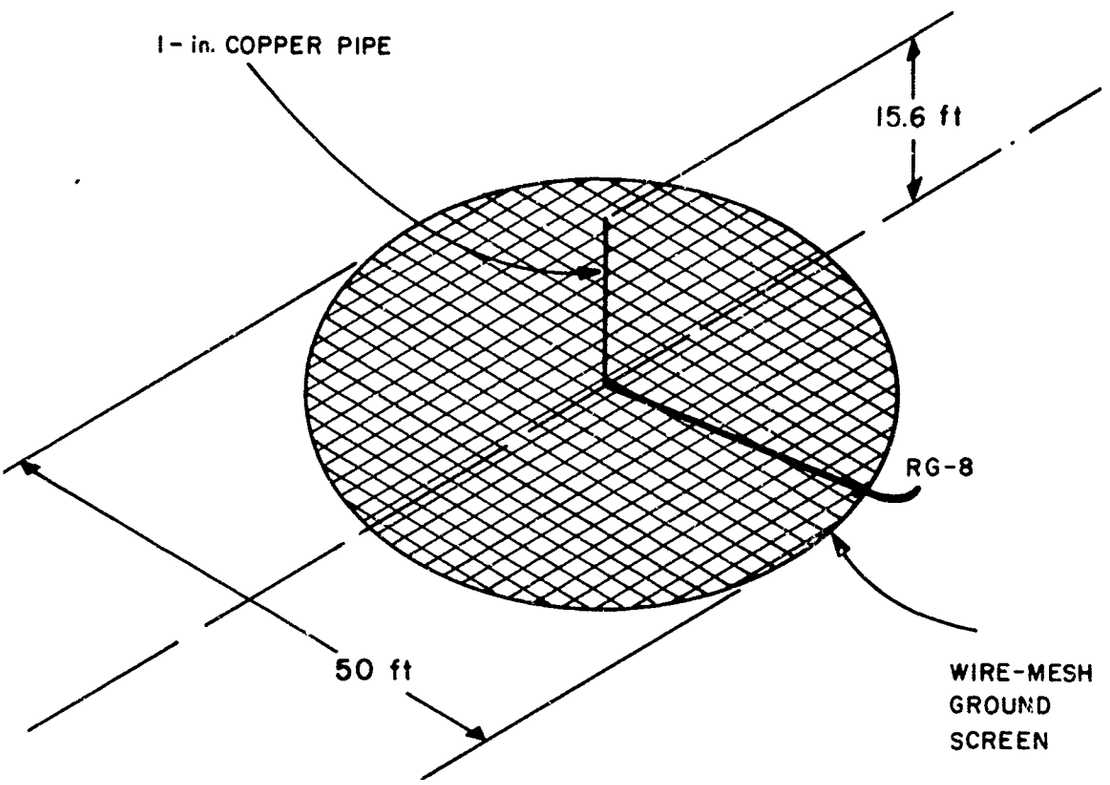

NOTE: COAXIAL FEED LINE RUNS UNDER
GROUND SCREEN AND SHIELD
SOLDERER TO SCREEN AT CENTER

D - 4172 - 206

FIG. 11 ISOMETRIC VIEW OF MONOPOLE ANTENNA

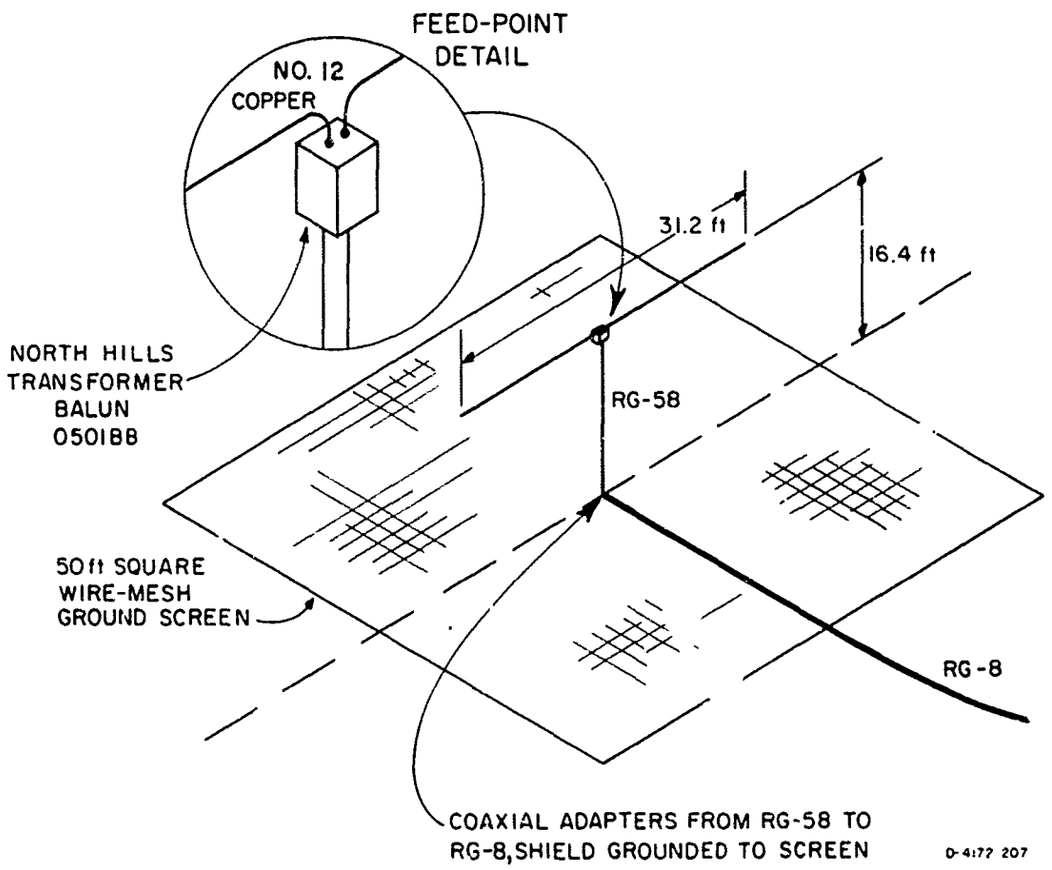

FIG. 12 ISOMETRIC VIEW OF BALANCED DIPOLE ANTENNA

III PATTERN MEASUREMENT TECHNIQUES

The antenna patterns were measured by towing a special transmitter (Xeledop*) on specified courses (circles and linear passes) around the antennas with an aircraft modified especially for this purpose. The signals received by the test antennas on the ground were recorded, together with the position of the aircraft. Later, these data were scaled into punched cards and plotted as stereographic contour maps, each of which shows one antenna's response to one frequency and one polarization. The operation of the pattern-measuring system has been described in previous reports[1,2] and the details of the basic system are not covered in this report. However, those changes made that are pertinent to this set of measurements are discussed, as is the technique for measuring power patterns.

A. The Xeledop

The heart of the pattern-measuring system is the Xeledop transmitter, which is towed behind the aircraft. On a cycle of about 1.5 seconds, the Xeledop pulses through eight selected frequencies between 2 and 30 Mc/s. For these tests, the frequencies were 2, 2.67, 4, 5, 6, 8, 10, and 15 Mc/s. All the electronics and batteries are contained in a central sphere. Arms extending out from the sphere are fed as a balanced dipole antenna, the total length of which is always less than one half wavelength. The Xeledop can be towed to transmit either horizontally (E_ϕ) or vertically (E_θ when corrected for transmitting dipole pattern)

*An acronym denoting Transmitting Elementary Dipole with Optional Polarization.

polarized waves. The electrical symmetry of the Xeledop is such that radiated polarization depends only upon its physical orientation.

Two separate checks were conducted daily during the measurement period to ensure that the radiated power of the Xeledop remained constant. The first check consisted of repeating one orbit that had been flown the previous day so that the data could be compared for two successive days. The second check consisted of monitoring the radiated power with a wavemeter mounted on a special measuring stand, constructed so that the same physical relationship always exists between Xeledop and wavemeter. Output measurements were taken each morning and evening; thus, the readings could be compared from day to day, and before and after use.

B. Aircraft Tracking

In addition to the Xeledop transmitter, the aircraft carries a low-power radio beacon transmitter and a modified transponder unit. Both are used for position information: The beacon is tracked by ground equipment, which provides azimuth and elevation information for data reduction; the airborne transponder works with a similar unit on the ground to indicate slant range for the pilot's information. The latter, displayed on a meter, is called the Pilot's Deviation Indicator or PDI.

The ground-tracking unit is a Rawin AN/GMD-1 Weather Balloon Tracker (referred to as the GMD). A steerable dish antenna tracks the aircraft beacon transmitter. Azimuth, elevation, and a sequence number (called the GMD time) are printed on adding machine paper every 6 seconds.

Although the operating frequency of the GMD is approximately 1.6 Gc/s, it has been found that metal and wooden towers--such as those normally found on an antenna farm--do not perturb the

signal enough to cause erratic operation of the tracking unit. However, the dish will start to "hunt" for the beacon if the signal is blocked by a large object, such as a building. For the measurements at Lake Almanor, the GMD was not elevated on a tower, but was situated on the edge of a small lake near the equipment van. This was done so that the effect of the attenuation and scattering of the GMD signal by the trees could be determined for planning the measurements to be made in Thailand.

It was found that the GMD could track fairly well above 35° elevation (breaking point between trees and sky); below this angle, manual assistance was required. As the elevation angle decreases and thus the amount of foliage between the beacon and the dish increased, the amount of manual slewing required increased. For elevation angles below about 20°, the GMD became practically useless. For elevation angles below 30°, it was necessary to rely on the pilot to fly a circular orbit, aided by the Pilot's Deviation Indicator (PDI) and a circle drawn on an aerial photograph of the site area. Also, when flying at elevation angles below 35°, the pilot called out visual check points to the ground station to provide azimuth position information, which were recorded with the data.

C. Power Plots

1. Background and Definitions

Because the ionosphere tends to randomly polarize energy passing through it, the critical element in evaluating the HF communications antennas is the total energy radiated or received as a function of direction, independent of polarization. For near-vertical-incidence paths--the intended use of these field-expedient antennas--the polarization is not truly random in tropical areas. But "polarization" for near-vertical incidence is a matter of

antenna orientation and can be treated separately from the evaluation of the radiation pattern.

The technique described here offers a practical method of measuring these power patterns over the entire hemisphere above the antennas, especially providing the explicit pattern data required near the zenith where these antennas normally operate. For various practical reasons discussed below, the measurement of individual polarizations was limited to comparing the response along N-S and E-W lines directly overhead. This comparison is shown on each power plot as a small vector diagram showing the directions referred to the antenna axis and the relative field magnitudes.

Although not strictly reciprocal, as are individual polarization patterns, these power plots do apply to both ends of the communications system:

(1) For the transmitting case, they show the power directivity pattern of the antenna.

(2) For the receiving case, they approximate the time-average response of the antenna to randomly polarized incident waves. Note, however, that response at any given instant--the fading effects--depend upon the actual polarization of both antenna and incident field.

To examine this equivalence, consider the derivation of a power plot from orthogonal-polarization pattern samples, such as the usual E_ϕ and E_θ plots. The latter are maps of many samples, each effectively taken in a plane tangential to a hemisphere over the antennas; the plane defined by the Φ and θ vectors is shown

in Fig. 13. The plane containing these vectors will be called the normal plane because of its relationship to R_s, the vector from the antenna location to the measurement point. To find the power passing through such a sample point (transmitting case), one would take, by Poynting's theorem:

$$P = |E_\phi|^2 + |E_\theta|^2 \quad . \tag{1}$$

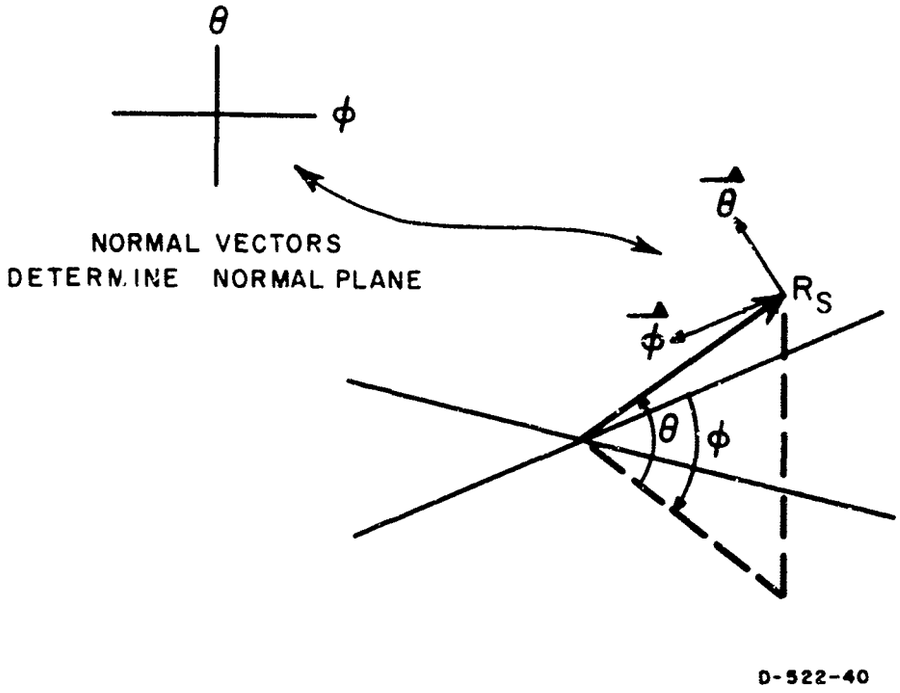

FIG. 13 DEFINITION OF NORMAL PLANE

For the receiving case, the time-average response to random polarization (imagine a rotating, constant amplitude field vector) is proportional to the magnitude of the receiving antenna's maximum response vector, regardless of the latter's orientation. To find this vector, consider the situation in Fig. 14, showing the E_ϕ and E_θ vectors lying in the normal plane at a given azimuth-elevation sample point. If we assume for the moment that the antenna's actual response is linearly polarized, then it must be one of two vectors: S_1 or S_2. Which S cannot be determined

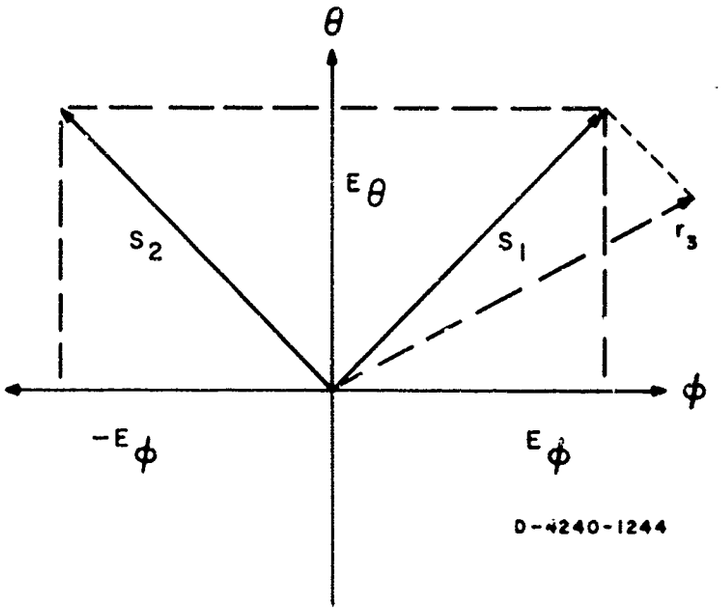

FIG. 14 DERIVATION OF S FROM E_ϕ AND E_θ SAMPLES

without a third measured response, such as the r_3 vector, shown dotted. However, for our purposes, the polarization is immaterial only the magnitudes $|S_1|$ and $|S_2|$ are of interest. Since the two magnitudes are equal, we can assign the value $S = |S_1| = |S_2|$ to this sample point, which represents the antenna's response to an optimally-polarized incident wave.

Note that P given by power summation and S given by field vector summation are identical. Therefore, a single stereographic contour map can fill both needs described above: transmitting power pattern and time-average response pattern to randomly polarized incoming waves.

2. Measurement above 60°

Unfortunately, aircraft limitations prohibit collection of E_ϕ and E_θ in the normal manner above about 60°--by flying orbit at constant elevation angles. An alternative technique would be

to fly constant azimuth radials overhead (above) the antenna, towing the Xeledop first in the normal horizontal position collinear with the aircraft heading and then in a new orientation: horizontal but perpendicular to the aircraft heading. This would ideally provide measurements of E_θ and E_ϕ, respectively, as functions of elevation angle. However, this technique has several serious problems:

(1) Accurate polarization sampling requires that the aircraft always head to or from a point directly over the antenna. This is very difficult in strong winds, which are the rule, not the exception, at high altitudes. Also, any test antennas to be measured simultaneously must be relatively close together.

(2) Redundant measurements are taken near the zenith, because an E-W track measured with the collinear orientation provides the same information as a north-south track measured with the crosswise orientation. For all practical purposes, only one pair of passes is required at the zenith to define the antenna's energy response; the remainder simply provide additional samples of the polarization elipse overhead.

(3) At the zenith, the vectors E_ϕ and E_θ are strictly undefined, and they are difficult to interpret for elevation angles near the zenith.

(4) Strict E_ϕ and E_θ responses are not required to define the power pattern. Measuring orthogonal response vectors, independent of the coordinate system, is sufficient to derive the S values exactly, and for a wide range of conditions, measuring nearly orthogonal responses is sufficient within the inherent system accuracy limits.

For these reasons, consideration of the radial flight pattern technique was abandoned in favor of a simpler approach based upon flying an approximately square grid over the test site as shown in Fig. 15. The Xeledop is towed collinearly with the

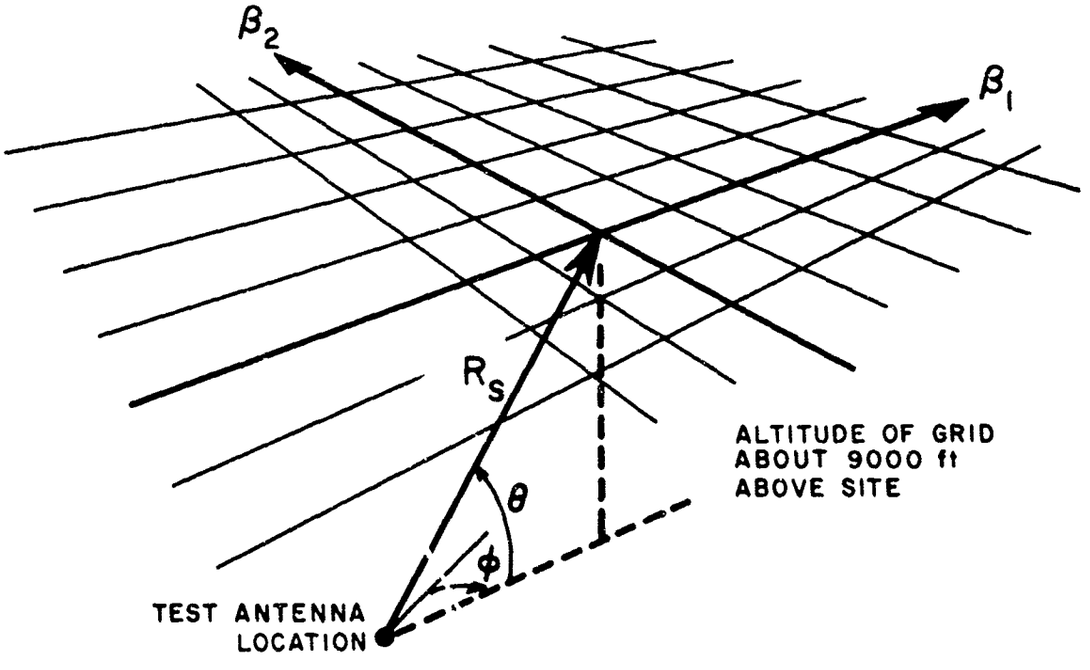

D-522-37R

FIG. 15 AIRCRAFT OVERHEAD-GRID FLIGHT PATTERN

aircraft heading on all passes. At each intersection point, roughly orthogonal measurements of the antenna's response in the

normal plane are obtained, which can be used to compute an S value in the same fashion as were the E_ϕ and E_θ vectors.

The test antenna does not see the full length of the Xeledop in general, but only the Xeledop's projection onto a plane tangential to the hemisphere. For the orbital technique with the Xeledop vertical, this projection ratio is simply the cosine of the elevation angle, which is used as a correction in reducing data for the E_θ plots. For the grid passes, this projection ratio, p, is somewhat more complex:

$$p(\phi, \theta, \beta) = \sqrt{1 - \cos^2 (\phi - \beta) \cdot \cos^2 (\theta)} \quad , \tag{2}$$

where

θ and ϕ are elevation and azimuth angles to the sample point

β is the aircraft heading.

If we receive signals a_1 and a_2 at an intersection of two grid passes with aircraft headings β_1 and β_2, then these signals must be normalized to a "unity" transmitter lying in the normal plane to give comparable response vector amplitudes $|r_1|$ and $|r_2|$:

$$|r_1| = a_1/p(\phi, \theta, \beta_1) \tag{3}$$

$$|r_2| = a_2/p(\phi, \theta, \beta_2) \quad . \tag{4}$$

It is also necessary to calculate the directions of $\vec{r}_1$ and $\vec{r}_2$ in the normal plane:

$$\alpha_1 = \arctan [\tan (\phi - \beta_1)/\sin (\theta)] \tag{5}$$

$$\alpha_2 = \arctan [\tan (\phi - \beta_2)/\sin (\theta)] \quad . \tag{6}$$

At this point, we have $\vec{r}_1$ and $\vec{r}_2$, which are equivalent to the E_ϕ and E_θ vectors normally measured except that they are not exactly orthogonal. However, at high elevation angles, sin (θ) is nearly 1.0 so α_1 and α_2 approach ($\phi - \beta_1$) and ($\phi - \beta_2$) respectively, which are as close to orthogonal as the grid--within five or ten degrees.

If we plot r_1 and r_2 in the normal plane (Fig. 16), we can again estimate two s vectors (linear antenna responses) that would have the observed components, r_1 and r_2.

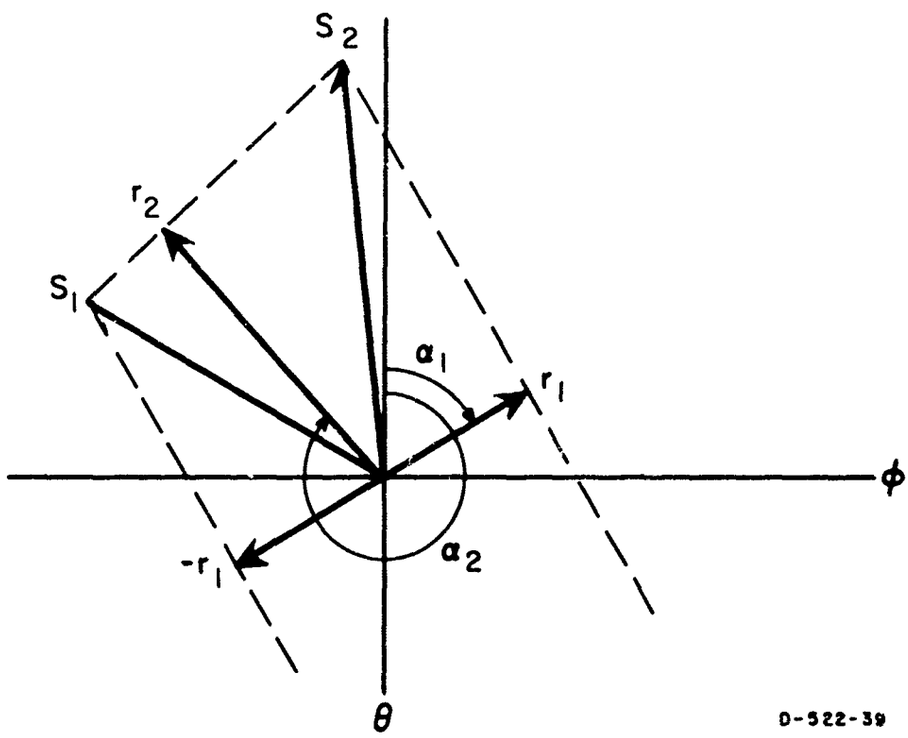

FIG. 16 DERIVATION OF S FROM r_1 AND r_2 SAMPLES

$$\gamma_1 = \arctan \left[- \frac{|r_2| \cos \alpha_1 + |r_1| \cos \alpha_2}{|r_2| \sin \alpha_1 + |r_1| \sin \alpha_2} \right] \qquad (7)$$

$$\gamma_2 = \arctan \left[- \frac{|r_2| \cos \alpha_1 - |r_1| \cos \alpha_2}{|r_2| \sin \alpha_1 - |r_1| \sin \alpha_2} \right] \tag{8}$$

$$|S_1| = \frac{|r_1|}{cc \ (\gamma_1 - \alpha_1)} \tag{9}$$

$$|S_2| = \frac{|r_1|}{\cos \ (\gamma_2 - \alpha_1)} \tag{10}$$

Although these magnitudes will not be equal, because $\vec{r}_1$ and $\vec{r}_2$ are not orthogonal, the error is rarely significant when converted into decibels because:

(1) $\vec{r}_1$ and $\vec{r}_2$ derived from grid data are usually nearly orthogonal, as noted previously.

(2) Significant error is only possible when $|r_1| \simeq |r_2|$, a condition that occurs only in a small number of cases.

Thus, very few sample points (grid intersections) have to be eliminated due to large differences--more than 3 dB--in the values of $|S_1|$ and $|S_2|$. For those having acceptable differences, S is set equal to the average of $|S_1|$ and $|S_2|$ (when in dB) to minimize the possible error in S.

The final power plot is a map of the S values for all measured elevation angles, 3° to the zenith. For angles below about 60°, the S values are computed from sets of E_θ and E_ϕ values calculated for matching (θ, Φ) points. These interpolated sets of values are a natural output of the first stage of the contour plotting computer program used to draw the basic E_ϕ and E_θ

stereographic maps. The area above 60° (with some overlap) is filled in with the approximate S values derived from an overhead grid consisting of 10 passes in each direction. All of the S values are corrected for inverse-distance amplitude variations from the nominal hemispherical radius.

To give some idea of the polarization directly overhead, a pair of vectors are shown in the corner of each power contour plot giving the two aircraft headings used in the grid relative to each antenna's nominal zero azimuth. The vector magnitudes are proportional to the relative field strengths observed overhead for the two directions. Although the polarization is still ambiguous in most cases, the true polarization is evident and surprising in some, such as Fig. A-28 showing the 23-ft-high unbalanced dipole below its resonance.

3. Data Reduction for Overhead Grid

The overhead data are processed with a multiphase system that includes the CDC-3200, B5500, and IBM 7090 computers and the Calcomp and Benson-Lehner automatic plotters. The data-reduction process is the same in part as that which creates the normal antenna patterns.

In order to locate the intersection points of the overhead passes, the ground track of the plane is plotted using the elevation and azimuth data as recorded by the GMD and the altitude, H, of the plane during the pass. (Note that the ground track will not be the same as the heading because of wind drift.) The plot is also a check on the accuracy of the tracking equipment. Because the equipment tracks inaccurately once the aircraft goes above 75° elevation, it is necessary to fit a straight-line approximation to the valid points below this elevation along each path. A program has been developed to compute the slope and distance D from the X, Y position of two end points of the pass.

Each point is associated with a specific time. We refer to these as T_U and T_L, or upper and lower time. The line is divided into segments:

$$S_G = \frac{D}{T_U - T_L} \quad .$$

The location of each time increment along the track is computed. The grid intersections are found by solving simultaneously the equations of each north/south line with all of the east/west lines. The output of the program consists of a plot of the new ground tracks showing the time increments along each track and the intersection (x, y). This plot is checked for accuracy and similarity to the original uncorrected plot. The intersection times for each north/south and east/west track is estimated to 0.1 unit accuracy.

The next program uses these grid intersection points described as occuring at a given (x, y) position relative to the GMD location and at a certain GMD "time" corresponding to the markings on the strip charts. The aircraft headings, β_1 and β_2, and amplitude data for each three seconds are read in from cards. The amplitude-data cards are similar to those read from orbit (E_ϕ or E_θ) data except that where the Xeledop signals have been covered by interfering noise (usually in nulls), the noise level is read and flagged as such on the card. This serves as an upper bound for what the test antenna's response could have been. All the amplitude data are read into an array as a function of GMD time. The array locations, number as T, would then correspond to successive 3-second intervals, synchronized to the GMD marks.

For each grid intersection, the program computes the azimuth and elevation angles, Φ and θ, from x, y and the aircraft altitude after having corrected the (x, y) origin to the test

antenna location rather than to that of the GMD. It next finds the pair of amplitude samples on each pass bracketing the intersection point. These signals are referred to as $a_1(T)$, $a_1(T + 1)$ for the β_1 heading and as $a_2(T)$ and $a_2(T + 1)$ for the β_2 heading. The T's indicate the half GMD time mark numbers appropriate to each pass. The four amplitudes are then corrected for variation in slant range from the nominal value.

The flow diagram in Fig. 17 shows the testing and interpolating used to compute S_1 and S_2 [Eq. (9) through (10)], which are converted to decibels and averaged to a_{AVE}, the desired value for that intersection. The latter is then punched on cards along with its (x, y) position. This process is repeated for all grid points.

Finally, these overhead grid points are combined with the E_ϕ and E_θ data for the power contour plots. These E_ϕ and E_θ values are interpolated to fit a regular azimuth elevation spacing by the contouring program when it generates their plots. This provides two matching sets of samples which can be directly combined [Eq. (1)] to find the power values. Since no noise threshold information is available here, only points having both E_ϕ and E_θ values are calculated. These power values are combined with the a_{AVE} values from the overhead grid into one list describing the power plot. The list is normalized to set its maximum equal to 0 dB and contoured.

D. Relative Gains

The term "relative" gain is used here to distinguish it from "absolute" gain, which is usually derived theoretically and expressed in decibels above a fixed reference level, e.g., isotropic. Because the receiving system is calibrated in parallel and the input impedances are known, the gains of the various antennas in both polarizations can be compared, or "related." However,

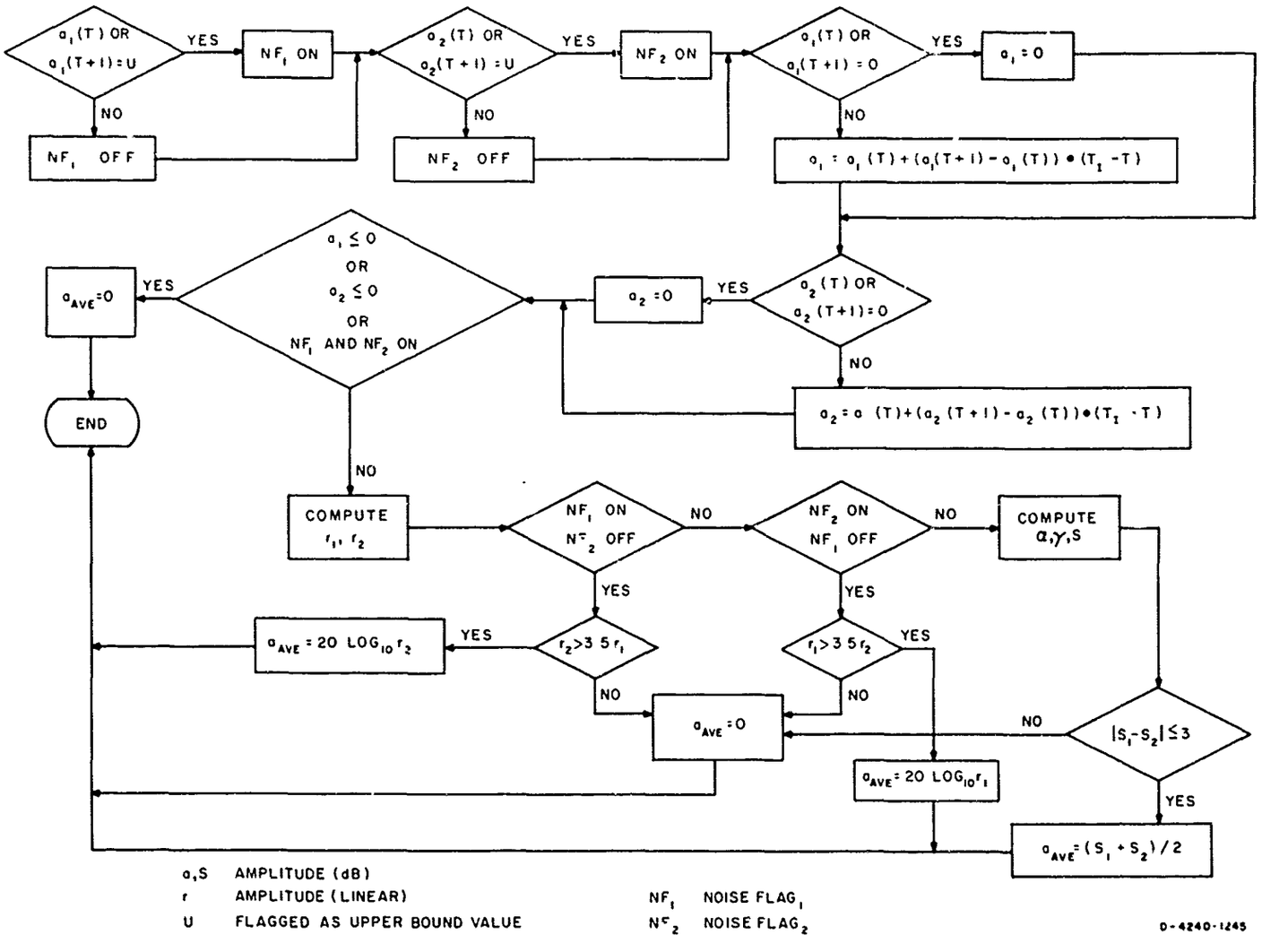

FIG. 17 FLOW CHART OF DATA PROCESSING TO COMPUTE POINTS FOR POWER PLOTS

because the Xeledop's absolute power output is unknown, absolute gains cannot be derived from the measured data without assuming the gain of one antenna.

Note that these comparisons are only strictly valid on a given frequency; comparisons between frequencies again require an assumed gain characteristic for one antenna.

Two types of gain figures are shown in Table I: relative voltage and E_θ/E_ϕ. The first, relative voltage, uses the values directly measured: voltages across impedances within 1.2 to 1 VSWR of 50 Ω at the receiving/recording equipment van. These voltage values--after correction for feed cable losses--are in decibels referred to an arbitrary level chosen for computer programming convenience, and are the normalizing constants for the contour plots, i.e., 0 dB on each plot. Thus, the relative voltage column effectively compares the voltages to be expected across (or power delivered to) 50-Ω loads at each antenna's feed point terminals for each pattern's maximum.

The next column, E_θ/E_ϕ, tabulates the differences in response between E_θ (vertical) and E_ϕ (horizontal) polarization, with a plus sign indicating the E_θ response was higher. For example, on the 2:1 inverted L at 5 Mc/s, the E_θ maximum (0 dB on the pattern contour plot) was about 3 dB higher than the E_ϕ maximum, while at 8 Mc/s the E_ϕ response was about 5 dB higher than the E_θ response.

The accuracy of the data in Table I is determined by the contour interval (3 dB) of the contour plots since they are tabulations of the maximum data point value of each plot. Thus, the E_θ/E_ϕ values are accurate to within about 1.5 dB. Comparisons between antennas--relative voltage gains include an additional 0.5 dB error due to the difference between the actual van input impedance and 50 Ω.

Table II presents relative power gains into matched loads, which were derived from the values from Table I through the following procedure:

(1) The mismatch loss to 50 Ω for each antenna at each measured frequency was estimated from the impedance data given in Sec. IV.

(2) These estimated losses were added to each of the maximum received signal values to estimate the power that would have been delivered to a matched load.

(3) To simplify comparisons, the maximum for each frequency was arbitrarily chosen as a 0-dB reference, and all of the relative gain values for that frequency were normalized to this maximum.

The resulting values include the 2-dB errors from Table I voltages plus an error in the mismatch loss estimates. These losses are determined from antenna impedance, which is measured by a technique that finds the magnitude and angle of the reflection coefficient, with an accuracy of about ±5 percent in the magnitude $|\rho|$. Since the mismatch losses required to correct the gains become a more sensitive function of $|\rho|$ as it increases from 0 to 1 (or the VSWR as ρ increases from 1 to infinity), the relative gain estimates suffer a small error at low antenna VSWR and a large error for high antenna VSWR, all due to a constant 5-percent error in $|\rho|$. Although the effect of this error is minimized by the technique outlined in Sec. IV-A, it should still be noted that an error is present. In Table II those values for which the sum of the errors, including the voltage gain errors, is potentially in excess of 3 dB have been indicated by an "x". Potential errors of the unmarked values are less than 3 dB.

Table I

RELATIVE VOLTAGE GAINS ACROSS 50-OHM LOADS AT PAT ERN MAXIMA

Antenna and Design Frequency, f_o	Measurement		Relative Voltage (dB)	E_θ/E_ϕ (dB)
	Frequency, (Mc/s)	Polarization		
30° Slant Wire (4 Mc/s)	2.0	θ	-50.1	+5.7
		φ	-55.8	
	4.0	θ	-28.9	+6.6
		φ	-35.5	
	6.0	θ	-30.5	+4.8
		φ	-35.3	
2:1 Inverted L (8 Mc/s)	2.6	θ	-66.4	
	5.0	θ	-44.8	+3.4
		φ	-48.2	
	8.0	θ	-32.6	-5.1
		φ	-27.5	
5:1 Inverted L (10 Mc/s)	4.0	θ	-29.6	+5.4
		φ	-35.0	
	6.0	θ	-30.3	+4.7
		φ	-35.0	
	10.0	θ	-26.6	+0.6
		φ	-27.2	
Unbalanced Dipole 23 ft High (8 Mc/s)	5.0	θ	-50.2	+6.0
		φ	-56.2	
	8.0	θ	-22.1	-0.5
		φ	-21.6	
	15.0	θ	-20.3	-2.5
		φ	-17.8	
Unbalanced Dipole 2 ft High (6 Mc/s)	2.0	θ	-54.9	
	4.0	θ	-45.1	+0.6
		φ	-45.7	
	6.0	θ	-31.8	-6.0
		φ	-25.8	
	10.0	θ	-40.0	-4.9
		φ	-35.1	
Sleeve Dipole (5 Mc/s)	5.0	θ	-44.8	+4.7
		φ	-49.5	
	8.0	θ	-45.4	+2.8
		φ	-48.2	
Monopole (15 Mc/s)	2.0	θ	-72.5	-
	4.0	θ	-49.8	-
	5.0	θ	-61.8	-
	6.0	θ	-48.1	-
	8.0	θ	-39.3	-
	10.0	θ	-27.1	-
	15.0	θ	-10.8	-
Balanced Dipole (15 Mc/s)	4.0	φ	-53.8	-
	5.0	φ	-63.0	-
	6.0	φ	-47.8	-
	8.0	φ	-37.9	-
	10.0	φ	-28.0	-
	15.0	φ	- 9.8	-

Table II

RELATIVE POWER GAINS INTO MATCHED LOADS

AT PATTERN MAXIMA

Measurement Frequency (Mc/s)	Antenna		Potential Error*	Gain	
	Type	Design Frequency, f_o (Mc/s)		E_θ (dB)	E_ϕ (dB)
4.0	30° Slant Wire	4		0.0	- 6.6
	5:1 Inverted L	10	x	- 0.2	- 5.6
	Unbalanced Dipole 2 ft high	8	x	-13.5	-14.1
	Balanced Dipole	15	x		-20.1
5.0	2:1 Inverted L	8	x	- 0.0	- 3.4
	Sleeve Dipole	5	x	- 0.2	- 4.9
	Unbalanced Dipole 23 ft high	8	x	- 5.2	-11.2
6.0	5:1 Inverted L	10	x	0.0	- 4.7
	Unbalanced Dipole 2 ft high	8		- 8.2	- 2.2
	30° Slant Wire	4		- 3.2	- 9.0
	Balanced Dipole	15	x		-17.6
	Monopole	15	x	-17.9	
8.0	Unbalanced Dipole 23 ft high	8		- 0.5	0.0
	2:1 Inverted L	8	x	- 7.8	- 2.7
	Sleeve Dipole	5	x	-17.9	-20.7
15.0	Balanced Dipole	15			0.0
	Monopole	15		- 0.8	
	Unbalanced Dipole 23 ft high	8	x	- 4.0	- 1.5

*Potential amplitude errors greater than ±3 dB due to VSWR measurement errors. All gains on one frequency normalized to set highest equal to 0.0 dB.

IV IMPEDANCE MEASUREMENTS

Impedance measurements were made of all the antennas as an aid to patterns analysis and deriving relative gain figures. They are illuminating in themselves, however, since the grounding rods or counterpoise wires are clearly shown to be an active part of the antenna system. They also give an indication of how poor the ground was during the time of measurement.

A. Measurement Technique

These measurements were taken with an Alford automatic impedance plotter, which provides a rapid and continuous display of impedance at the antenna feed point over a wide frequency band. This capability makes it economically feasible to take a large number of measurements without missing any significant characteristics [which might be lost if a discrete-point technique (RX meter) were used]. The price of this convenience and continuity is the accuracy of any given point. The plotter measured impedances indirectly by finding the load's reflection coefficient (compared to 50 Ω) and displaying that value on a Smith chart. The equipment accuracy is expressed as a percentage of the reflection coefficient (±5%, ±5°); hence, the resistance and reactance numbers near the rim of the chart are not precise. For this reason, the data is presented on Smith charts, rather than as tables of resistance and reactance as a function of frequency.

The inaccuracy results from several parts of the plotter being frequency-sensitive. The "hybridge" (where the load and standard are compared) is rated down to only 2.5 Mc/s, and its performance deteriorates below that figure. The three "phase splitters" (networks that divide an oscillator signal into

reference and test signals) work well only over limited frequency bands, overlapping at about 4 and 11 Mc/s.

In order to minimize the errors at the ends of the frequency band of the phase splitters, the system was calibrated more often than recommended by the manufacturer. The manufacturer advises that the instrument be calibrated once at the middle of the frequency band of the phase splitter in use. It was found that if the instrument were calibrated at the middle and both ends of the frequency band of these phase splitters, there would be less discrepancy when comparing measurements from the upper frequency and lower frequency of two consecutive phase splitters. The impedance plotter was also calibrated at each frequency transmitted by the Xeledop so as to minimize errors when measuring the antenna VSWR at the frequencies at which data were taken for the radiation patterns and relative gain figures (see Sec. III-D).

In the previous measurements at Lodi, the unit was calibrated in the middile of the frequency band of each phase splitter, as recommended by the manufacturer. Later, the deviation from these simple calibrations and calibration over the range of specific frequencies was determined. Then the field data were corrected and smoothed by calculating these deviations into the data. Thus, the Lodi data have been smoothed through calculations and the data in this report have been corrected for major plotter errors by calibrating the instrumentation over smaller frequency bands. In some cases, at very high VSWR, the plotter indicated a reflection coefficient slightly greater than one. Any portions of the curve where this occurred are shown by a dashed line on the Smith charts.

B. Discussion of Results

Impedance measurements were made on all antennas after they were erected in their measurement situations. Thus, the impedance

plots (Figs. 18 to 26) show the impedance of the antenna as it was while radiation patterns of the antennas were being measured.

For the cases where match to the antenna is very poor (near anti-resonance), relatively high currents appear on the outside of the feeding coaxial line. These currents show up in two ways: as radiation during pattern measurements and as perturbations in the impedance curves. The Smith chart for the 23-ft-high dipole (Fig. 22) shows the presence of these currents very clearly in the form of small loops between the frequencies of 10 and 15 Mc/s. Similar loops are also evident on the Smith chart of the 2-ft-high dipole (Fig. 23) around 4.0 Mc/s and 7.0 Mc/s. These small loops are quite similar to those evident in the measurements at Lodi.

If a further comparison is made between the impedance measurement indicated in this report and those made at Lodi, some information can be deduced about the conductivity of the ground. The impedance plots of the dipoles and monopole antenna compare fairly well, while there is a discrete difference between the impedances of the slant-wire and inverted L's. However, the latter group of antennas are more dependent on ground characteristics, due to the grounding systems of these antennas (i.e., counterpoises and grounding rods).

In addition to impedance plots of the antennas at their pattern measurement heights, impedance measurements were made at resonant frequency of half-wave dipoles with the height above ground as a variable. The 6 Mc/s dipole was the 2-ft-high unbalanced dipole used for pattern measurements and the 3 Mc/s dipole was the same antenna but the radiators were lengthened to 77.8 ft. In all cases, the dipoles were unbalanced and the shield of the RG-58 coaxial line was grounded only at the measurement point (at the impedance plotter). More detailed information on dipole impedance as a function of height can be found in other reports.[3,4]

The normalized curves in Figs. 27 and 28 show variations of impedance and resonant frequency which are typical of half-wave dipoles near a lossy ground.

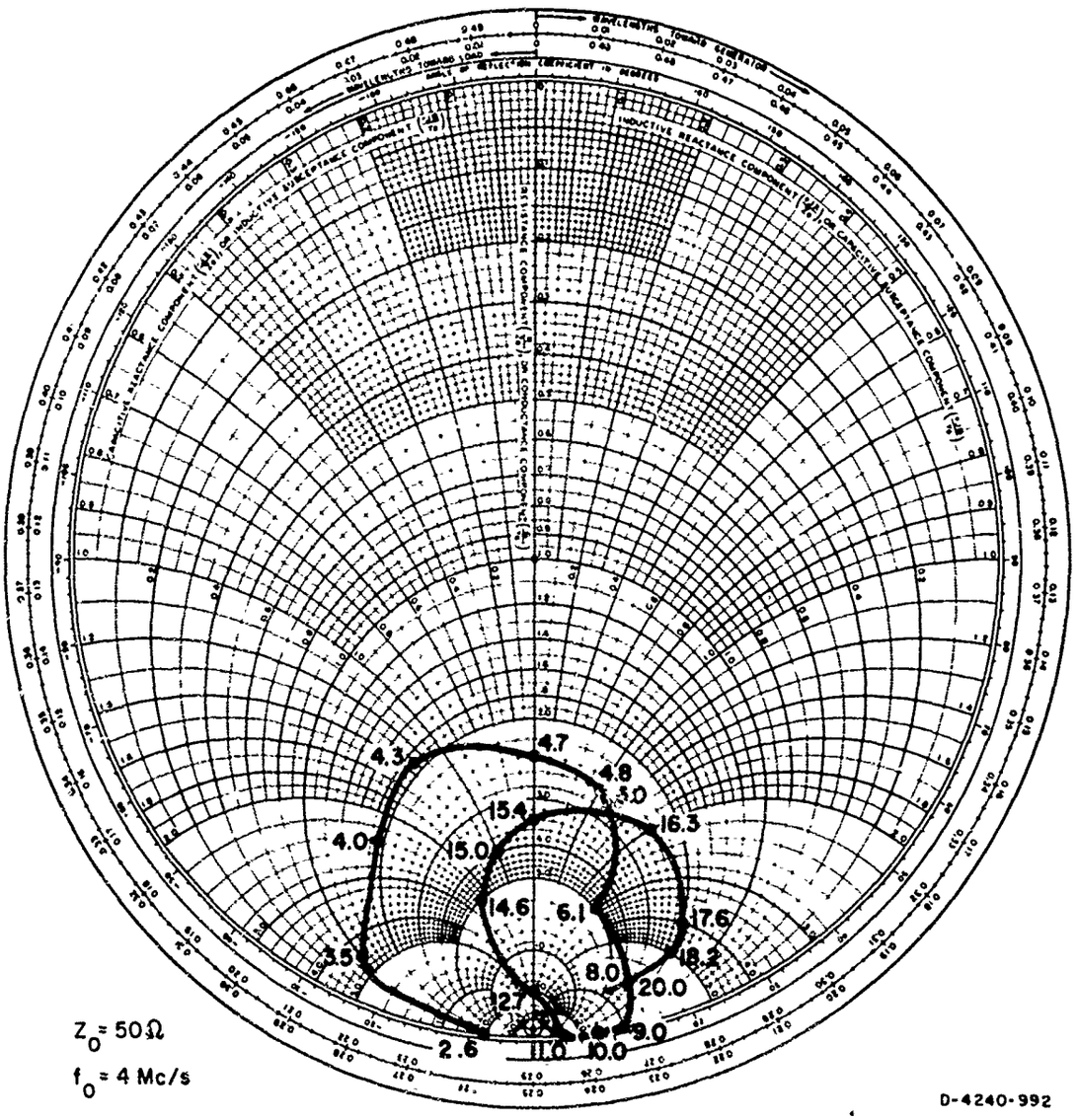

FIG. 18 SMITH CHART REPRESENTATION OF ANTENNA IMPEDANCE FOR 30° SLANT-WIRE ANTENNA (2.6 to 20.0 Mc/s)

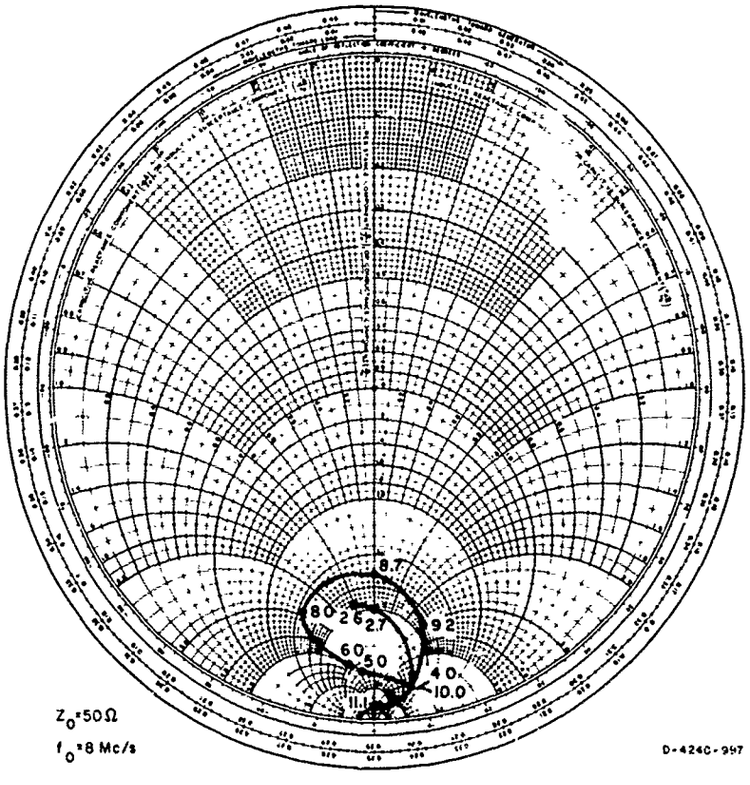

FIG. 19 SMITH CHART REPRESENTATION OF ANTENNA IMPEDANCE FOR 2:1 INVERTED L ANTENNA (2.6 to 11.1 Mc/s)

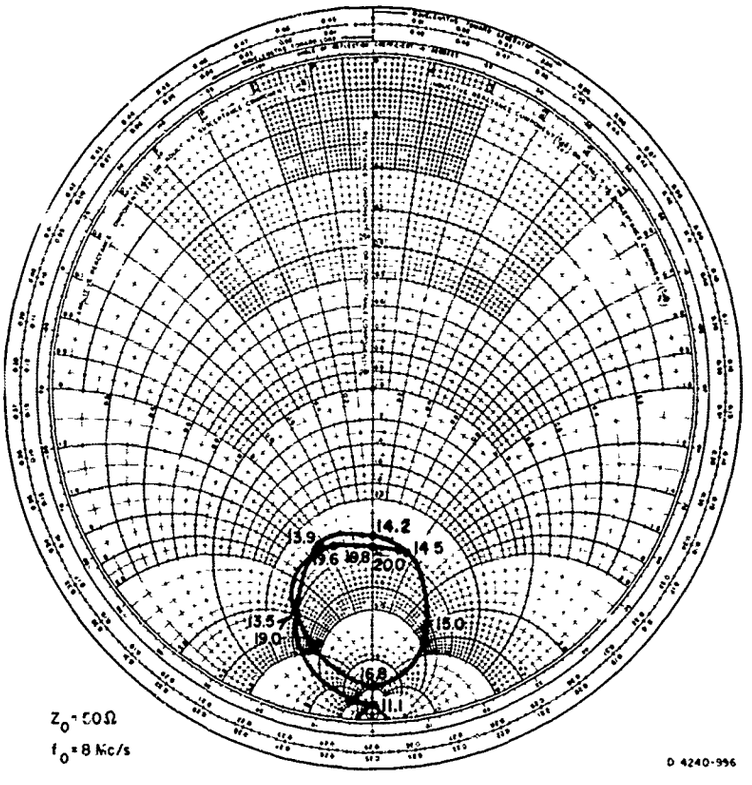

FIG. 20 SMITH CHART REPRESENTATION OF ANTENNA IMPEDANCE FOR 2:1 INVERTED L ANTENNA (11.1 to 20.0 Mc/s)

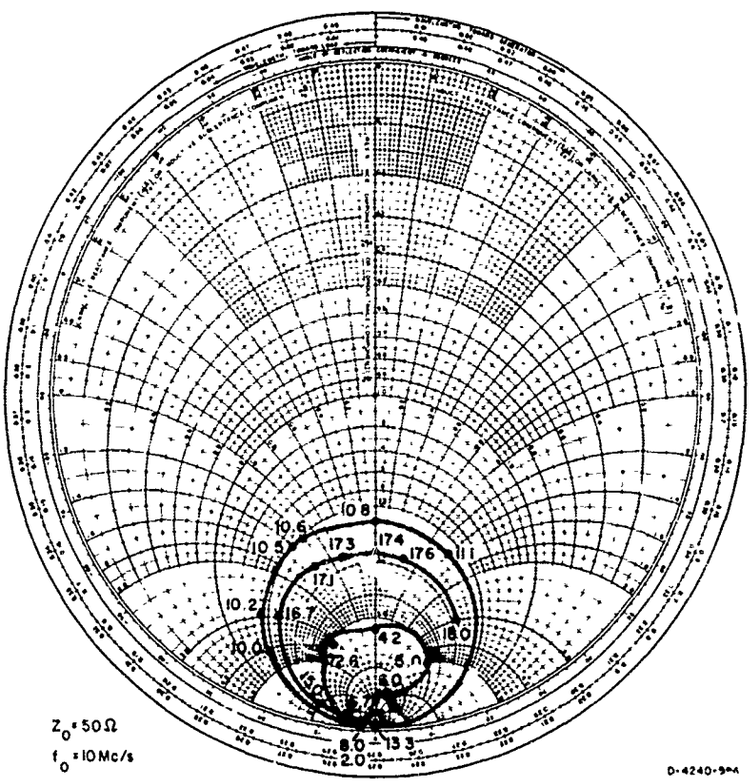

FIG. 21 SMITH CHART REPRESENTATION OF ANTENNA IMPEDANCE FOR 5:1 INVERTED L ANTENNA (2.0 to 18.0 Mc/s)

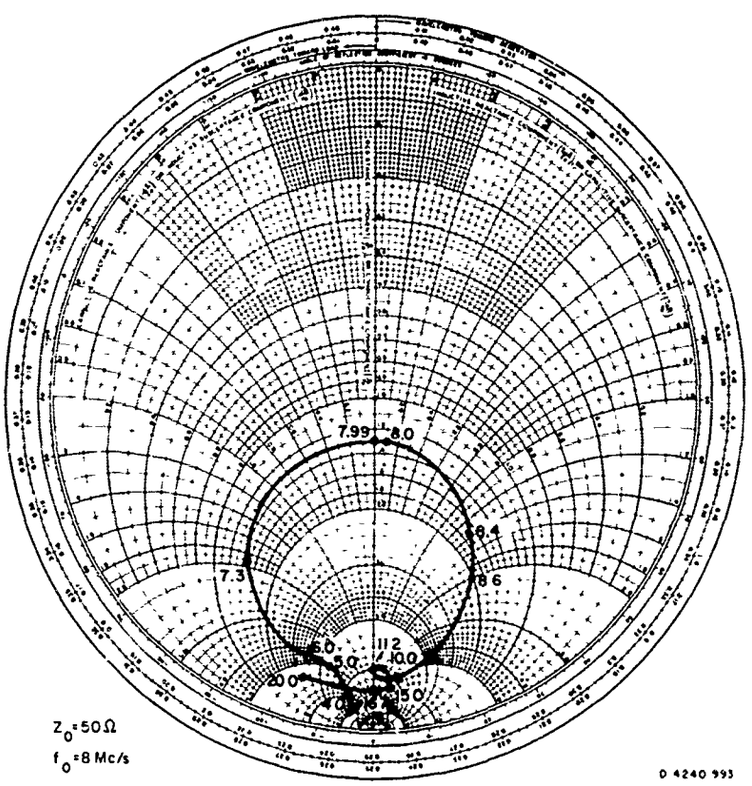

FIG. 22 SMITH CHART REPRESENTATION OF ANTENNA IMPEDANCE FOR 23-FOOT-HIGH UNBALANCED DIPOLE ANTENNA (4.0 to 20.0 Mc/s)

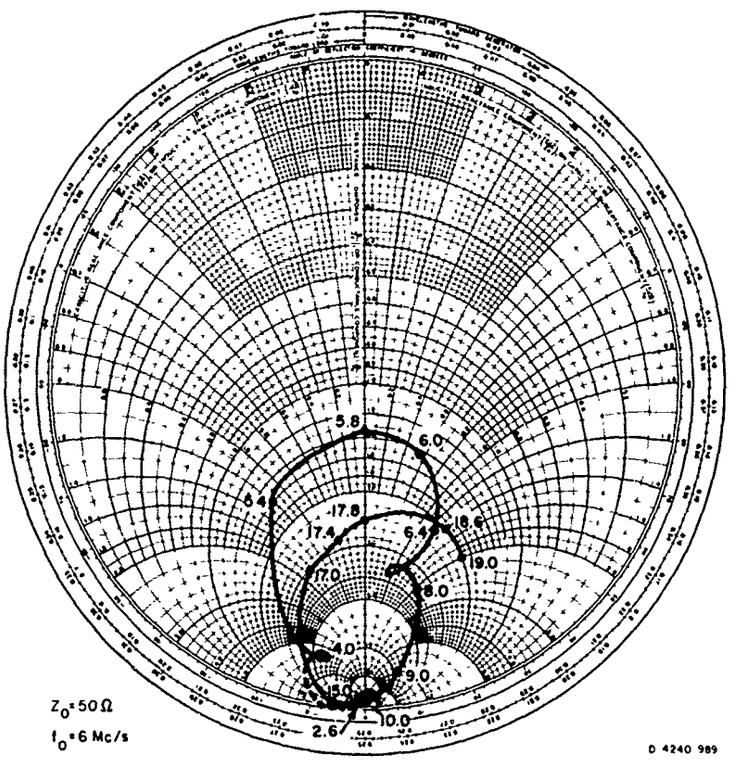

FIG. 23 SMITH CHART REPRESENTATION OF ANTENNA IMPEDANCE FOR 2-FOOT-HIGH UNBALANCED DIPOLE ANTENNA (2.0 to 19.0 Mc/s)

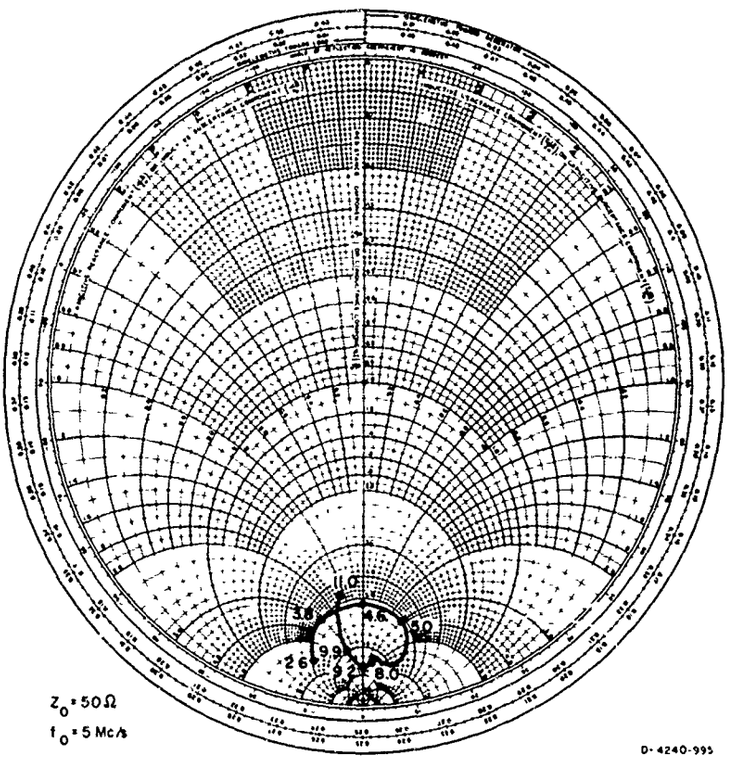

FIG. 24 SMITH CHART REPRESENTATION OF ANTENNA IMPEDANCE FOR SLEEVE DIPOLE ANTENNA (2.6 to 11.0 Mc/s)

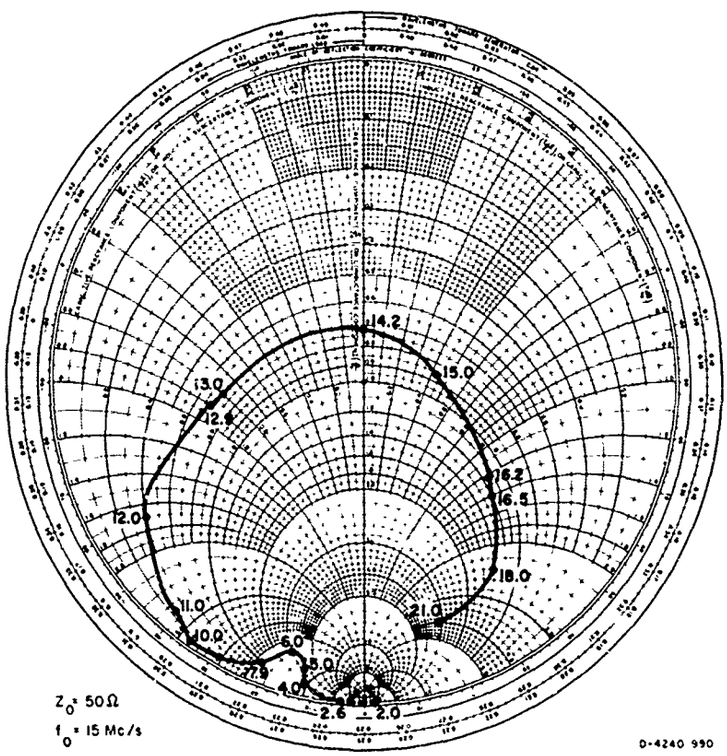

FIG. 25 SMITH CHART REPRESENTATION OF ANTENNA IMPEDANCE FOR MONOPOLE ANTENNA (2.0 to 21.0 Mc/s)

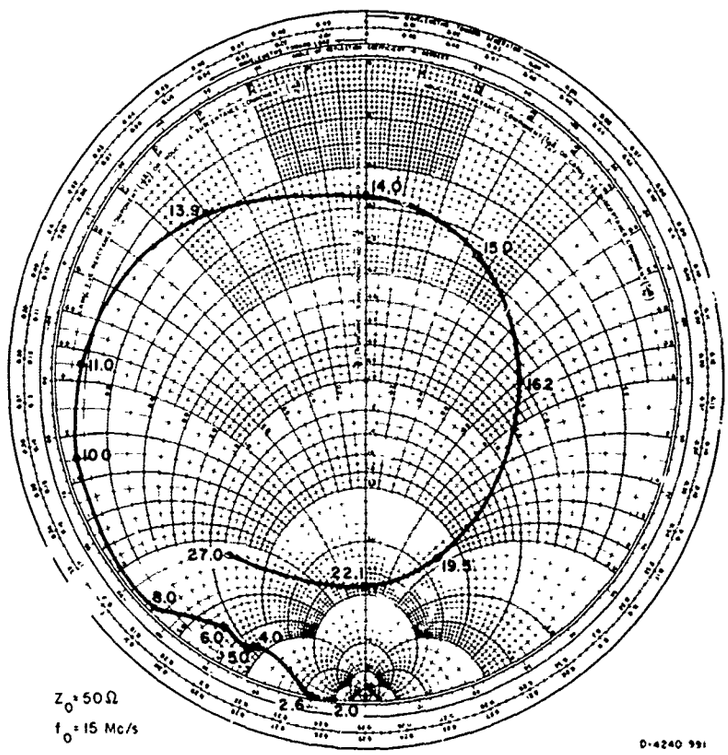

FIG. 26 SMITH CHART REPRESENTATION OF ANTENNA IMPEDANCE FOR BALANCED DIPOLE ANTENNA (2.0 to 27.0 Mc/s)

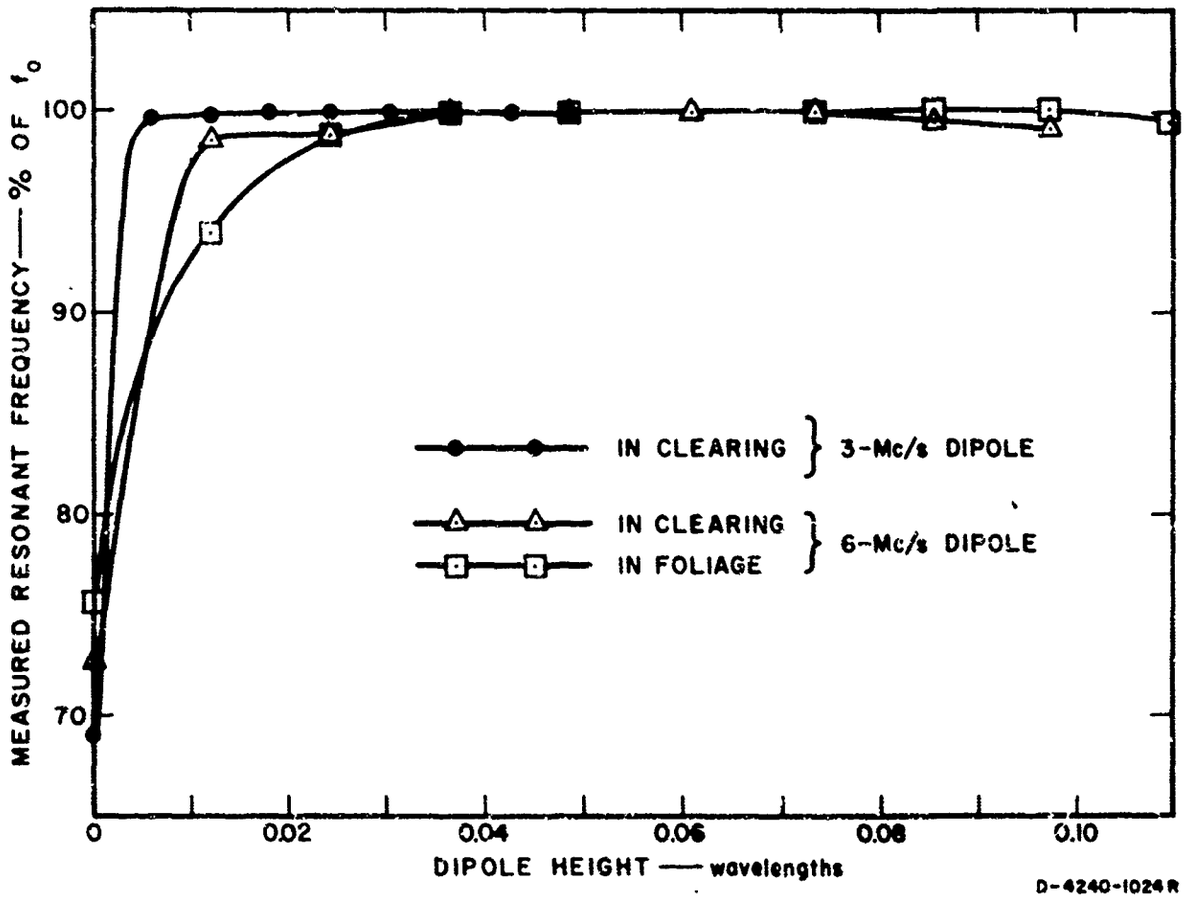

FIG. 27 NORMALIZED CURVES OF RESONANT FREQUENCY AS A FUNCTION OF HEIGHT FOR DIPOLES

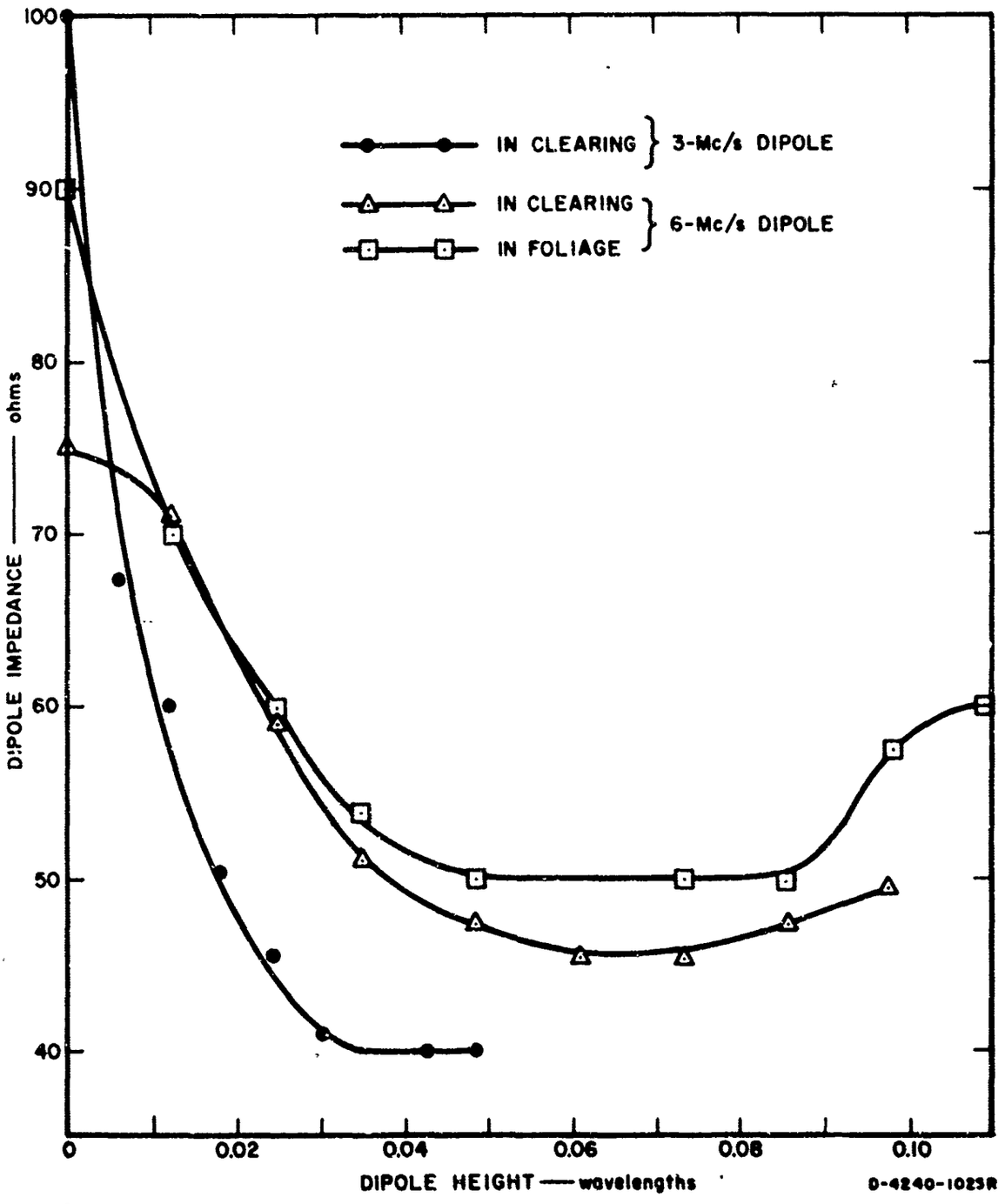

FIG. 28 NORMALIZED CURVES OF DIPOLE IMPEDANCE AT RESONANT FREQUENCY AS A FUNCTION OF DIPOLE HEIGHT

V DISCUSSION OF RESULTS

This section makes some preliminary comparisons between the results reported here on antennas in a pine forest and the results reported earlier on essentially similar antennas in open farmland, since significant changes in both patterns and impedances were observed.

For many of the antennas, such as the inverted L's, the resistive component of the impedance increased considerably. It is not clear whether this was entirely or even partly due to the change from open space to forest because the electrical ground parameters also changed.

The extent to which these two site differences--trees and ground--affected the patterns is more apparent. The ground seems to have affected most the elevation plane patterns of antennas with major radiating structures very close to the ground (the 30° slant wire at 6 Mc/s, for example). The 23-ft-high dipole at resonance (Figs. A-29 and A-30) was relatively unaffected by either ground or trees in either polarization. No major changes are evident even at the lower elevation angles; thus, the trees apparently had little or no effect on the dipole's radiation pattern at 8 Mc/s. Of course, this does not prove whether or not its efficiency as a vertical-incidence antenna changed due to energy loss in the dipole's near field; it only shows that the pattern shape did not change.

The effect of the trees was clearly evident for the monopole at the higher frequencies. Azimuthal patterns measured on this antenna at the farmland site and elsewhere have been constant within a few dB up to 15 Mc/s. This also holds true here, where the antenna was built in the forest as described in Sec. II-H,

up to 6 Mc/s (Figs. A-51 through A-54). However, at 8 Mc/s and above, the azimuthal pattern breaks up dramatically (Figs. A-55 to A-57). This sudden change in pattern for a small change in frequency was unexpected and hence very significant. Turning to the 23-ft-high dipole at 15 Mc/s, the E_ϕ pattern (Fig. A-33) repeats the one measured at the farmland site almost exactly, while the E_θ pattern (Fig. A-32) is similar only at the higher elevation angles. The response at lower angles seems attenuated and distorted: The response at all azimuths is lower, but the sharp null at 255° azimuth at the farmland site is not evident here.

REFERENCES

1. W. A. Ray, "Full-Scale Pattern Measurement of Simple HF Field Antennas," Special Technical Report 10, Contract DA 36-039 AMC-00040(E), SRI Project 4240, Stanford Research Institute, Menlo Park, California (May 1966).

2. C. Barnes, "Xeledop Antenna Pattern Measuring Equipment, 2 to 50 Mc," Stanford Research Institute, Menlo Park, California (July 1965).

3. G. H. Hagn, J. E. van de Laan, D. J. Lyons, E. M. Kreinberg, "Ionospheric-Sounder Measurement of Relative Gains and Bandwidths of Selected Field-Expedient Antennas for Skywave Propagation at Near-Vertical Incidence," Special Technical Report 18, Contract DA 36-039 AMC-00040(E), SRI Project 4240, Stanford Research Institute, Menlo Park, California (January 1966).

4. T. S. Cory, W. A. Ray, "Measured Impedances of Some Tactical Antennas Near Ground," Research Memorandum 7, Contract DA 36-039 AMC-00040(E), SRI Project 4240, Stanford Research Institute, Menlo Park, California (February 1964).

DISTRIBUTION LIST

Organization	No. of Copies
Commanding General U.S. Army Electronics Command Fort Monmouth, New Jersey 07703 Attn: AMSEL-RD-DO ARMA Coordinator	1
Commanding General U.S. Army Electronics Command Fort Monmouth, New Jersey 07703 Attn: AMSEL-NL-R-4 R. N. Herring	28
Marine Corps Liaison Officer U.S. Army Electronics Command Fort Monmouth New Jersey 07703 Attn: AMSEL-RD-LNR	1
U.S. Army Electronics Command Liaison Officer Rome Air Development Center EMPL Griffiss Air Force Base, New York 13440 Attn: Capt. A. P. Toth	1
U.S. Army Electronics Command Liaison Officer Rome Air Development Center EMPL Griffiss Air Force Base, New York 13440 Attn: Capt. E. Hee	1
Commanding General U.S. Army Materiel Command Washington, D.C. 20315 Attn: ANCRD-DE-C	1
Director Advanced Research Projects Agency Remote Area Conflict Washington, D.C. 20301 Attn: Lt. Col. T. W. Doeppner	2

DISTRIBUTION LIST (continued)

Organization	No. of Copies
Commanding General U.S. Army Electronic Proving Ground Fort Huachuca, Arizona 85613 Attn: STEEP-ET	1
President U.S. Army Airborne Board and Special Warfare Board Fort Bragg, North Carolina 28307	1
Chief of Research and Development Department of the Army Washington, D.C. 20315 Attn: Lt. Colonel N. F. J. Allen	1
Office of the Chief of Communications-Electronics Department of the Army Washington, D.C. 20315 Attn: Electronics Systems Directorate	1
Dr. Thomas M. Griffiths Project Duty Department of Geography University of Denver Denver, Colorado 80202	1
Director Waterways Experiment Station P.O. Box 631 Vicksburg, Mississippi 39180 Attn: Mr. A. Rula	1
Advanced Research Projects Agency R&D Field Unit APO San Francisco 96309	1
Commanding General U.S. Army Electronics Command Fort Monmouth, New Jersey 07703 Attn: AMSEL-IO-T	1

Organization	No. of Copies
Director U.S. Naval Research Laboratory Washington, D.C. 20390 Attn: Code 2027	1
Rome Air Development Center (EMTLD) Griffiss Air Force Base New York 13440 Attn: Documents Library	1
Commanding Officer U.S. Army Combat Development Command Fort Bragg, North Carolina 28307 Attn: C. T. Swaringen	1
Commanding Officer U.S. Army War Limited Laboratory Aberdeen Proving Ground, Maryland 21005 Attn: CRD-AM-6	1
Director National Security Agency Fort George G. Meade, Maryland 20755 Attn: TDL	1
Remote Area Conflict Information Center (RACIC) Battelle Memorial Institute 505 King Avenue Columbus, Ohio 43201	1
Chief of Naval Research Naval Research Laboratory Washington D.C. 20390 Attn: Code 4324 Mr. Irwin Schiff	1
Major A. P. Sidon OSD/ARPA R&D Field Unit JUSMAG APO San Francisco 96346	70

DISTRIBUTION LIST (continued)

Organization	No. of Copies
Chief of Research and Development Headquarters, Department of the Army Washington, D.C. 20301 Attn: Chief, Environmental Sciences Division	1
Wilson Nuttall, Raimond Engineers, Incorporated Chesterton, Maryland 21620 Attn: Dr. Holdbridge	1
Wilson Nuttall, Raimond Engineers, Incorporated Chesterton, Maryland 21620 Attn: Library	1
Defense Intelligence Agency Washington, D.C. 20301 Attn: Special Warfare Off	1
Defense Documentation Center Cameron Station Alexandria, Virginia 22314	50
Atlantic Research Corporation Jansky & Bailey Division Shirley Highway at Edsall Road Alexandria, Virginia 22314	1
Director OSD/Advanced Research Projects Agency RDFO (ME) APO New York 09694	1
Commanding General U.S. Army Electronics Command Fort Monmouth, New Jersey 07703 Attn: AMSEL-RD-GFA Mr. John Chappell	1

Organization	No. of Copies
Commanding General U.S. Army Electronics Command Fort Monmouth, New Jersey 07703 Attn: AMSEL-RD-MAF	1
Major A. P. Sidon OSD/ARPA Research and Development Field Unit JUSMAG APO San Francisco 96346	1
Commanding Officer U.S. Army Strategic Communications Command--CONUS Fort Monmouth, New Jersey 07703 Attn: Capt. Smith (Fort Monmouth Facility)	1
Rome Air Development Griffiss Air Force Base, New York 13440 Attn: EMASA - Mr. Vincent Coyne	1
Rome Air Development Center Griffiss Air Force Base, New York 13440 Attn: EMD - Mr. Fred Diamond	1
Commander Aeronautical Systems Division Wright-Patterson Air Force Base, Ohio 45433 Attn: ASJT (Mr. Ricker)	1
U.S. Army Liaison Office MIT Lincoln Laboratory, Rm. A-210 Lexington, Massachusetts 02173 Attn: A. D. Bedrosian	1
Headquarters ESD (ESWE/Capt. Ruta) L.G. Hanscom Field Bedford, Massachusetts 01730	1
California Institute of Technology Jet Propulsion Laboratory 4800 Oak Grove Drive Pasadena, California 91103 Attn: STA-Library/ R. E. Walker, Supervisor	1

DISTRIBUTION LIST (concluded)

Organization	No. of Copies
Commanding General U.S. Army Security Agency Arlington Hall Station Arlington, Virginia 22212 Attn: IARD-R-E	1
Commanding General, USASA Arlington Hall Station Arlington, Virginia 22212 Attn: DCSR&D	3
DRC Incorporated P.O. Box 3537 Santa Barbara, California 93105	1
Director Advanced Research Projects Agency The Pentagon Washington, D.C. 20301 Attn: T IO	2
Commanding General U.S. Army Electronics Command Fort Monmouth, New Jersey 07703 Attn: AMSEL-HL-CT-R	1
Page Communications Engineers, Inc. 3300 Whitehaven Street Washington, D.C. 20007 Attn: Mr. Robert Hauptman	1
Director Air University Library Maxwell Air Force Base, Alabama 36112 Attn: AUL3T-66-453	1

Organization	No. of Copies
Commanding General Special Warfare Center Fort Bragg, North Carolina 28307	1
Commandant Special Warfare School Fort Bragg, North Carolina 28307	1
Dr. F. A. Fox A/Deputy Chief Scientist Department of Supply Box 2288/U G.P.O. Melbourne, Australia	1
Headquarters U.S. Marine Corps Washington, D.C. 20390 Attn: Code A04C Mr. R. J. Sgro	1

Appendix

ANTENNA CONTOUR PLOTS

This appendix contains all of the antenna pattern contour plots grouped by antenna in this order: 30° slant wire, 2:1 inverted L, 5:1 inverted L, 23-ft-high unbalanced dipole, 2-ft-high unbalanced dipole, sleeve dipole, monopole, and balanced dipole. For each antenna, the two individual polarization plots and the power plot are given for each measured frequency in order of increasing frequency. The title block at the lower right-hand side of each plot gives the antenna name, the polarization, and the frequency measured for that plot. The polarizations are defined exactly in Sec. III-A; as a reminder, E_ϕ is horizontal and E_θ is vertical. The antenna's design frequency, f_o, is indicated at the lower left corner of each page.

Each contour map shows all the amplitude data taken on one antenna, for one polarization, at one frequency. The plot can be visualized in several ways. For instance, one can picture placing a large hemisphere over the antenna being measured, then drawing the field-strength contours on its surface. The contour plots are two-dimensional maps of the hemisphere as it appears from directly above. Hence, the zenith angle is at the center of the plot, azimuth angles appear as radials, and elevation angles are concentric circles. The outer rim of the plot is the horizon, or 0-degree elevation. The azimuth angles numbered around the rim of the plot are in degrees relative to some principal axis of the antenna. As an example, for the balanced dipole antenna patterns, 0° azimuth on the plot is actually 142° from magnetic north. These angles are indicated on the two site maps (Figs. 3 and 4) by arrows labeled in degrees magnetic. The relationship of contour

plot azimuth to each antenna is also shown by the schematic diagram in the center of each E_θ or E_ϕ pattern plot.

The power plots do not have the antenna diagram, so it is necessary to refer to the previous voltage plot for the orientation. Instead of the antenna diagram, a pair of vectors are shown in the center of each power plot. These indicate the relative signal voltages (within 2-3 dB) received overhead the antennas from roughly orthogonal aircraft passes as described in Sec. III-C-2. The "polarization" of the antenna at the zenith can be inferred from this diagram in the cases where one vector is much larger than the other; otherwise the test antenna's actual polarization is ambiguous (see Fig. 16 and accompanying text).

In examining the plots, the accuracy limits of the measurement technique should be kept in mind. The details of these limits are discussed in the previous report, but generally, any features of the plot which are smaller than ±3° azimuth ±1/2 contour interval are insignificant due to limited data sampling and processing errors.

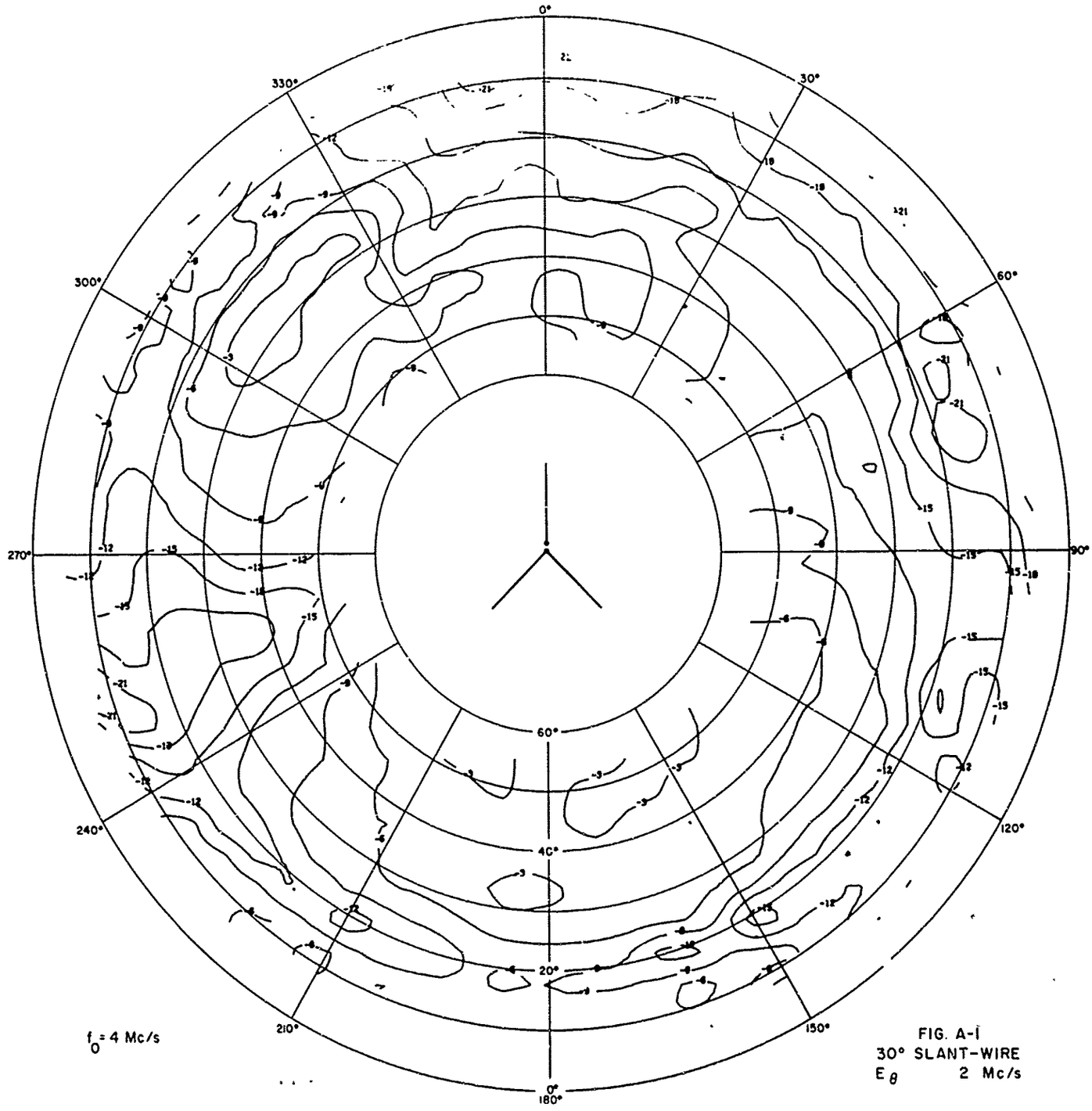

f_0 = 4 Mc/s

FIG. A-1
30° SLANT-WIRE
E_θ 2 Mc/s

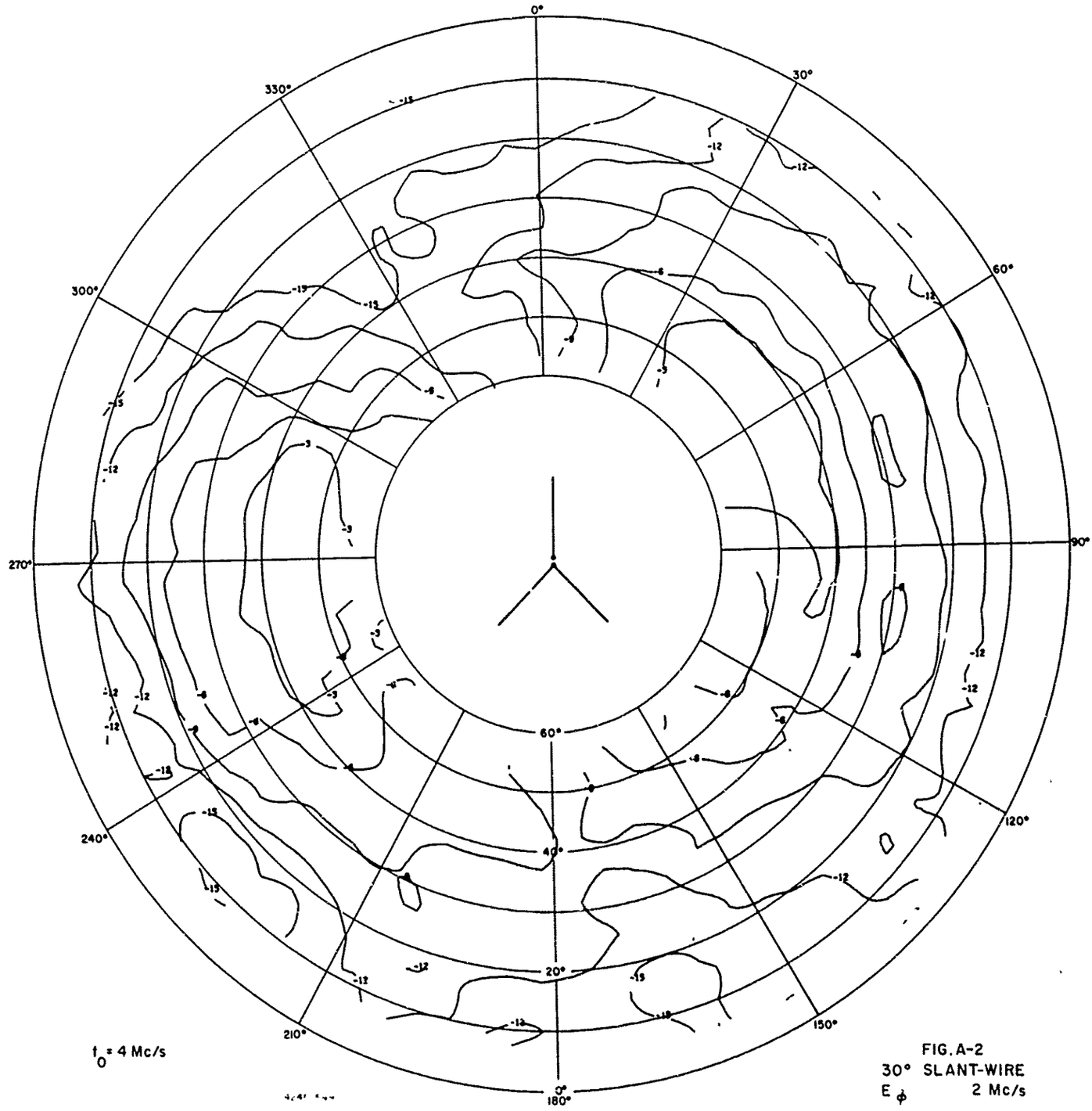

f_0 = 4 Mc/s

FIG. A-2
30° SLANT-WIRE
E_ϕ 2 Mc/s

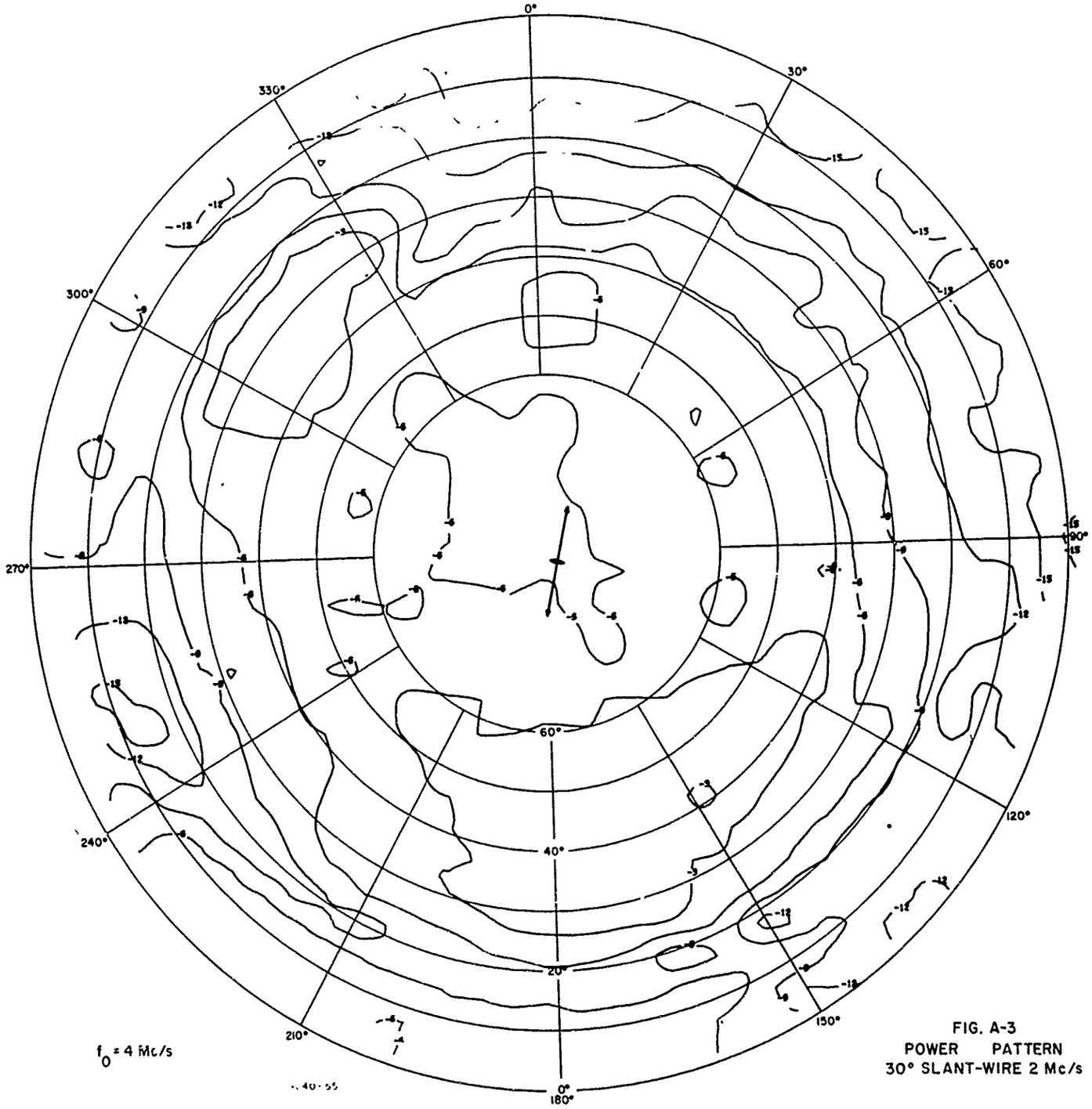

FIG. A-3
POWER PATTERN
30° SLANT-WIRE 2 Mc/s

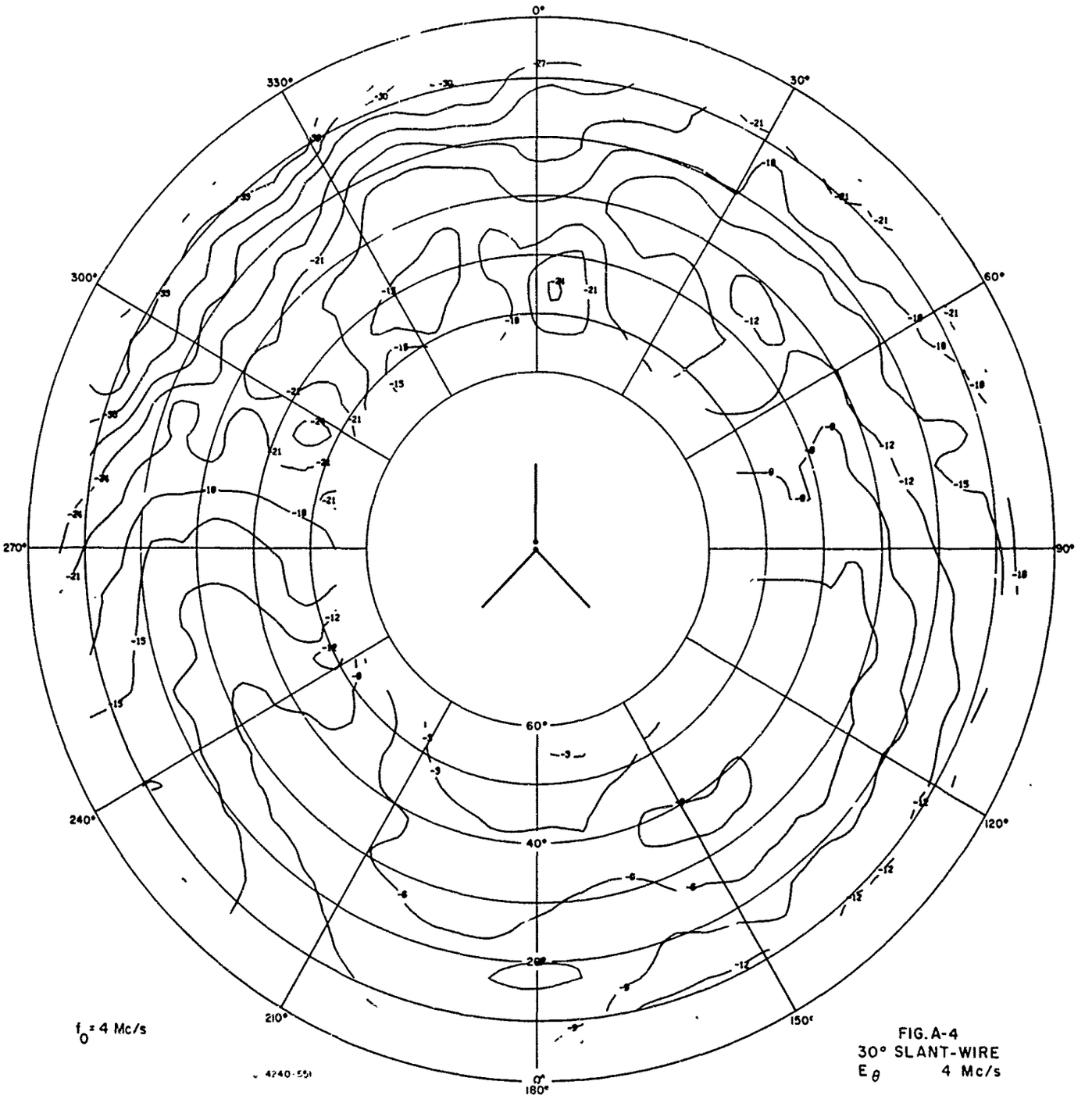

FIG. A-4
30° SLANT-WIRE
E_θ 4 Mc/s

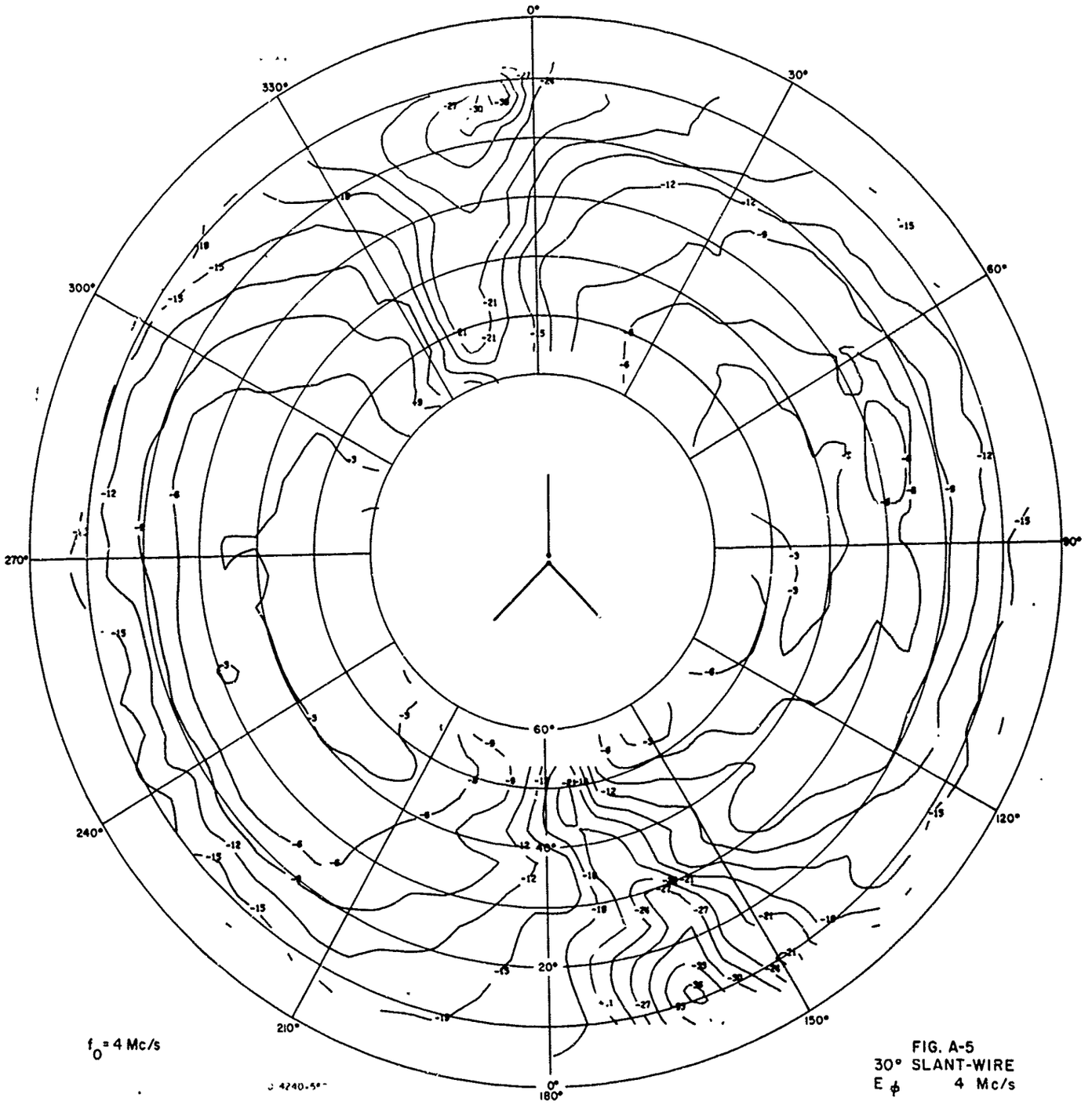

f_0 = 4 Mc/s

FIG. A-5
30° SLANT-WIRE
E_ϕ 4 Mc/s

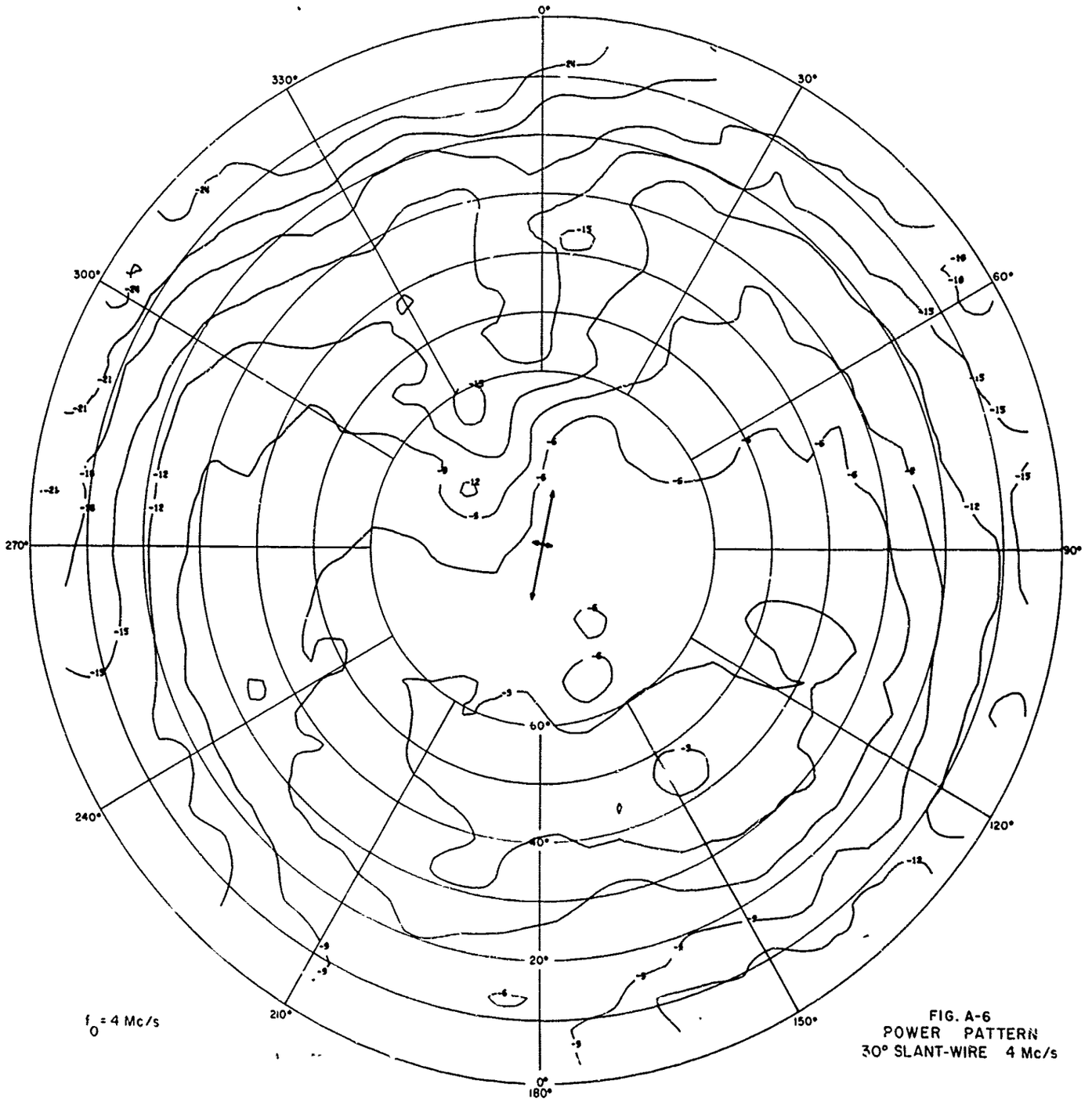

f_0 = 4 Mc/s

FIG. A-6
POWER PATTERN
30° SLANT-WIRE 4 Mc/s

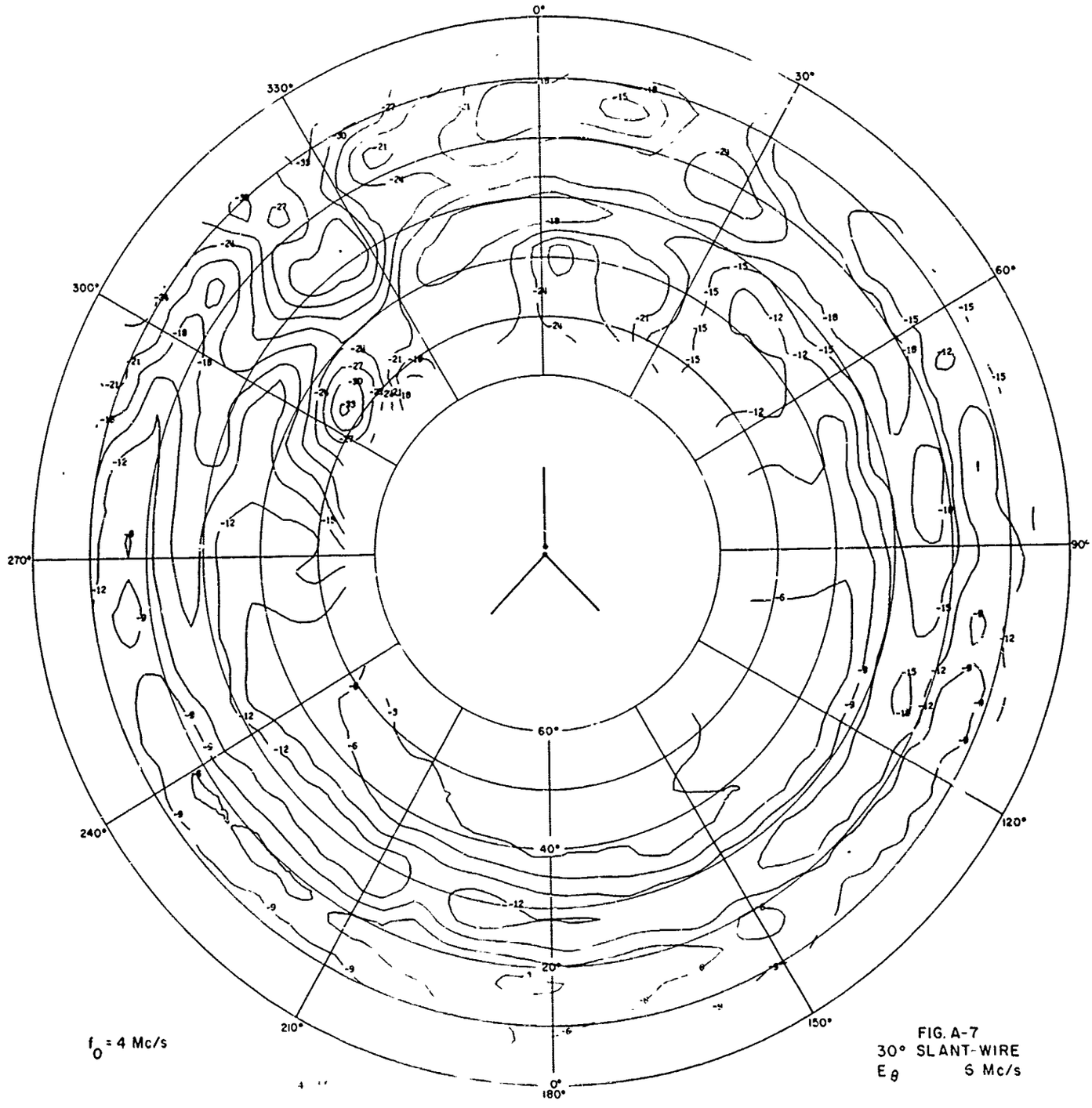

f_0 = 4 Mc/s

FIG. A-7
30° SLANT-WIRE
E_θ 5 Mc/s

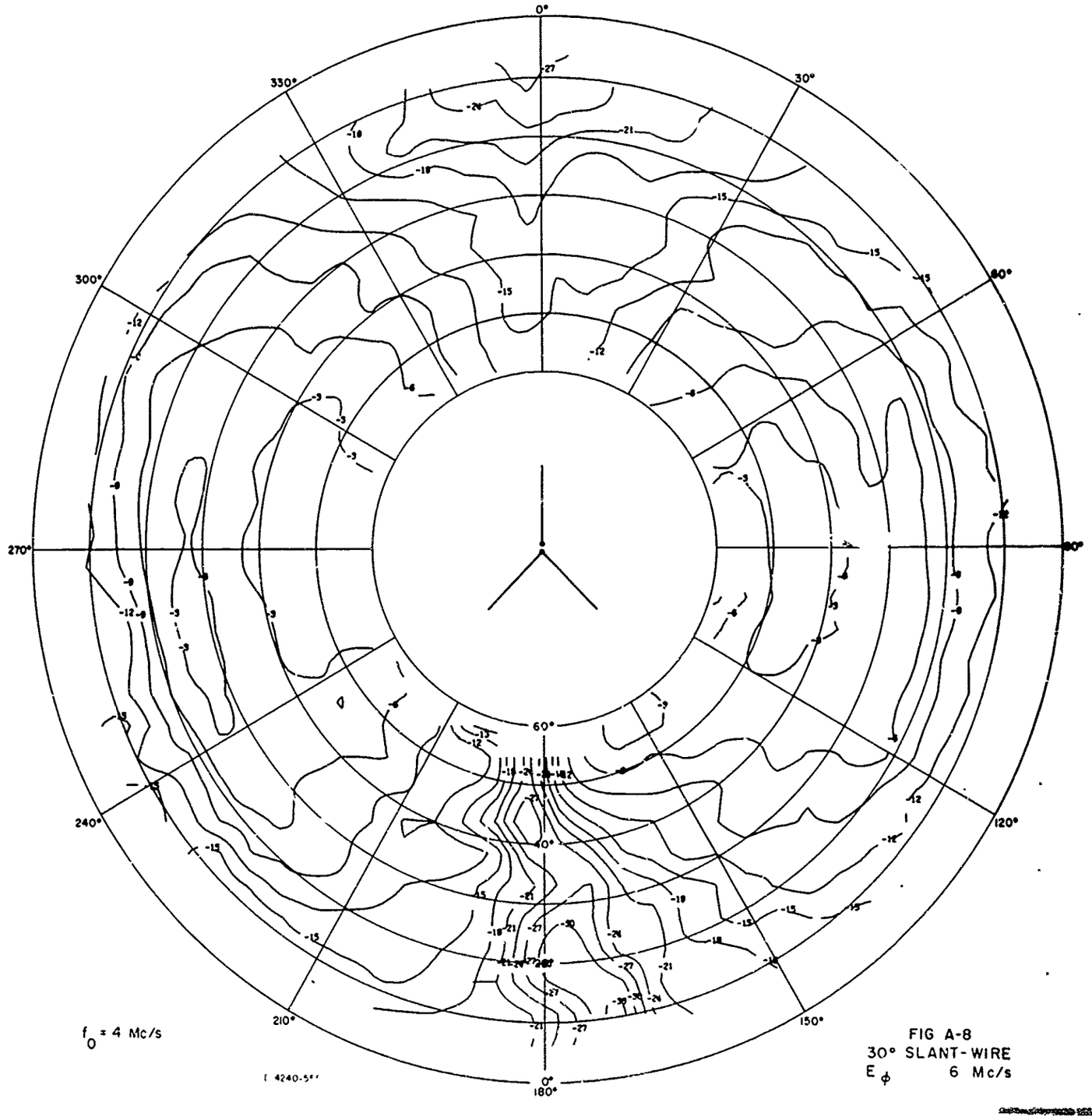

FIG A-8
30° SLANT-WIRE
E_ϕ 6 Mc/s

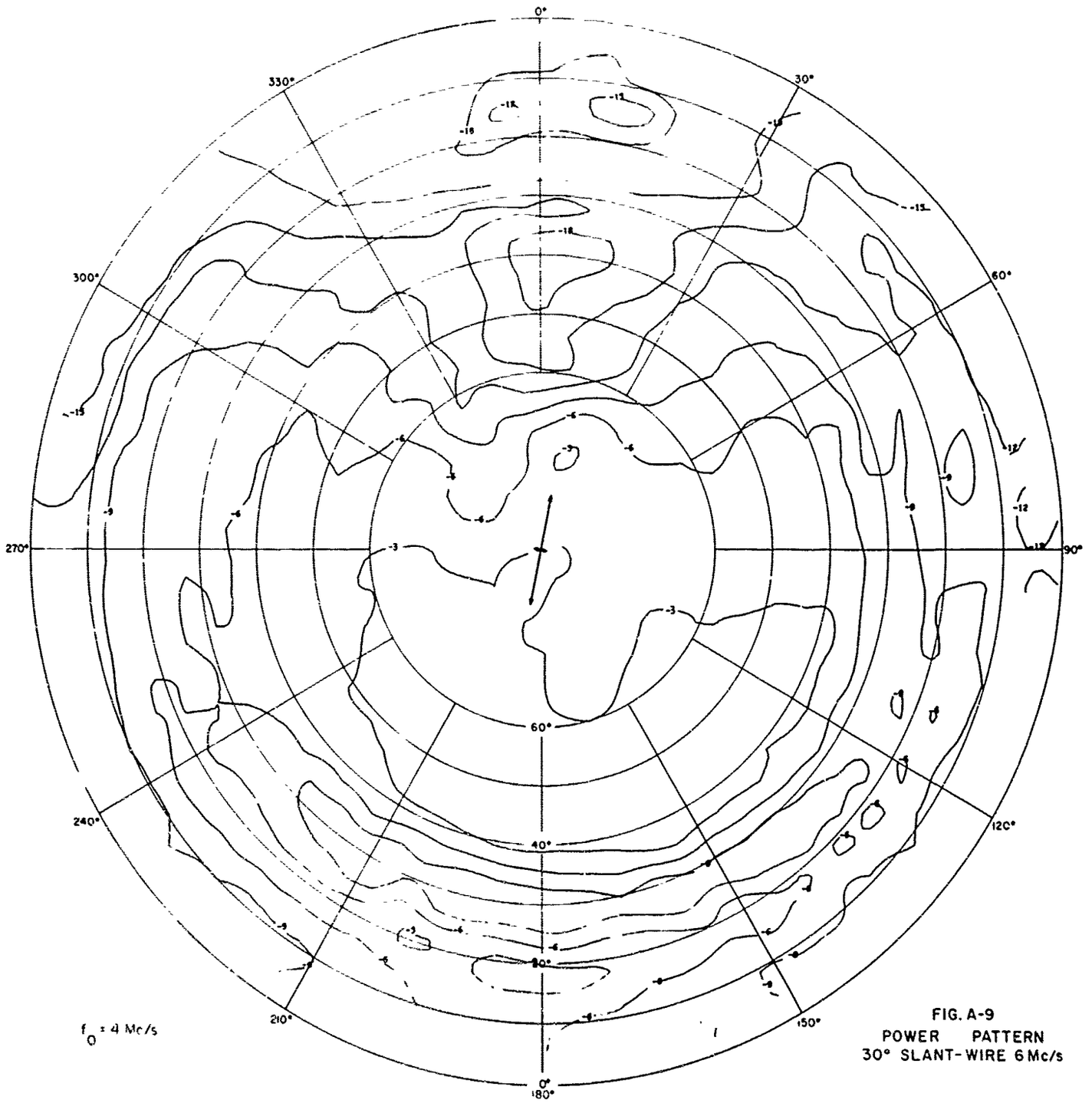

f_0 = 4 Mc/s

FIG. A-9
POWER PATTERN
30° SLANT-WIRE 6 Mc/s

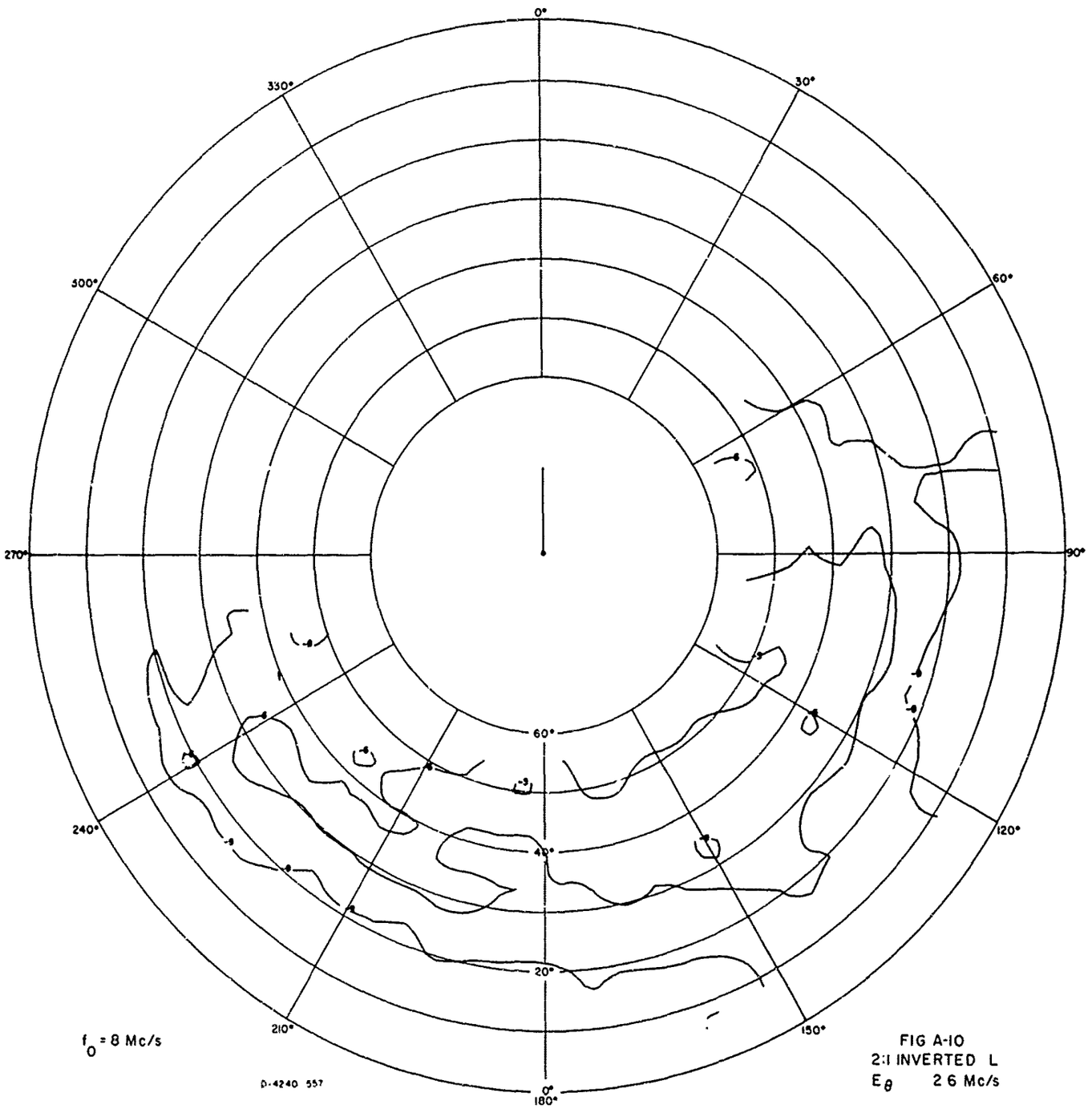

f_0 = 8 Mc/s

FIG A-10
2:1 INVERTED L
E_θ 2 6 Mc/s

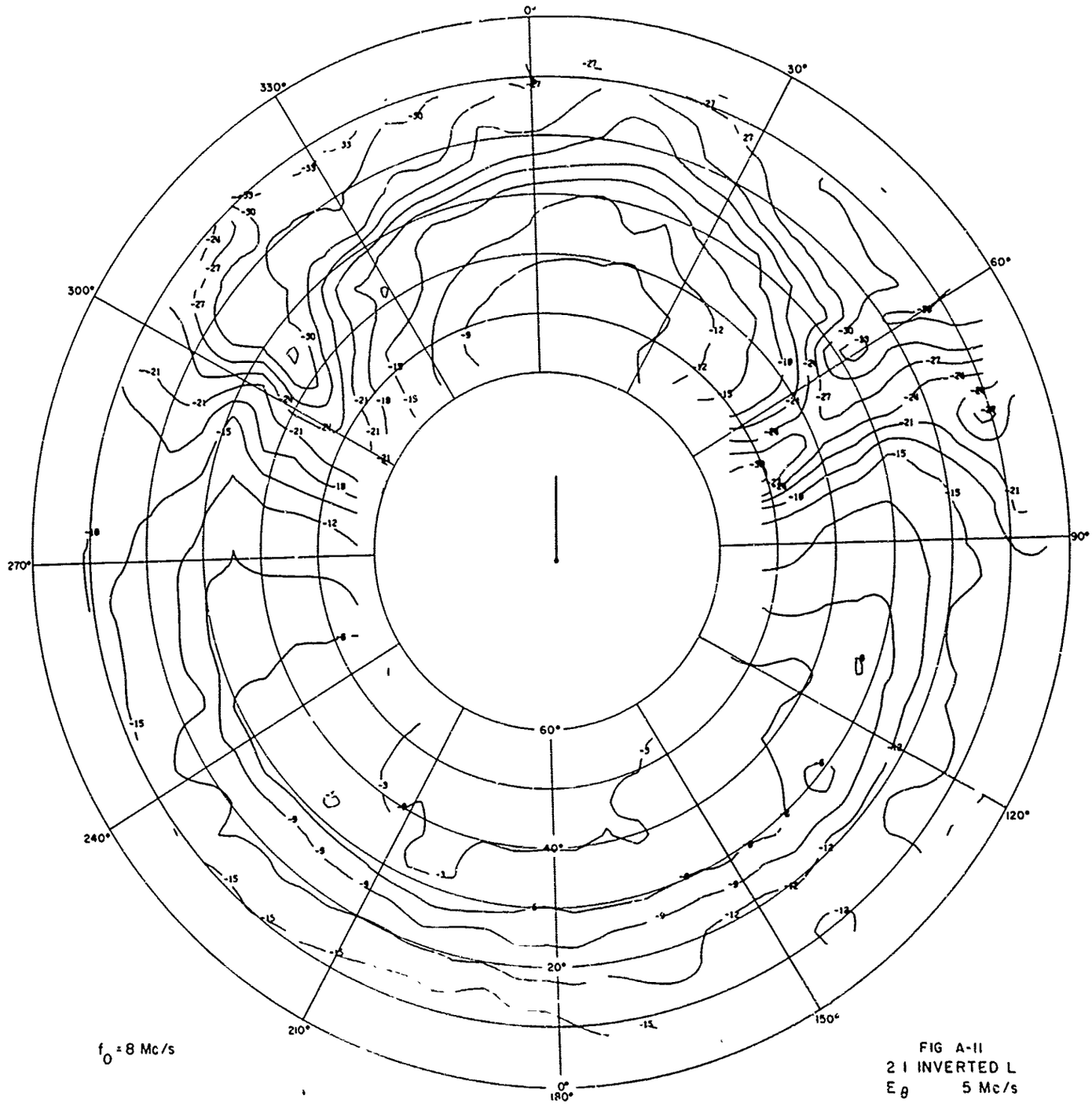

f_0 = 8 Mc/s

FIG A-11
2 I INVERTED L
E_θ 5 Mc/s

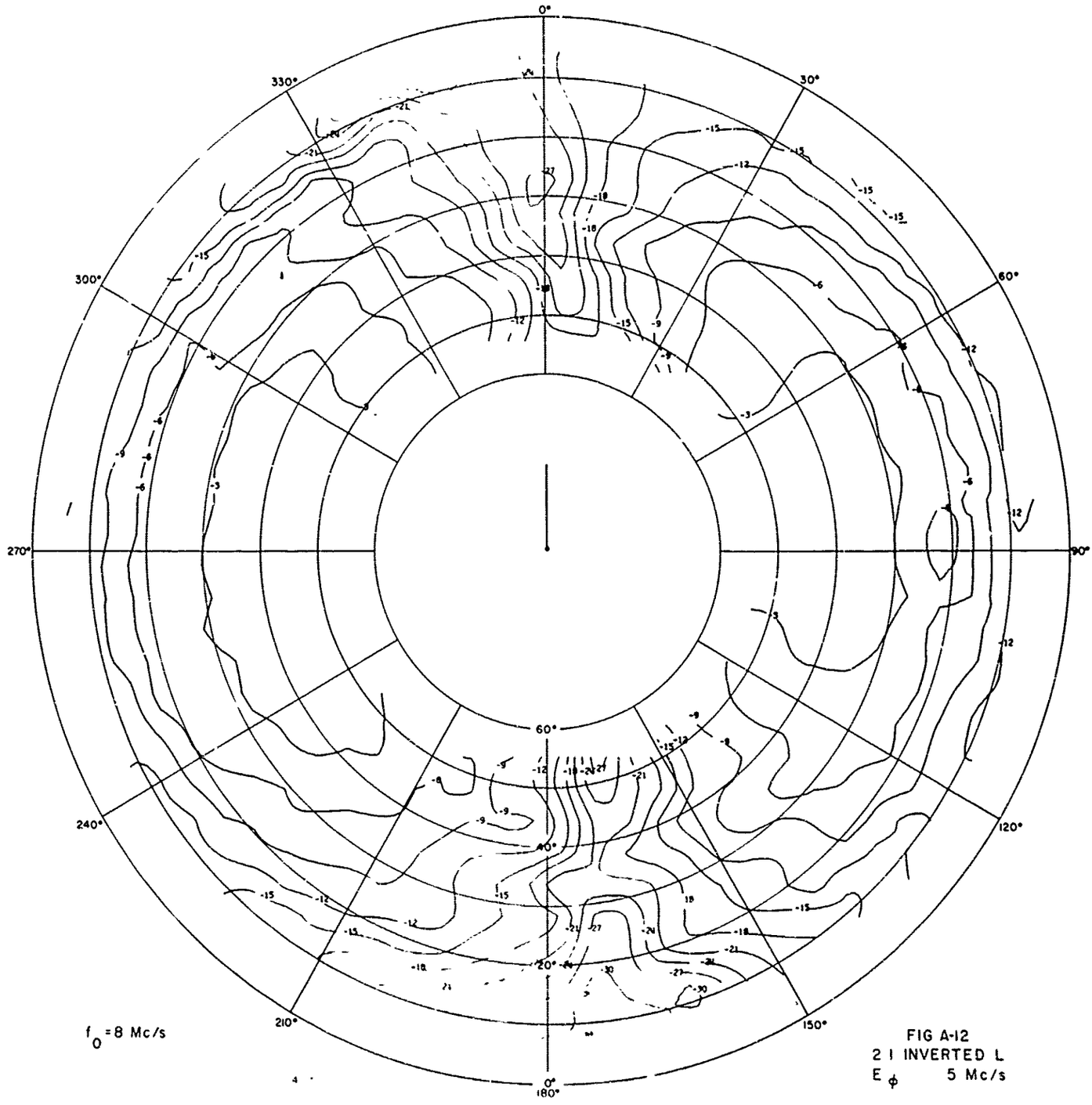

f_0 = 8 Mc/s

FIG A-12
2 I INVERTED L
E_ϕ 5 Mc/s

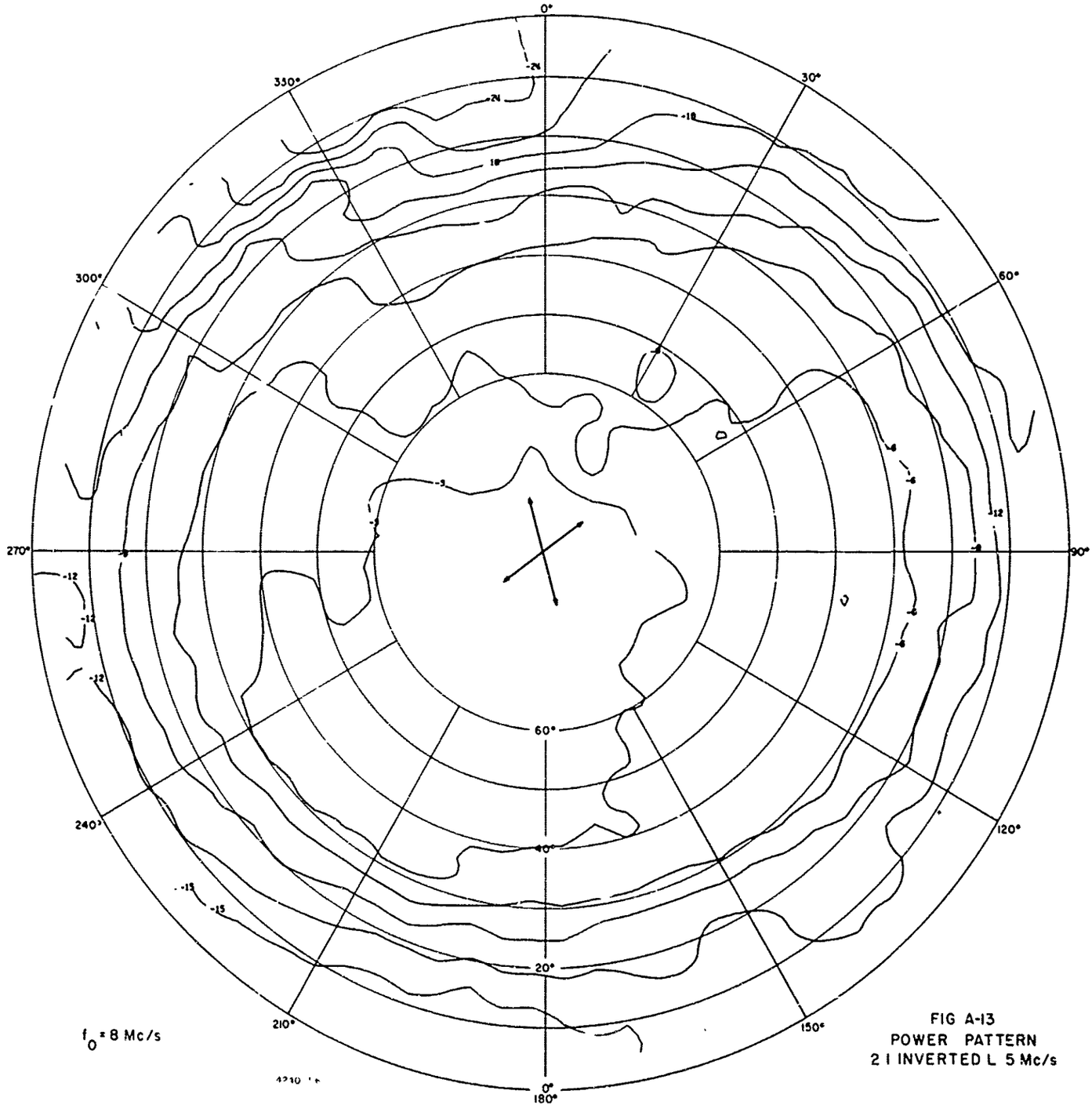

f_0 = 8 Mc/s

FIG A-13
POWER PATTERN
2 I INVERTED L 5 Mc/s

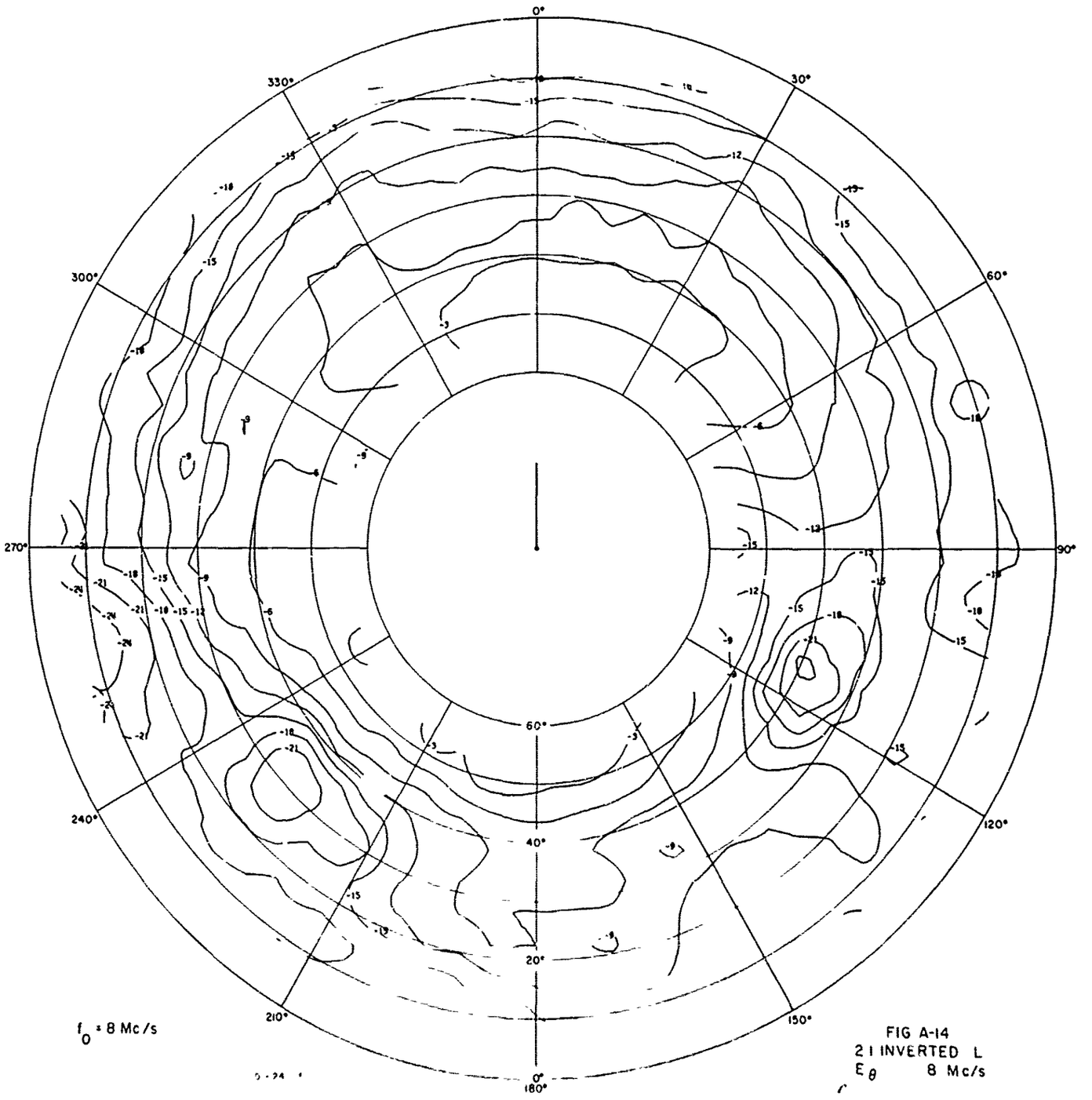

f_0 = 8 Mc/s

FIG A-14
21 INVERTED L
E_θ 8 Mc/s

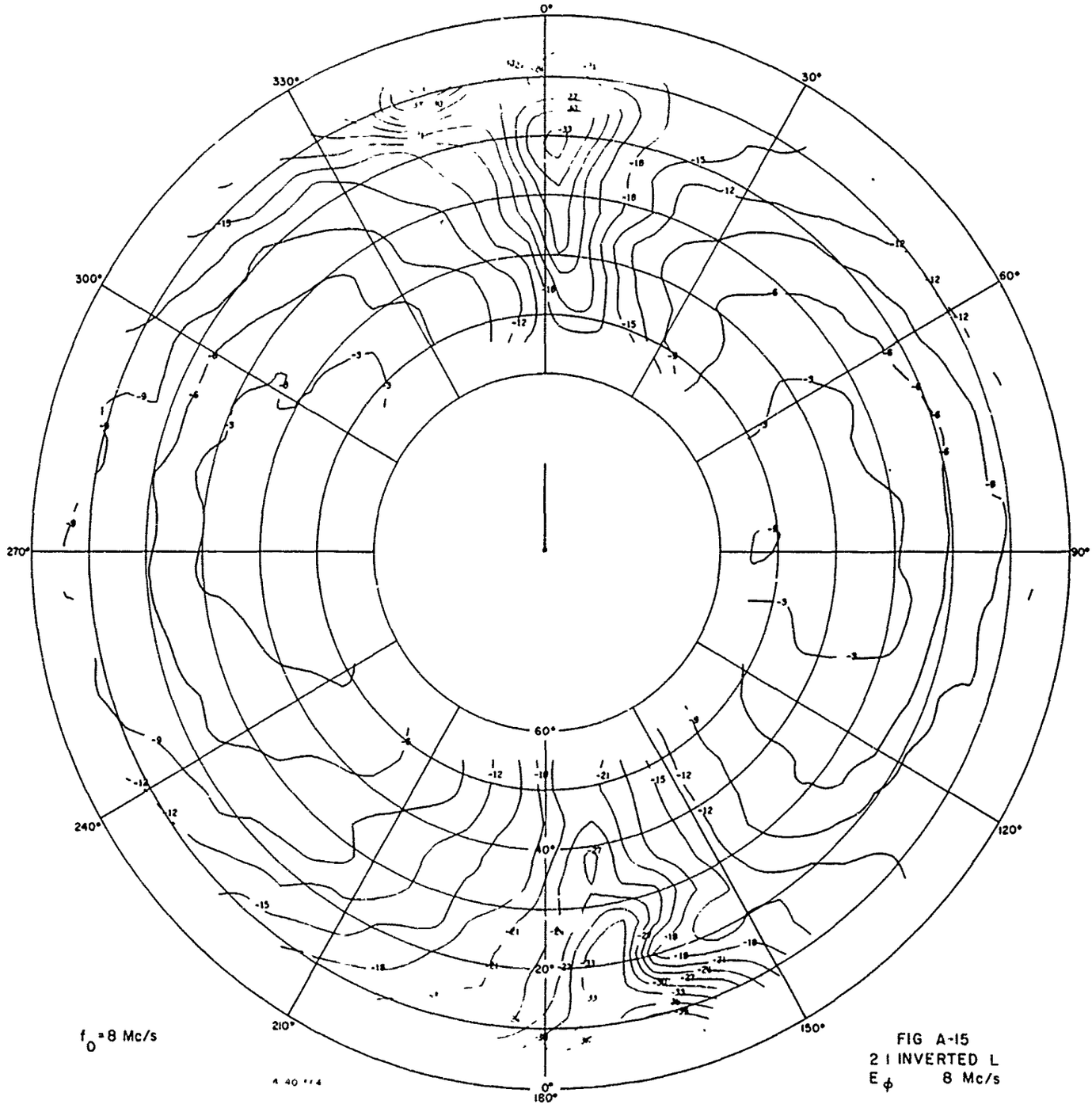

f_0 = 8 Mc/s

FIG A-15
2 I INVERTED L
E_ϕ 8 Mc/s

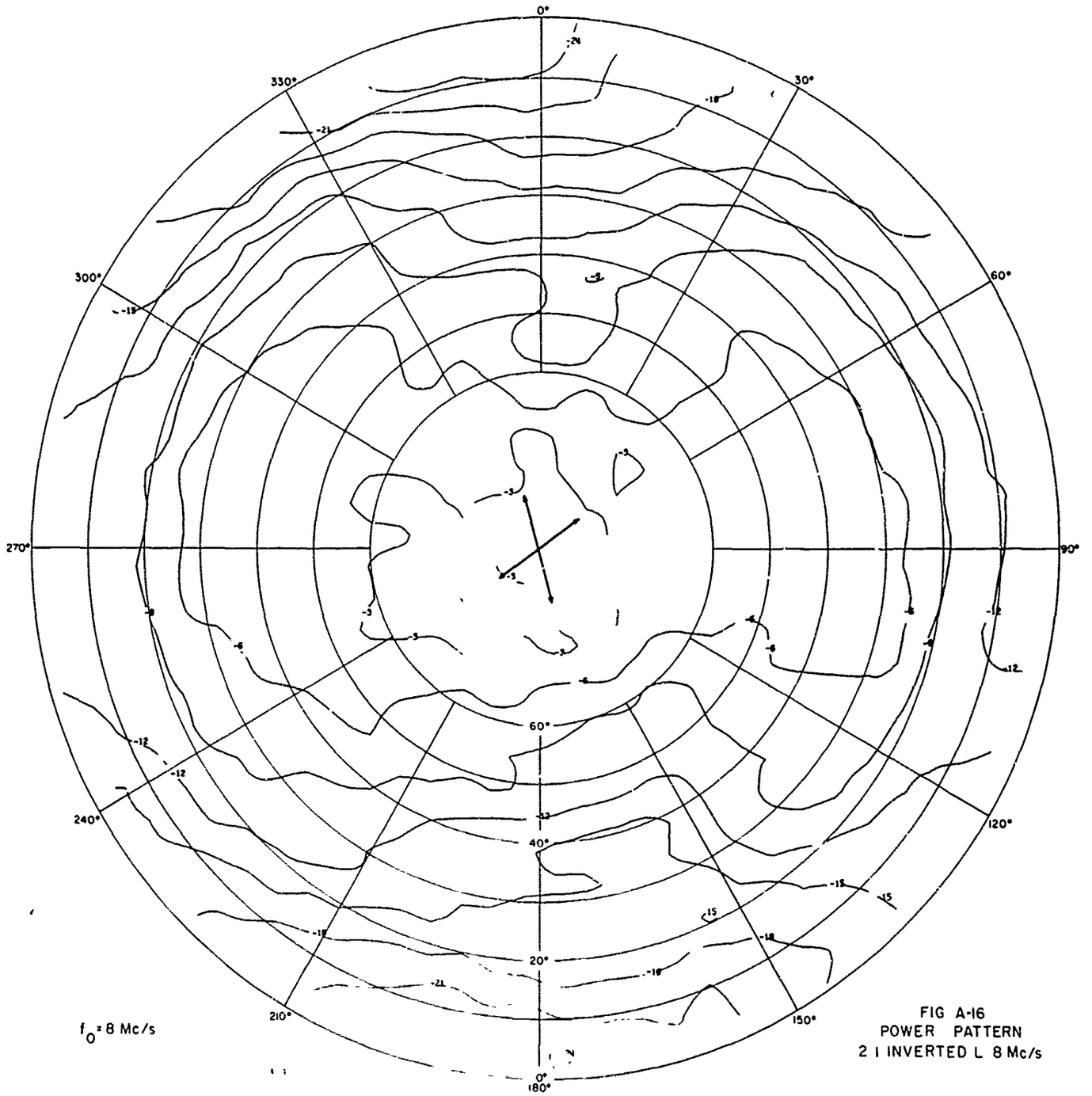

FIG A-16
POWER PATTERN
2 I INVERTED L 8 Mc/s

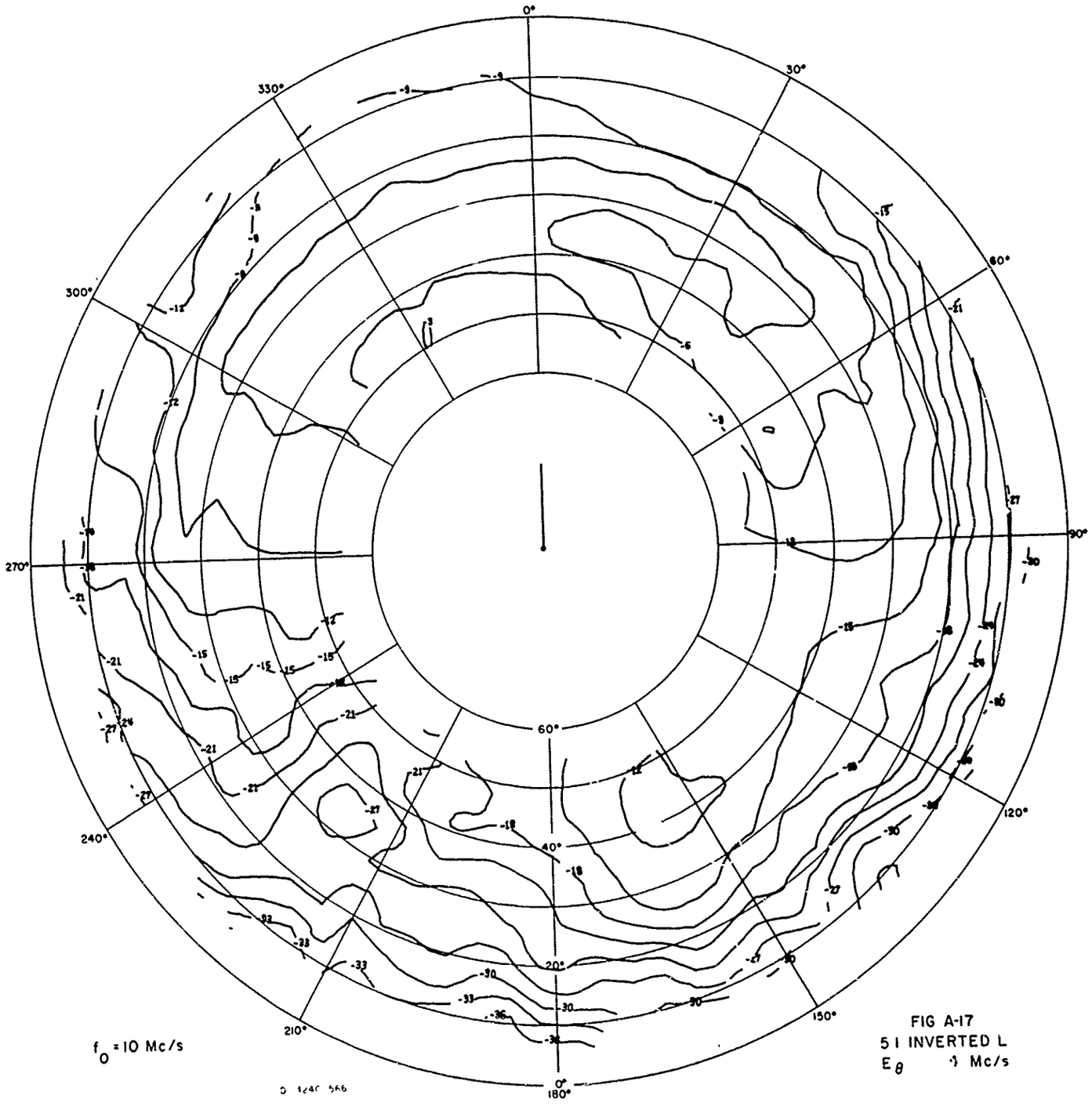

f_0 = 10 Mc/s

FIG A-17
5 I INVERTED L
E_θ 1 Mc/s

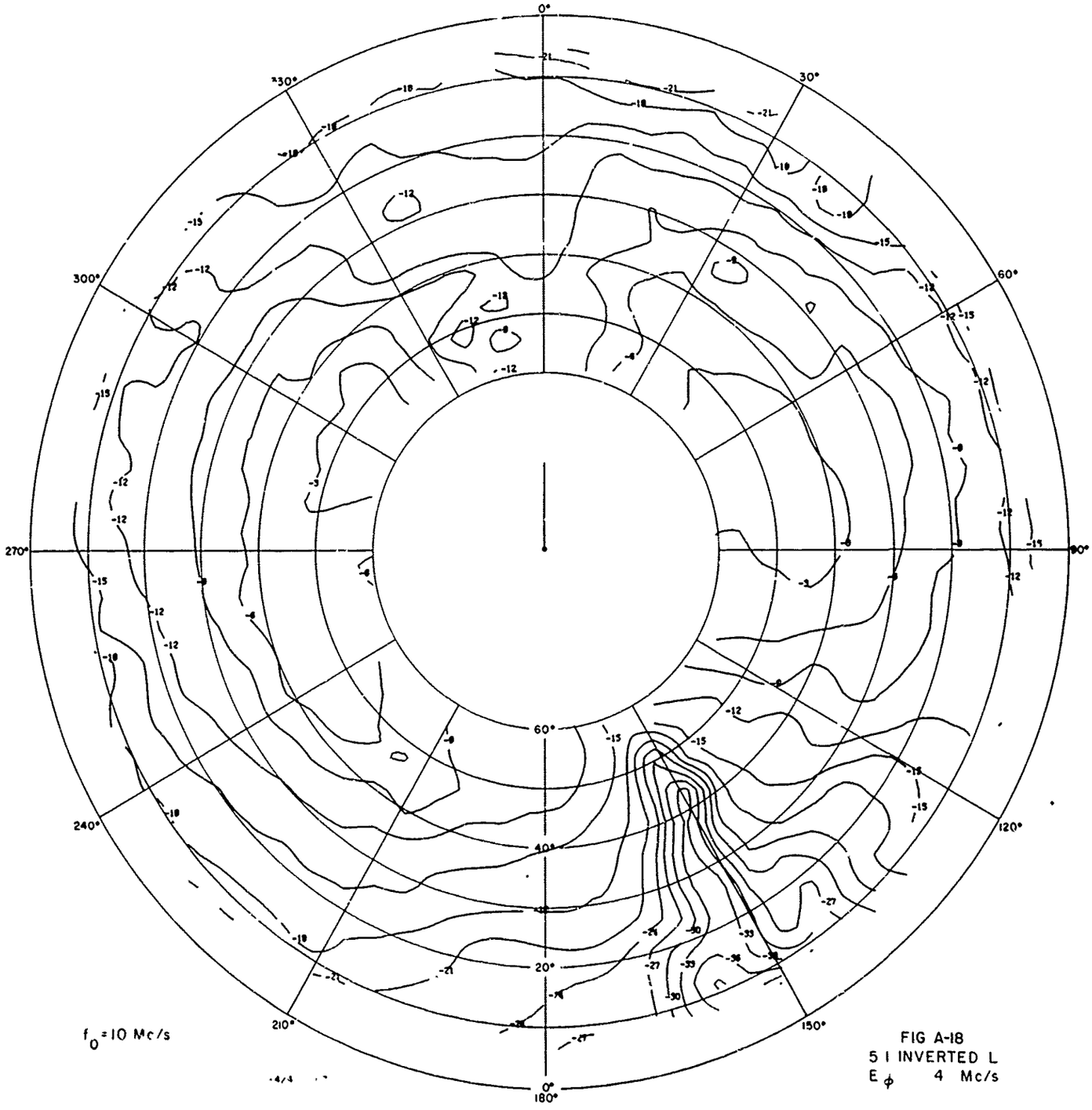

f_0 = 10 Mc/s

FIG A-18
5 I INVERTED L
E_ϕ 4 Mc/s

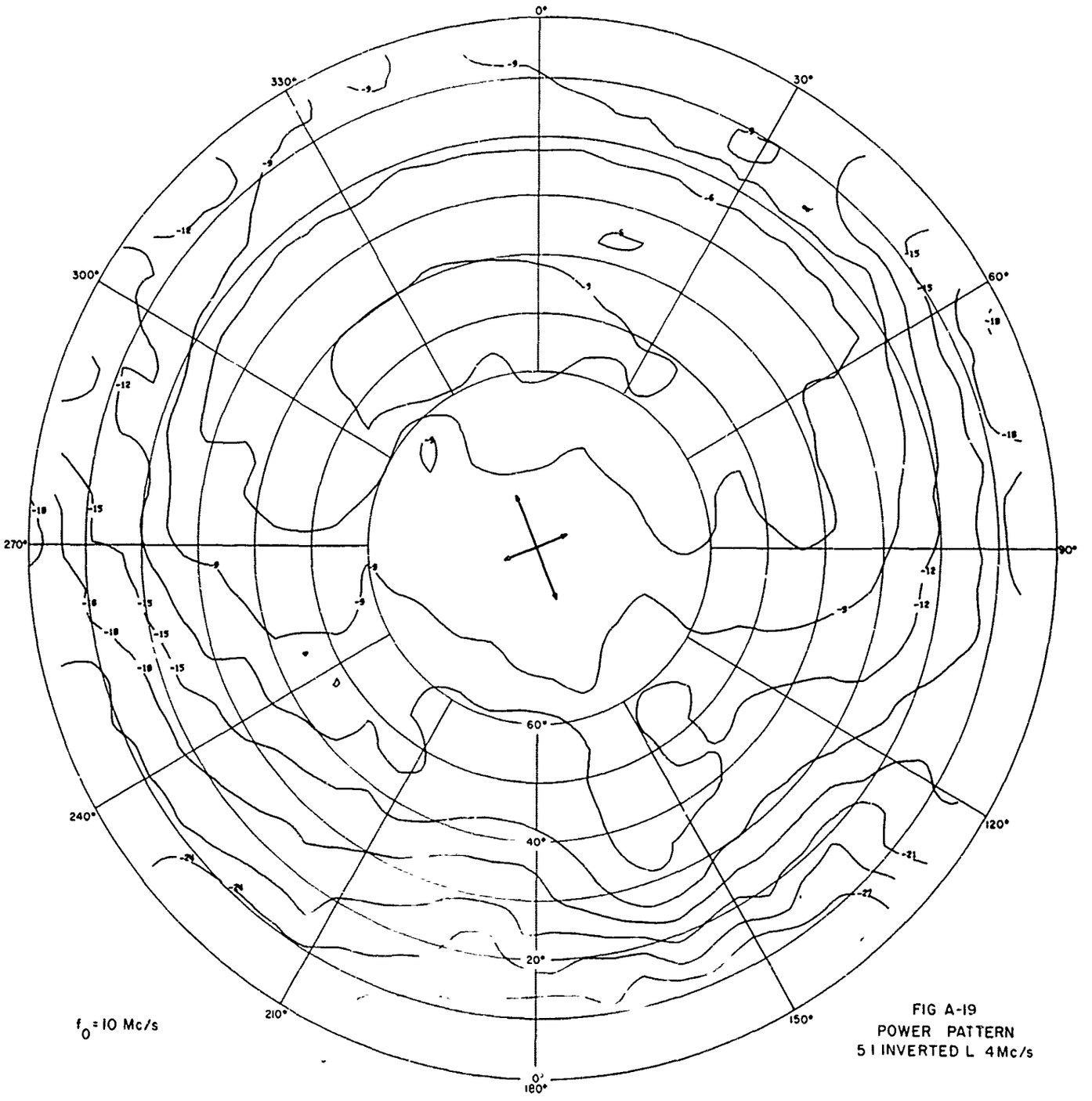

f_0 = 10 Mc/s

FIG A-19
POWER PATTERN
5 I INVERTED L 4 Mc/s

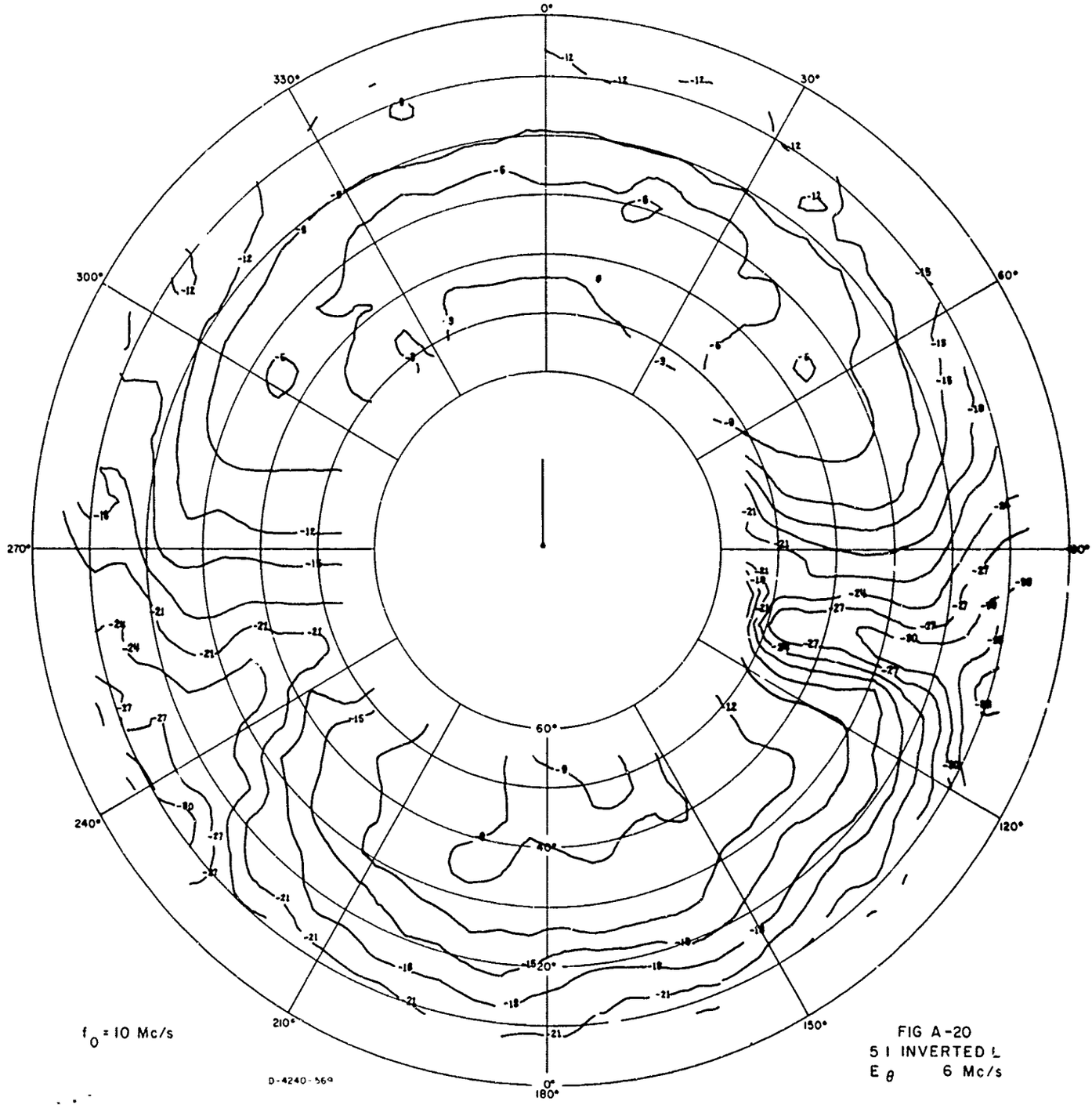

FIG A-20
51 INVERTED L
E_θ 6 Mc/s

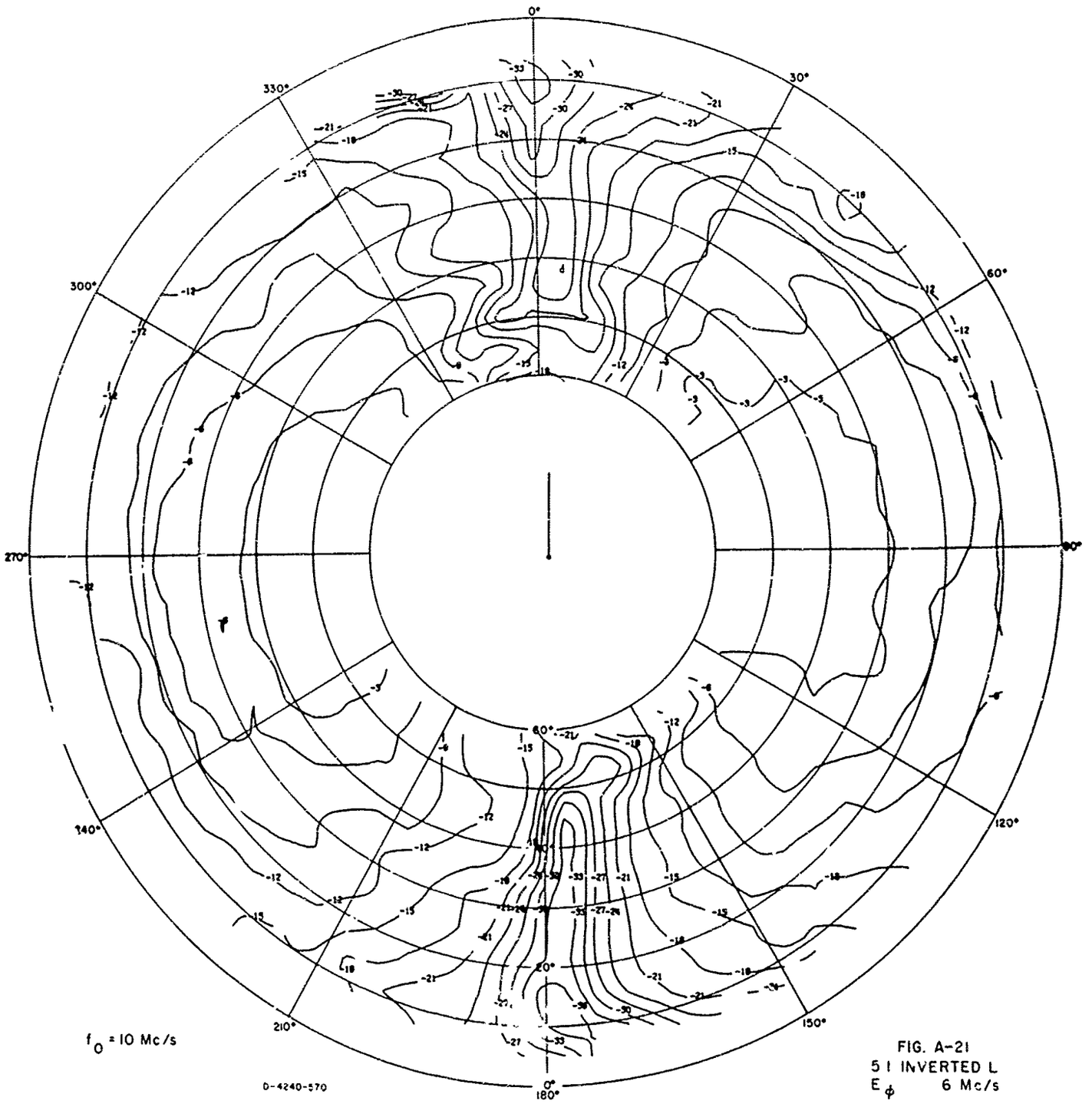

FIG. A-21
51 INVERTED L
E_ϕ 6 Mc/s

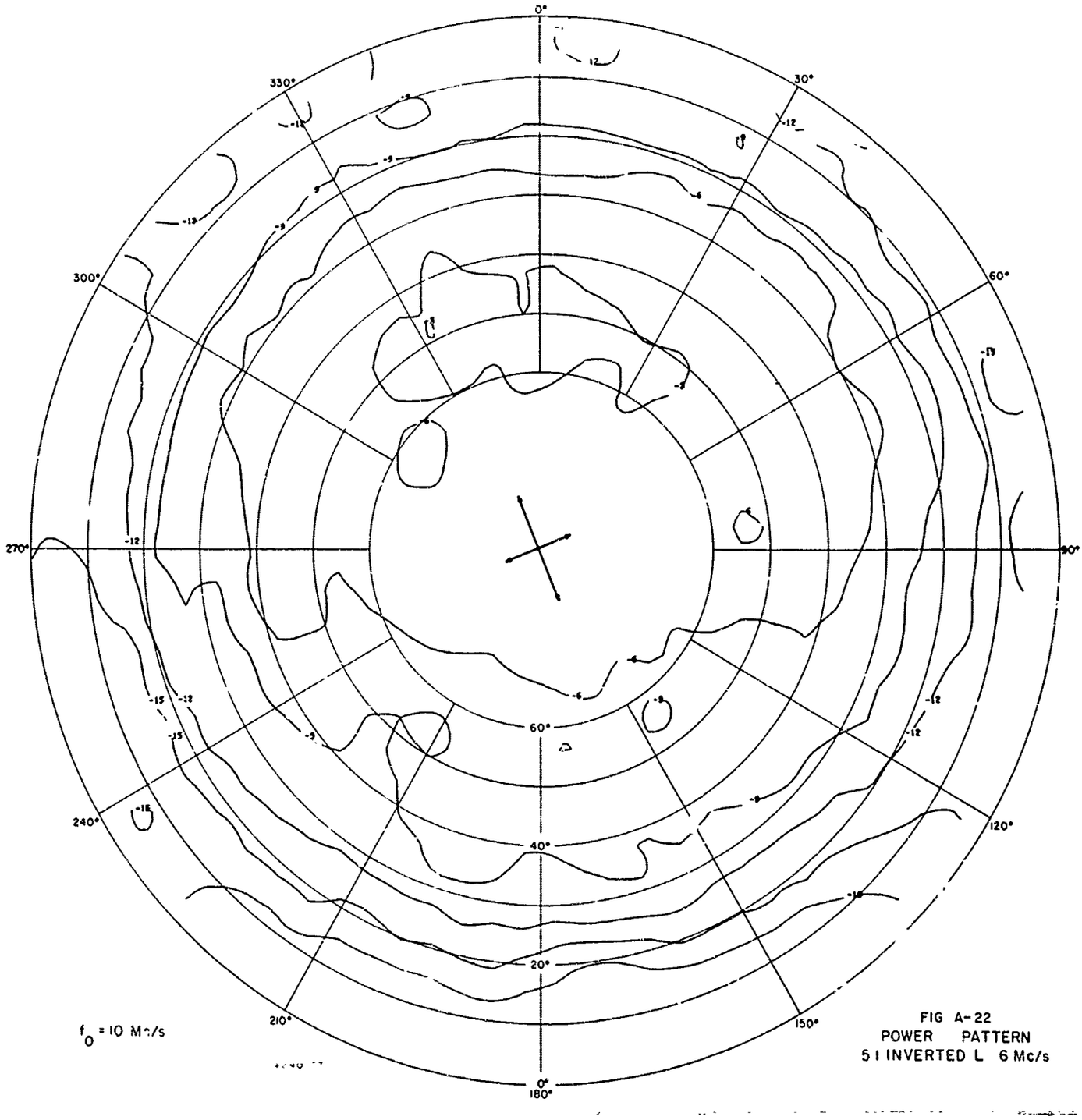

f_0 = 10 Mc/s

FIG A-22
POWER PATTERN
51 INVERTED L 6 Mc/s

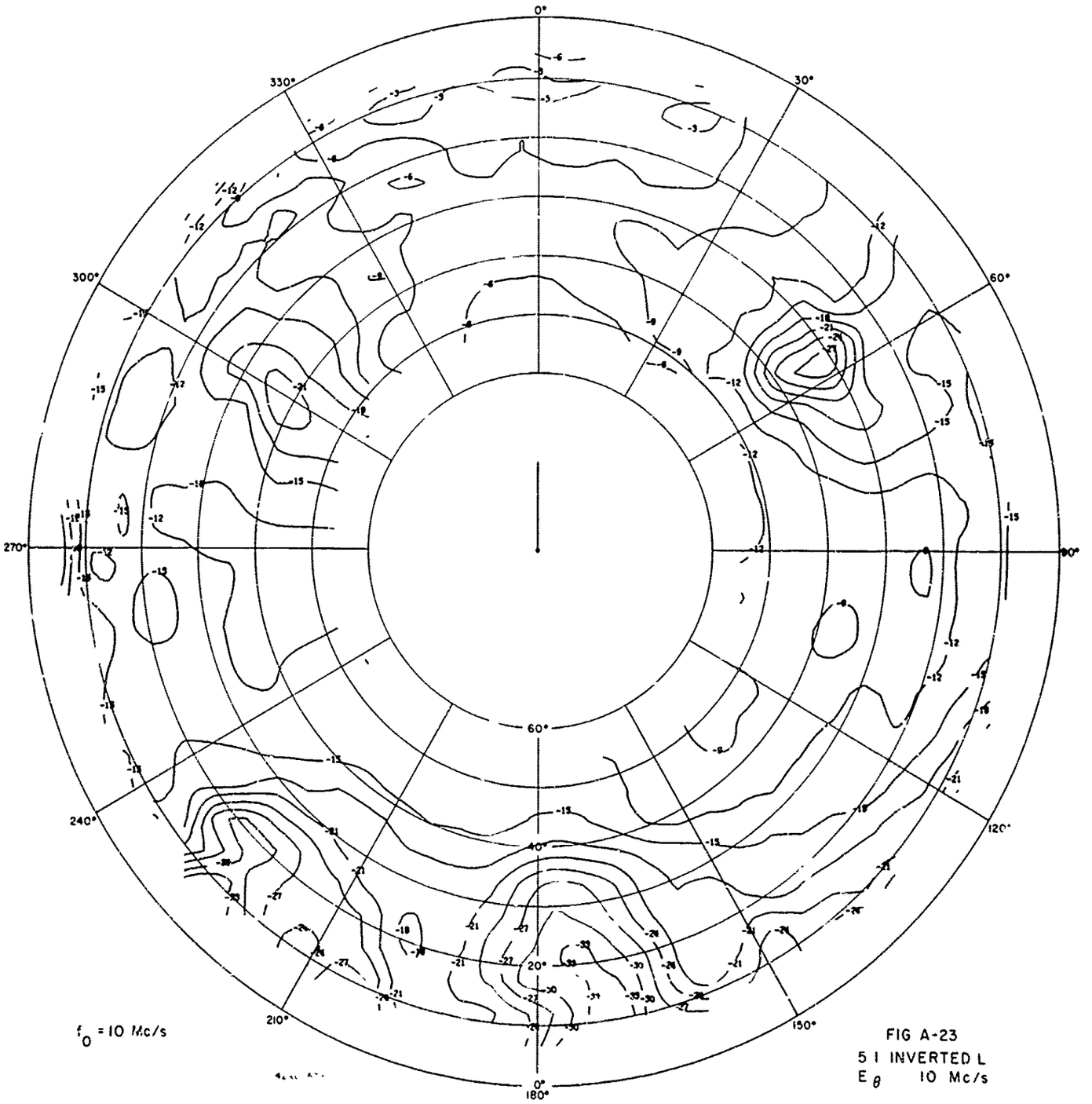

FIG A-23
5 I INVERTED L
E_θ 10 Mc/s

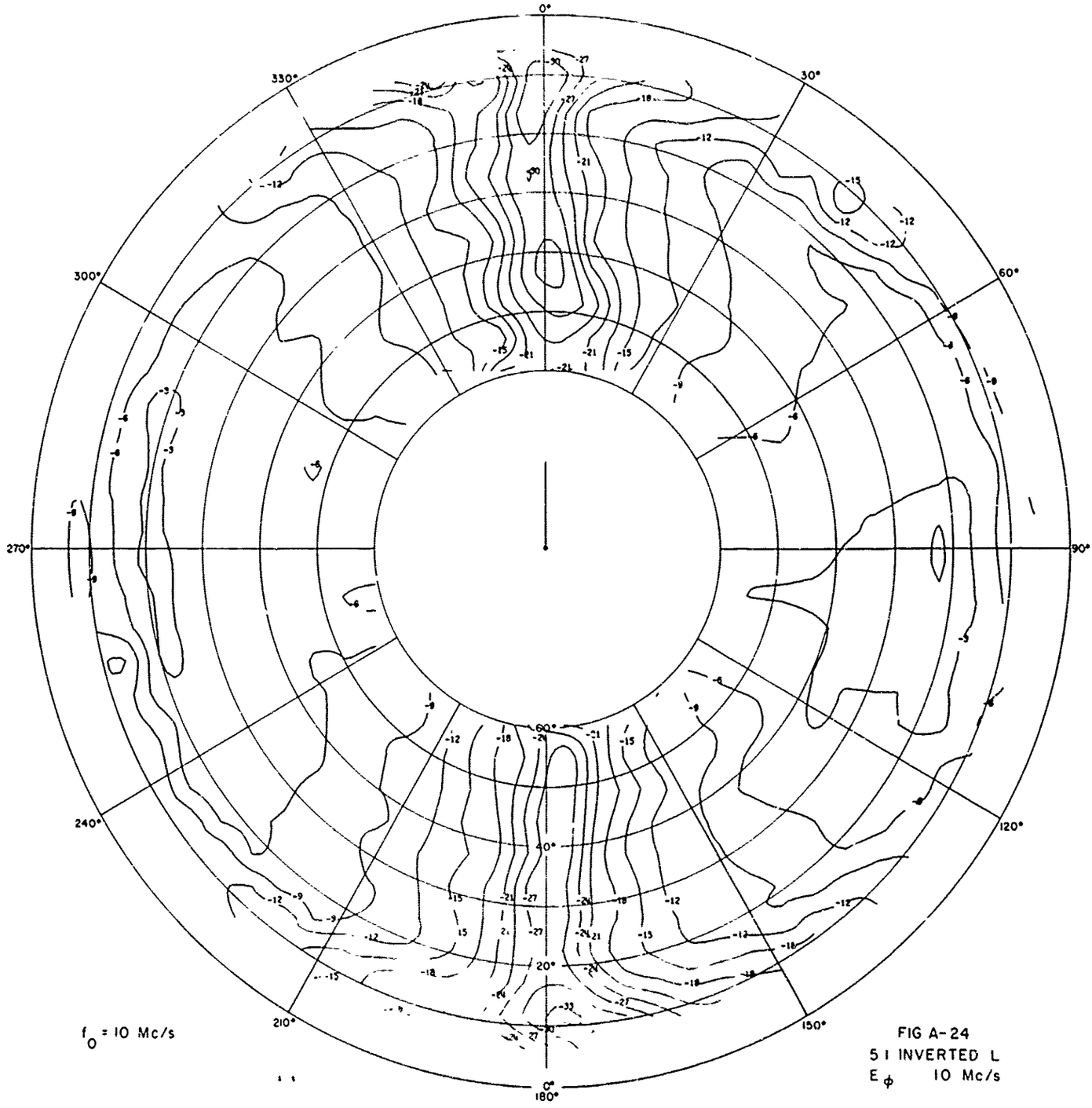

f_0 = 10 Mc/s

FIG A-24
5 I INVERTED L
E_ϕ 10 Mc/s

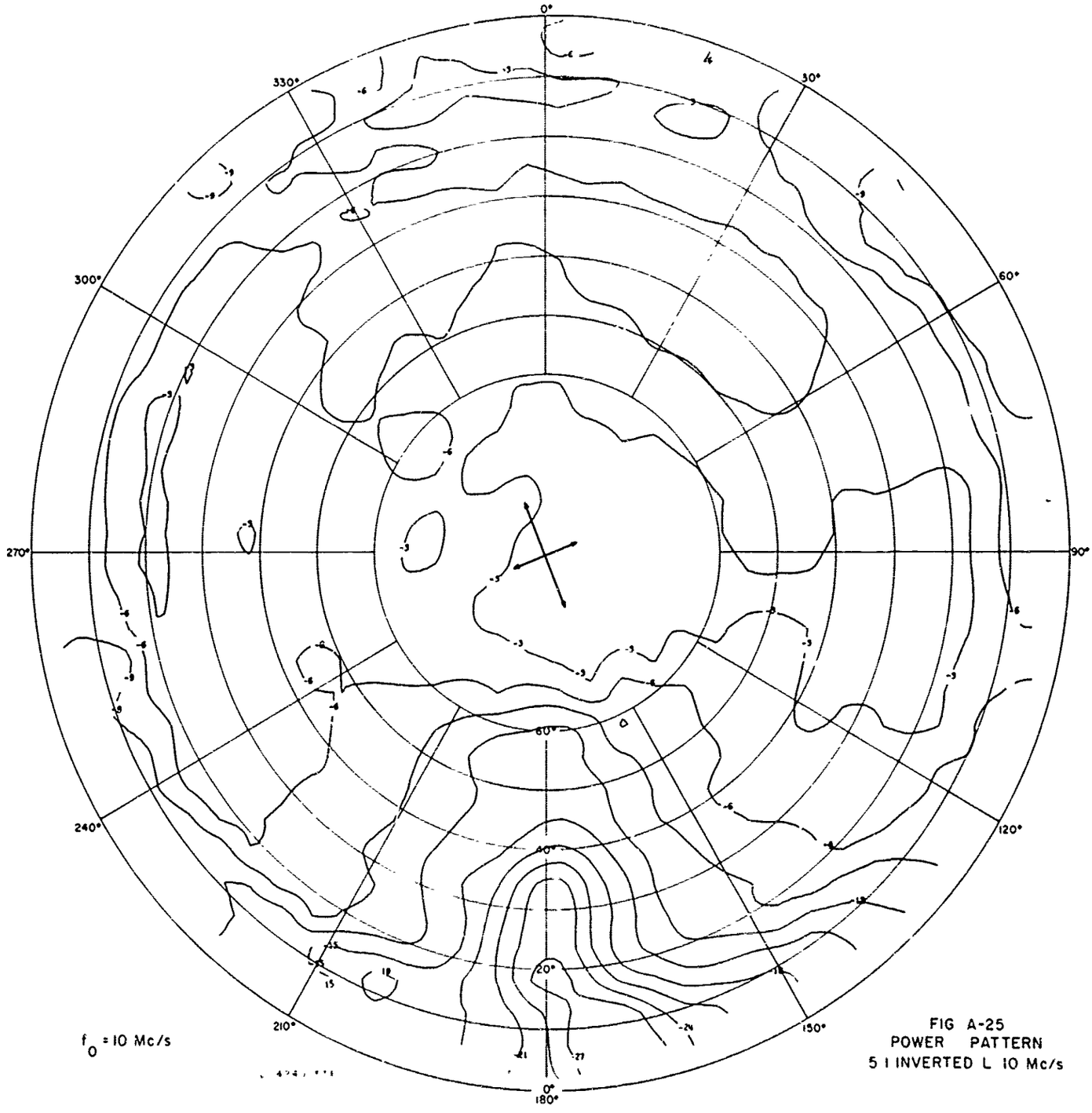

f_0 = 10 Mc/s

FIG A-25
POWER PATTERN
5 I INVERTED L 10 Mc/s

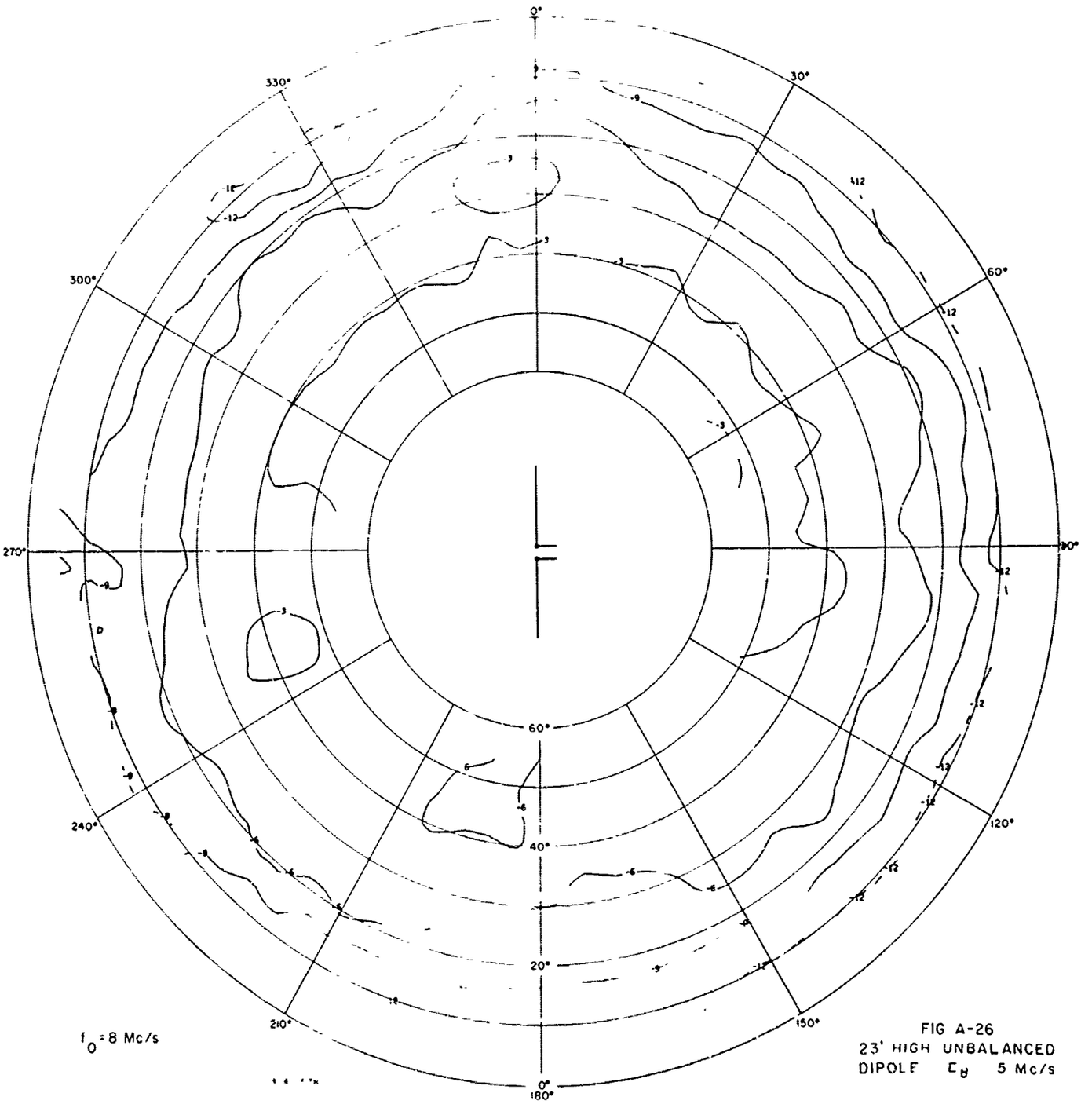

$f_0 = 8$ Mc/s

FIG A-26
23' HIGH UNBALANCED
DIPOLE E_θ 5 Mc/s

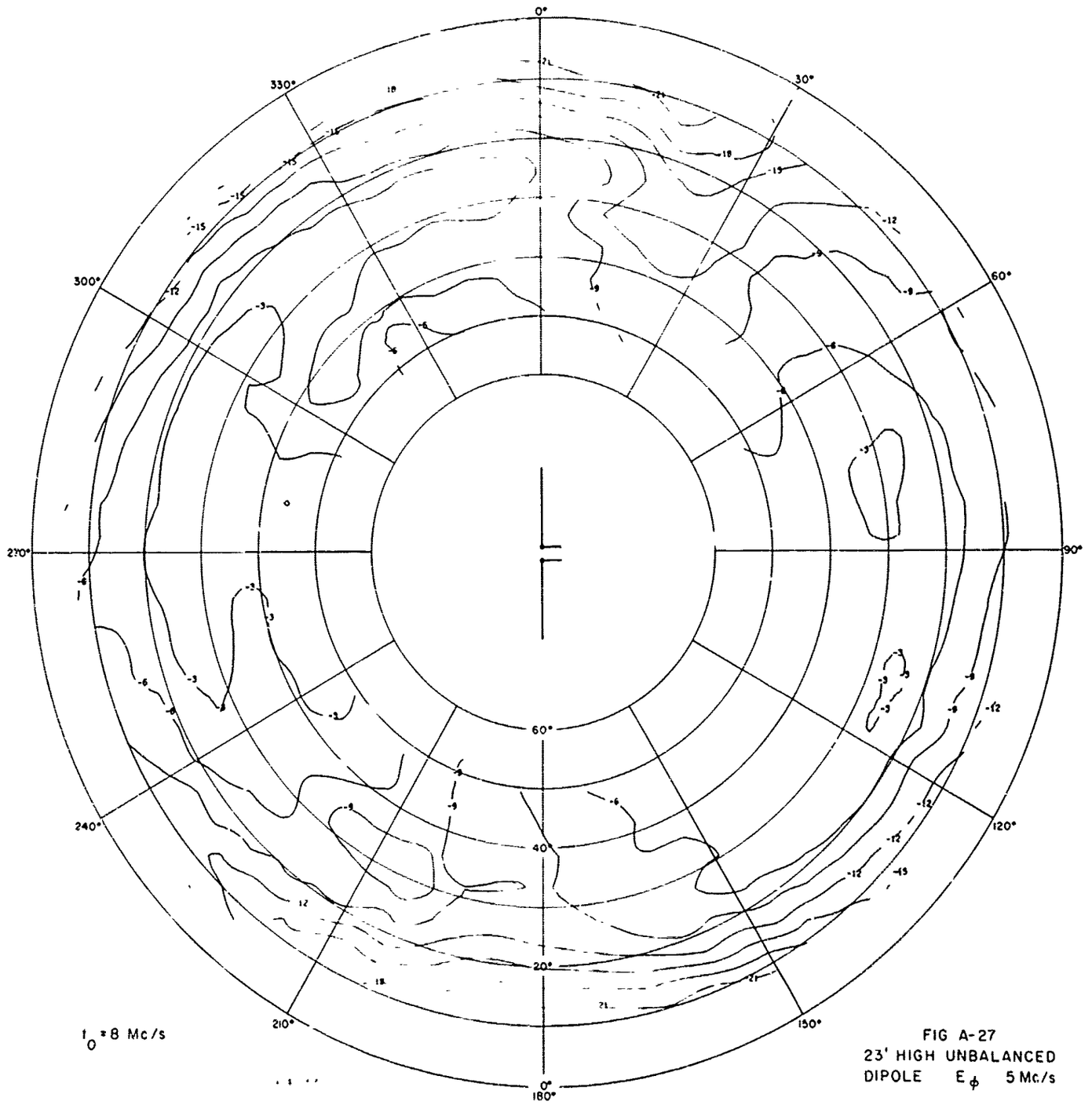

$f_0 = 8$ Mc/s

FIG A-27
23' HIGH UNBALANCED
DIPOLE E_ϕ 5 Mc/s

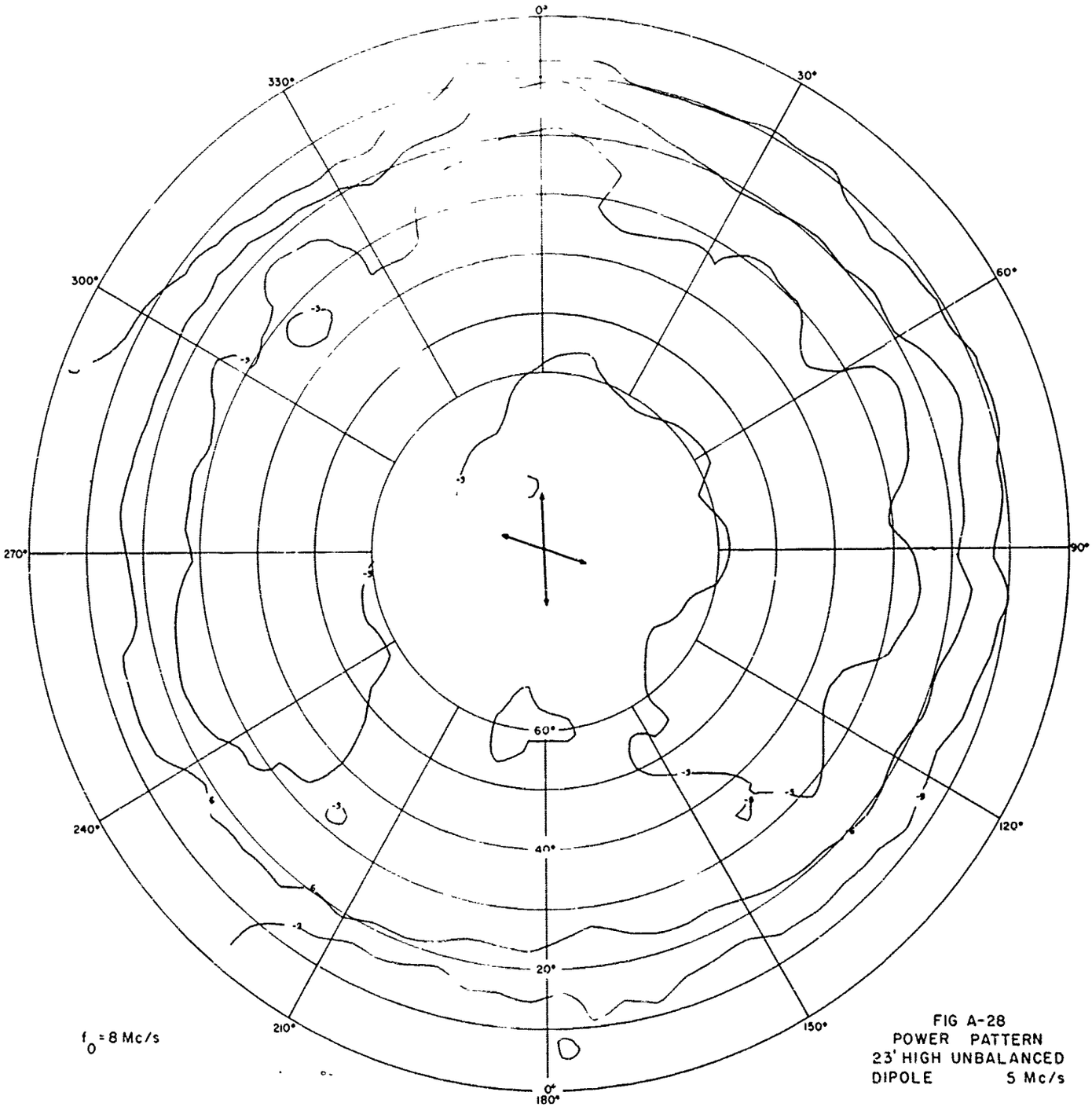

f_0 = 8 Mc/s

FIG A-28
POWER PATTERN
23' HIGH UNBALANCED
DIPOLE 5 Mc/s

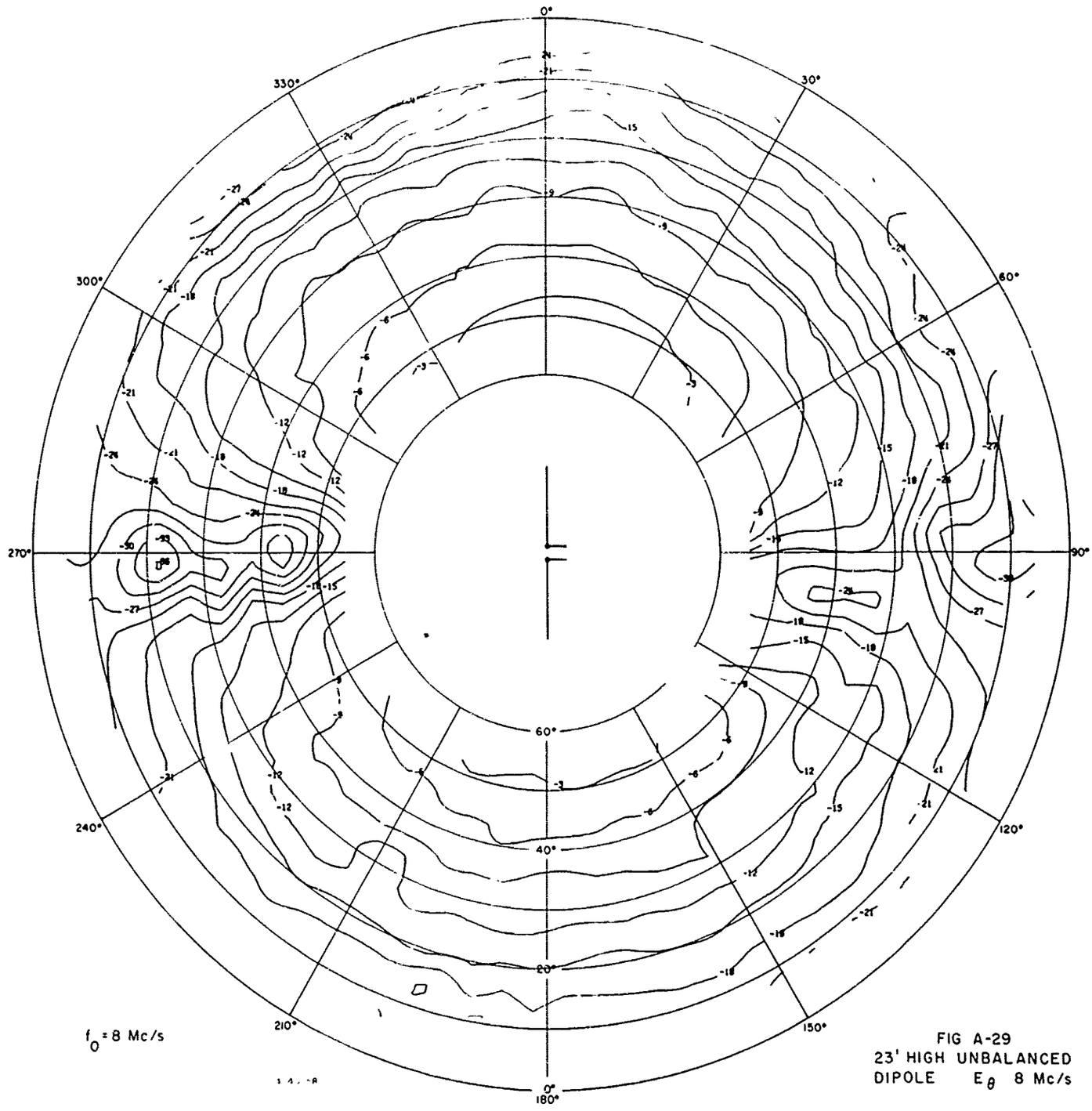

f_0 = 8 Mc/s

FIG A-29
23' HIGH UNBALANCED
DIPOLE E_θ 8 Mc/s

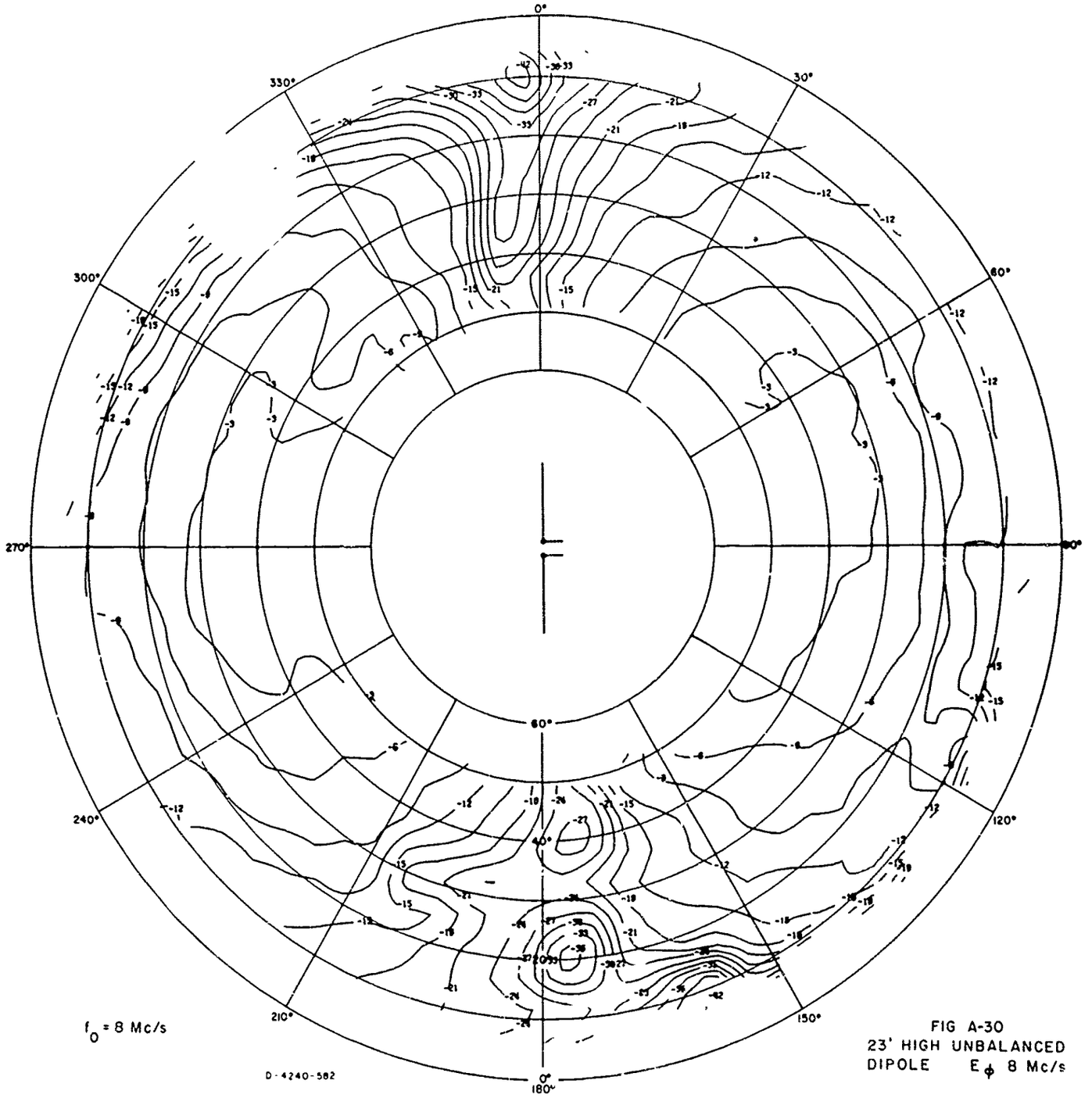

FIG A-30
23' HIGH UNBALANCED
DIPOLE E_ϕ 8 Mc/s

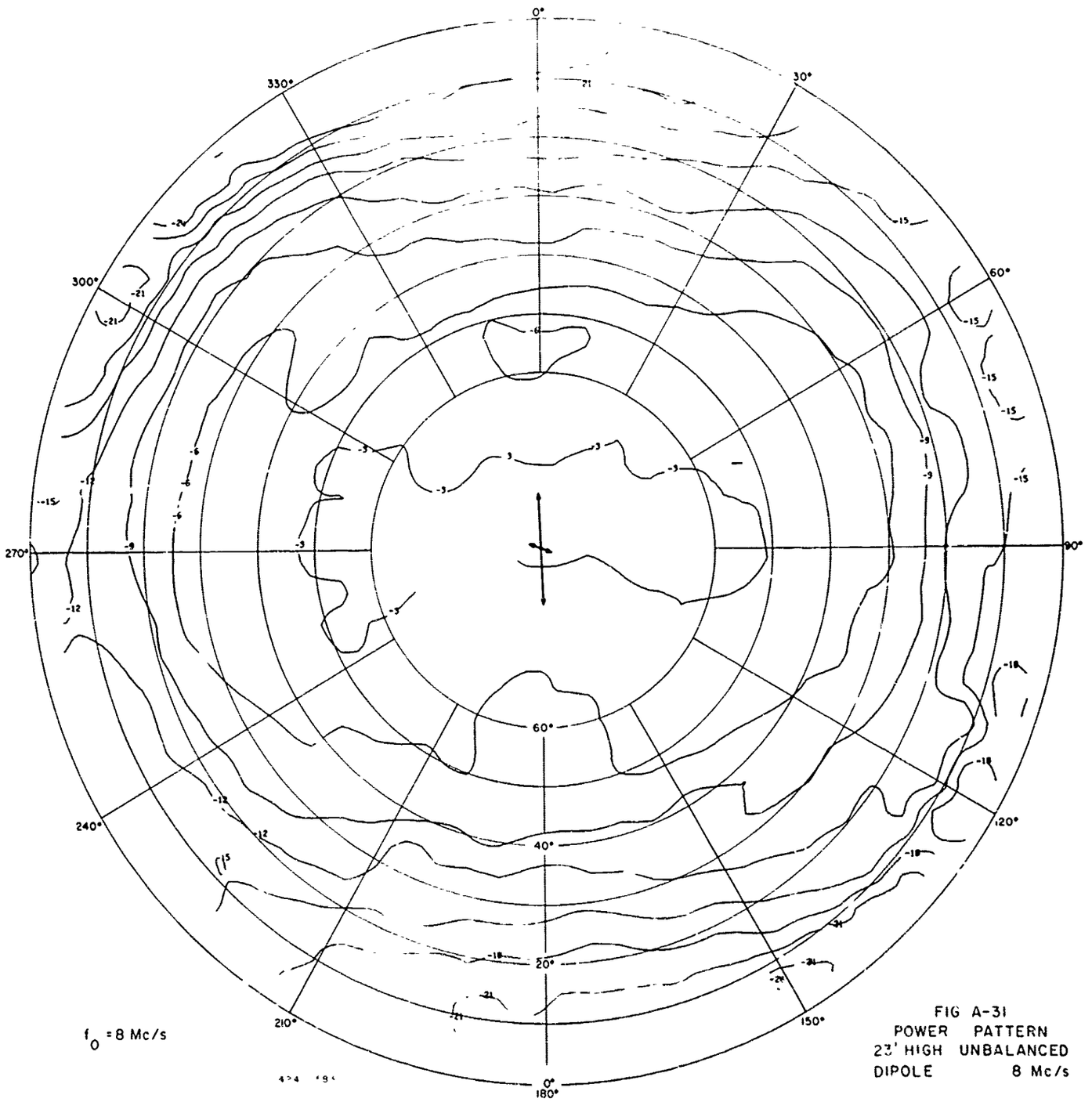

f_0 = 8 Mc/s

FIG A-31
POWER PATTERN
23' HIGH UNBALANCED
DIPOLE 8 Mc/s

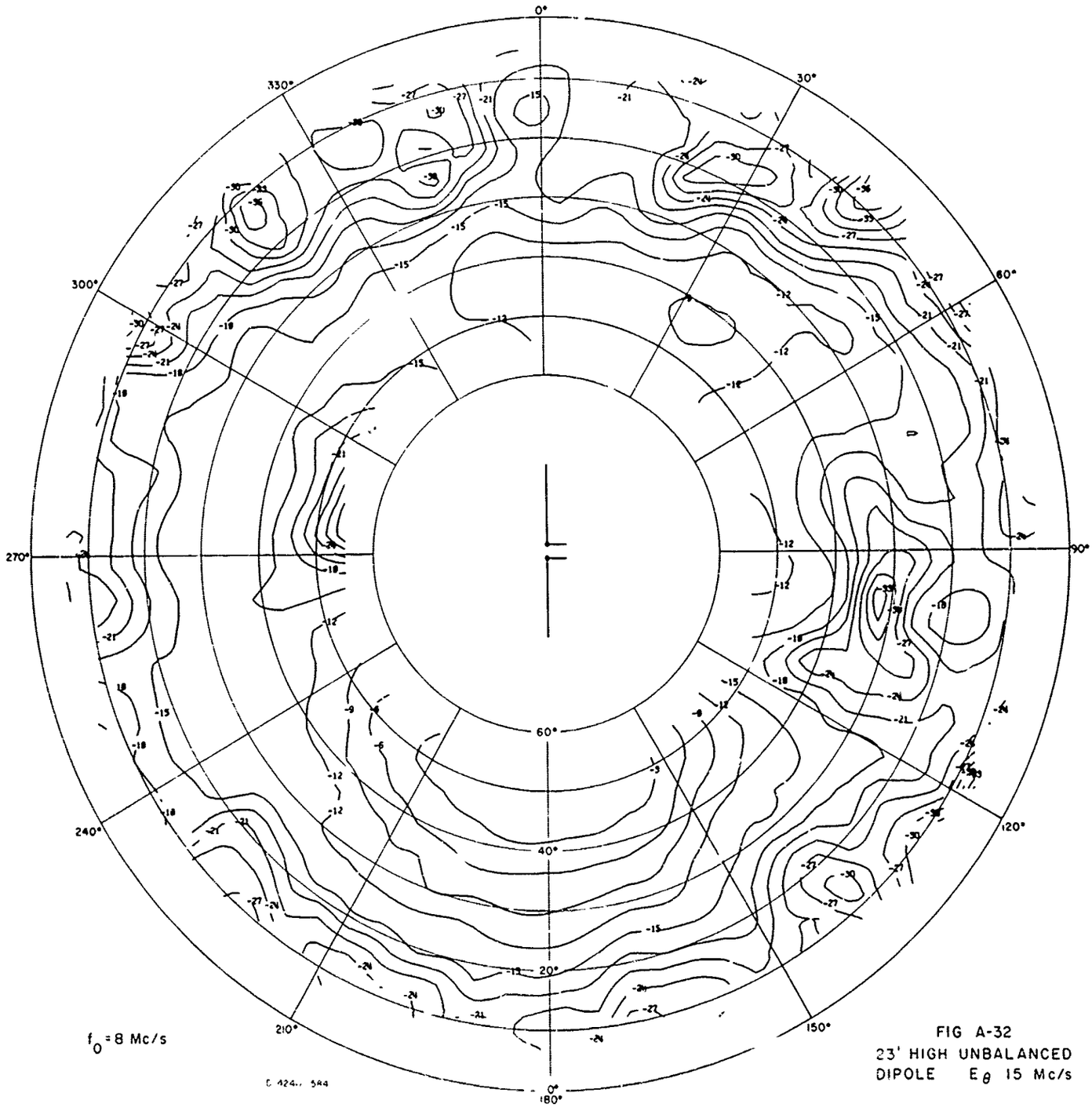

f_0 = 8 Mc/s

FIG A-32
23' HIGH UNBALANCED
DIPOLE E_θ 15 Mc/s

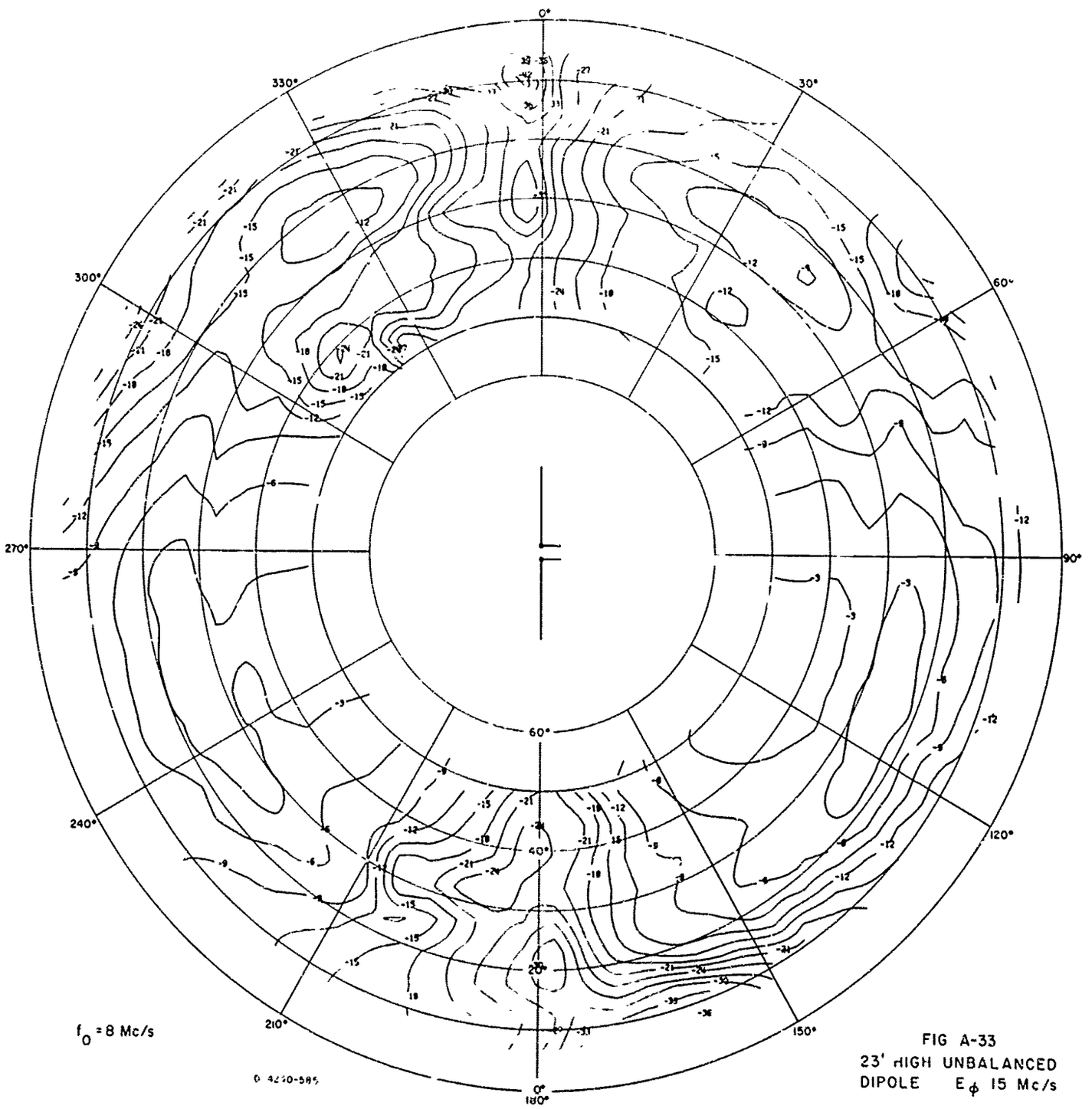

FIG A-33
23' HIGH UNBALANCED
DIPOLE E_ϕ 15 Mc/s

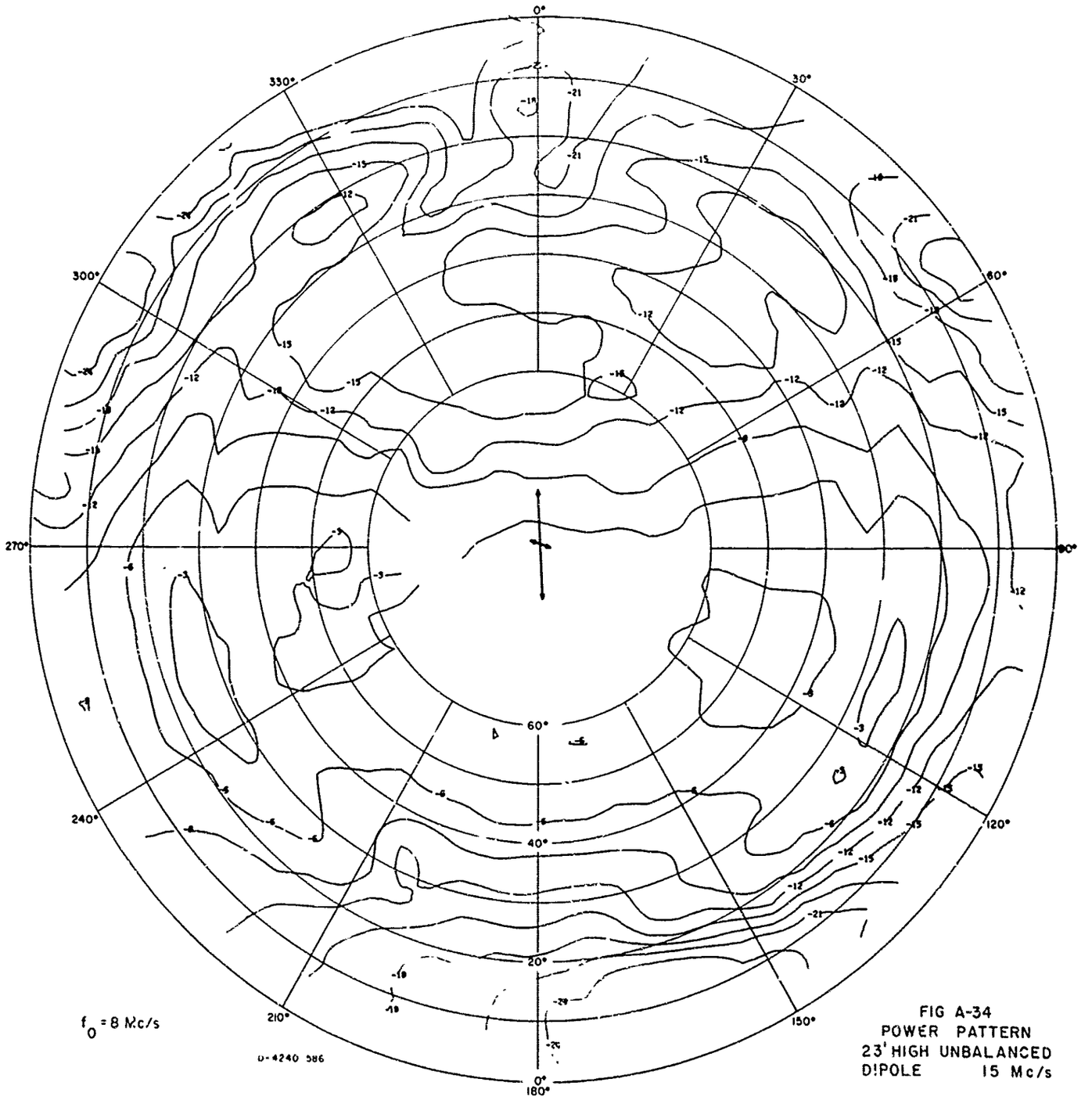

$f_0 = 8$ Mc/s

D-4240 586

FIG A-34
POWER PATTERN
23' HIGH UNBALANCED
DIPOLE 15 Mc/s

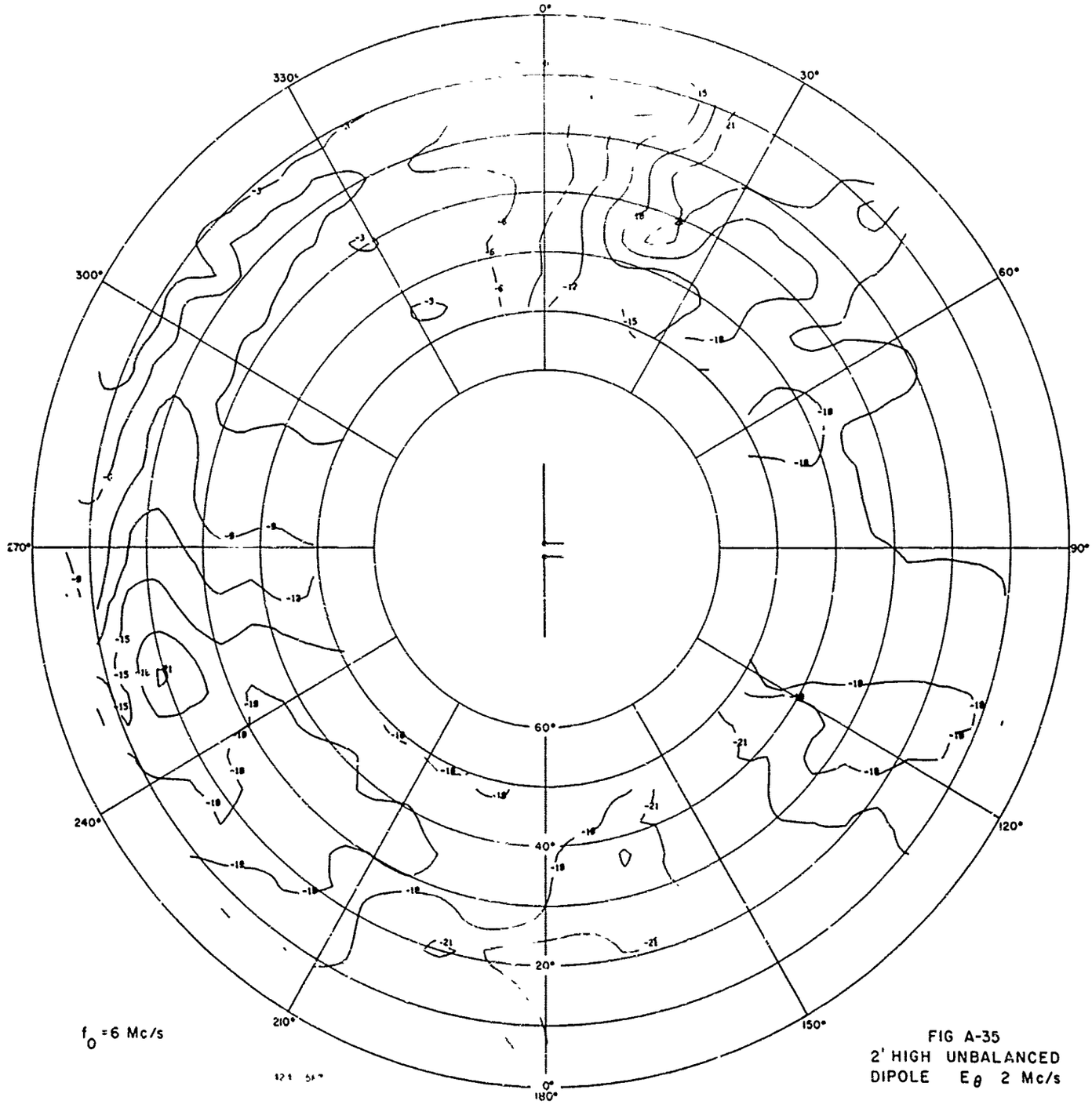

f_0 = 6 Mc/s

FIG A-35
2' HIGH UNBALANCED
DIPOLE E_θ 2 Mc/s

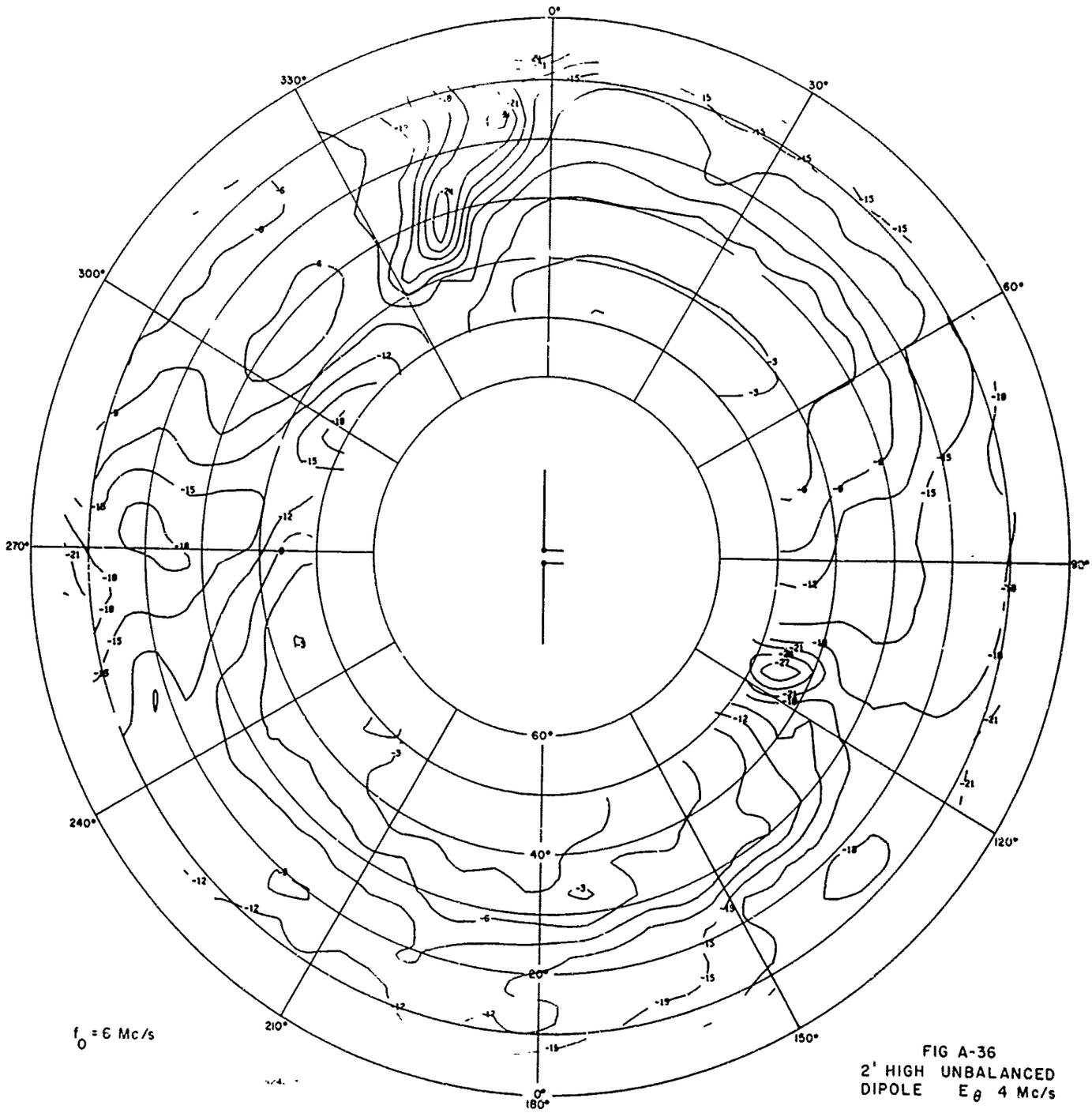

f_0 = 6 Mc/s

FIG A-36
2' HIGH UNBALANCED
DIPOLE E_θ 4 Mc/s

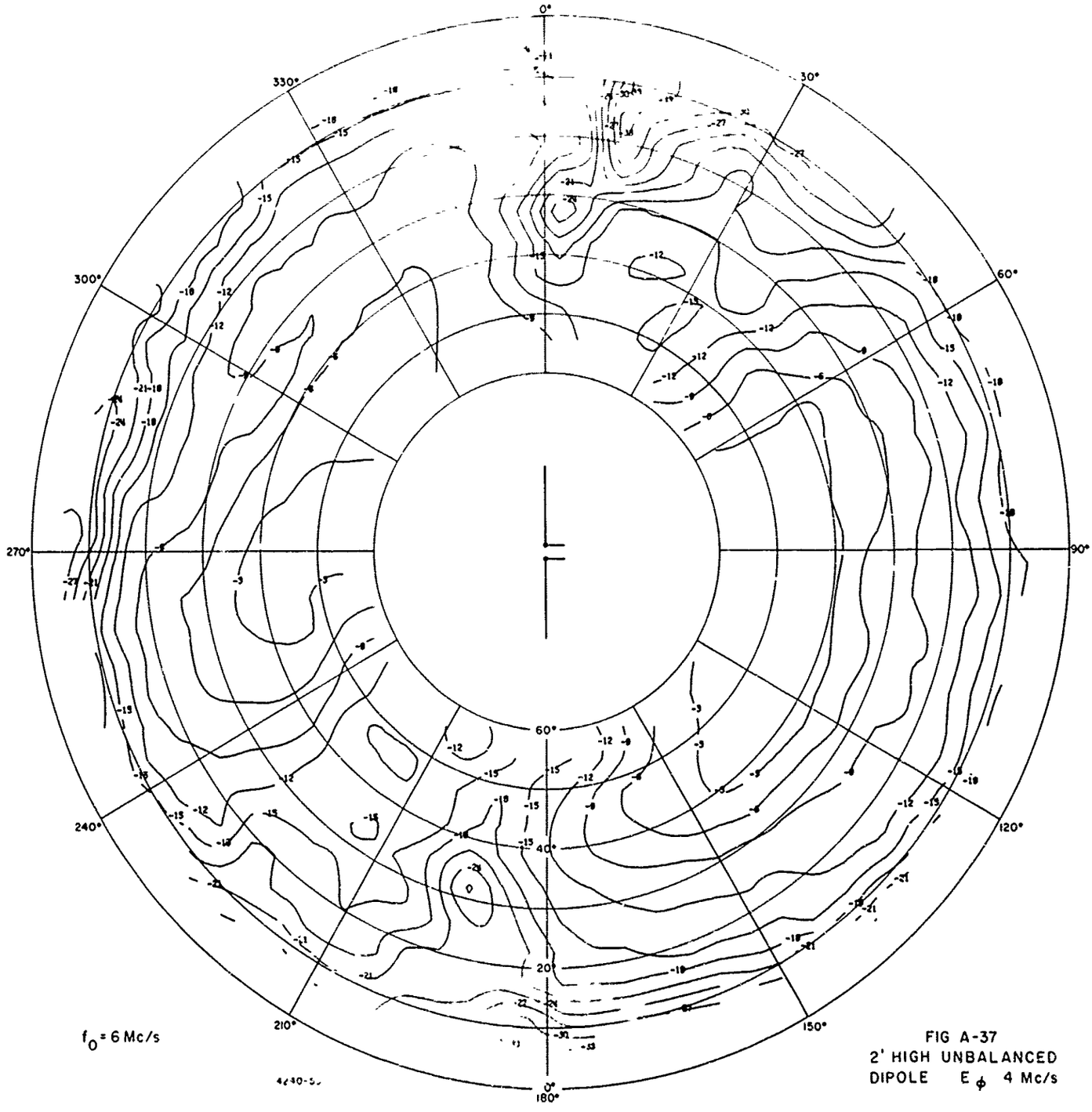

f_0 = 6 Mc/s

FIG A-37
2' HIGH UNBALANCED
DIPOLE E_ϕ 4 Mc/s

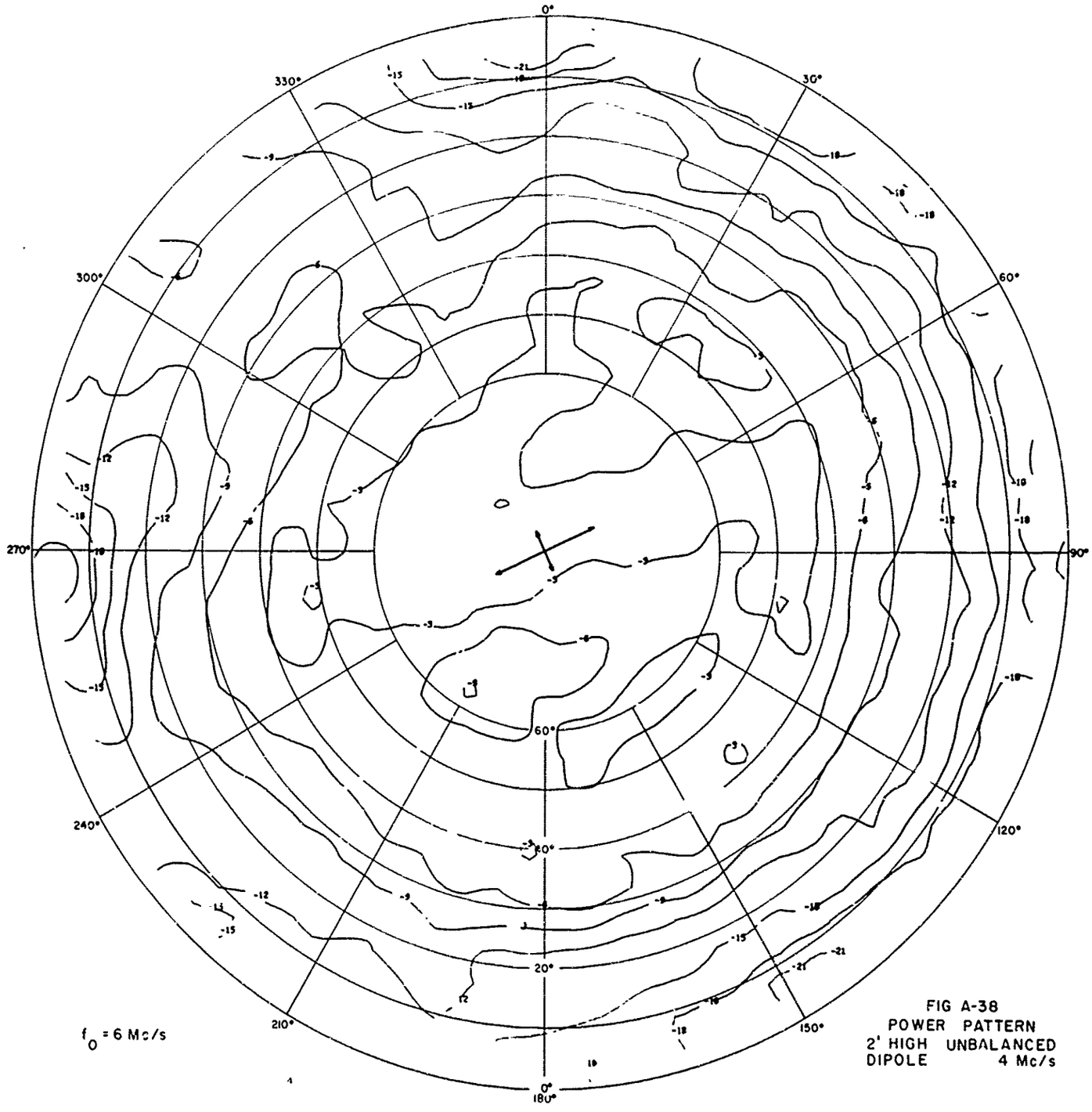

f_0 = 6 Mc/s

FIG A-38
POWER PATTERN
2' HIGH UNBALANCED
DIPOLE 4 Mc/s

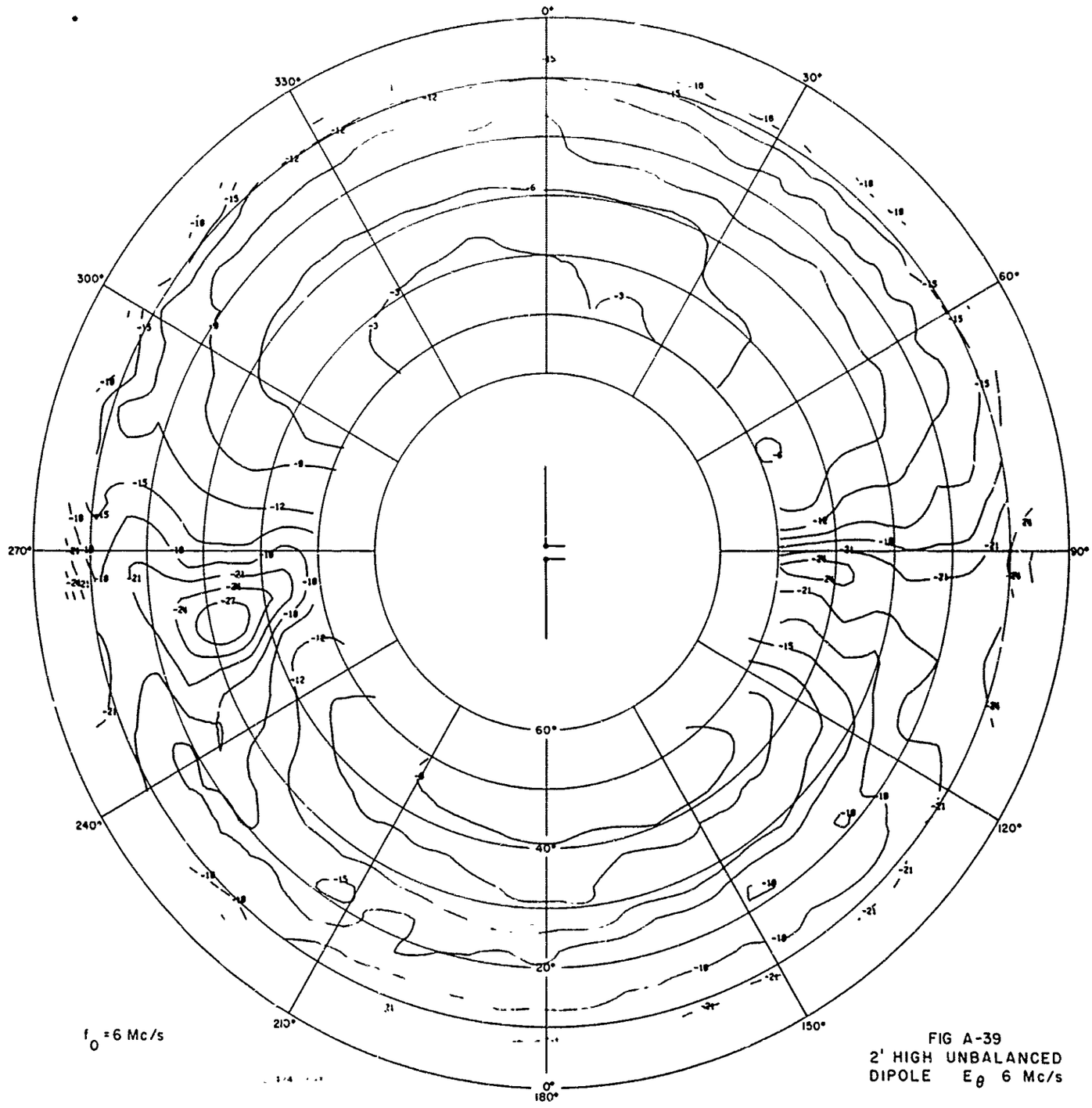

f_0 = 6 Mc/s

FIG A-39
2' HIGH UNBALANCED
DIPOLE E_θ 6 Mc/s

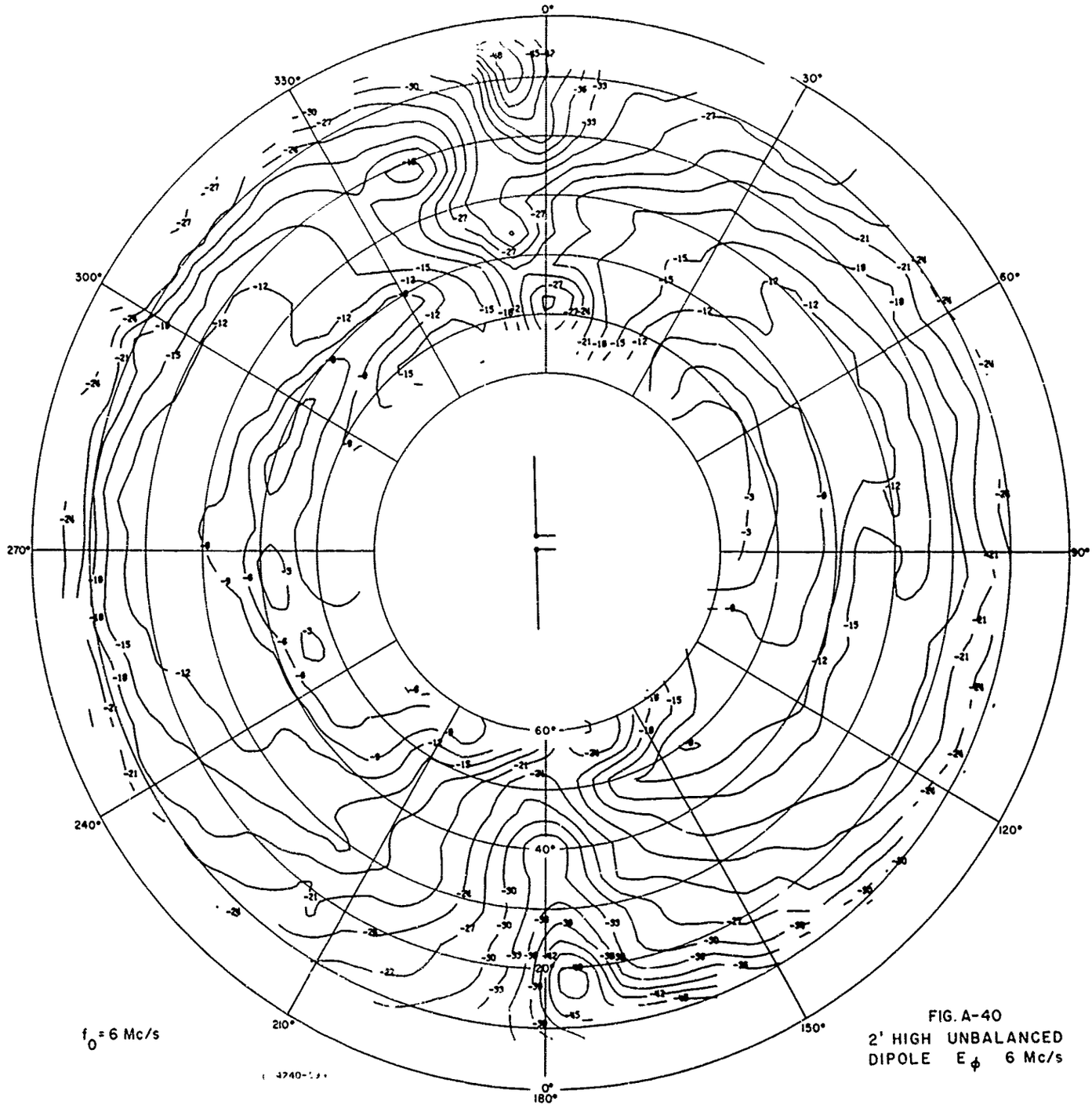

f_0 = 6 Mc/s

FIG. A-40
2' HIGH UNBALANCED
DIPOLE E_ϕ 6 Mc/s

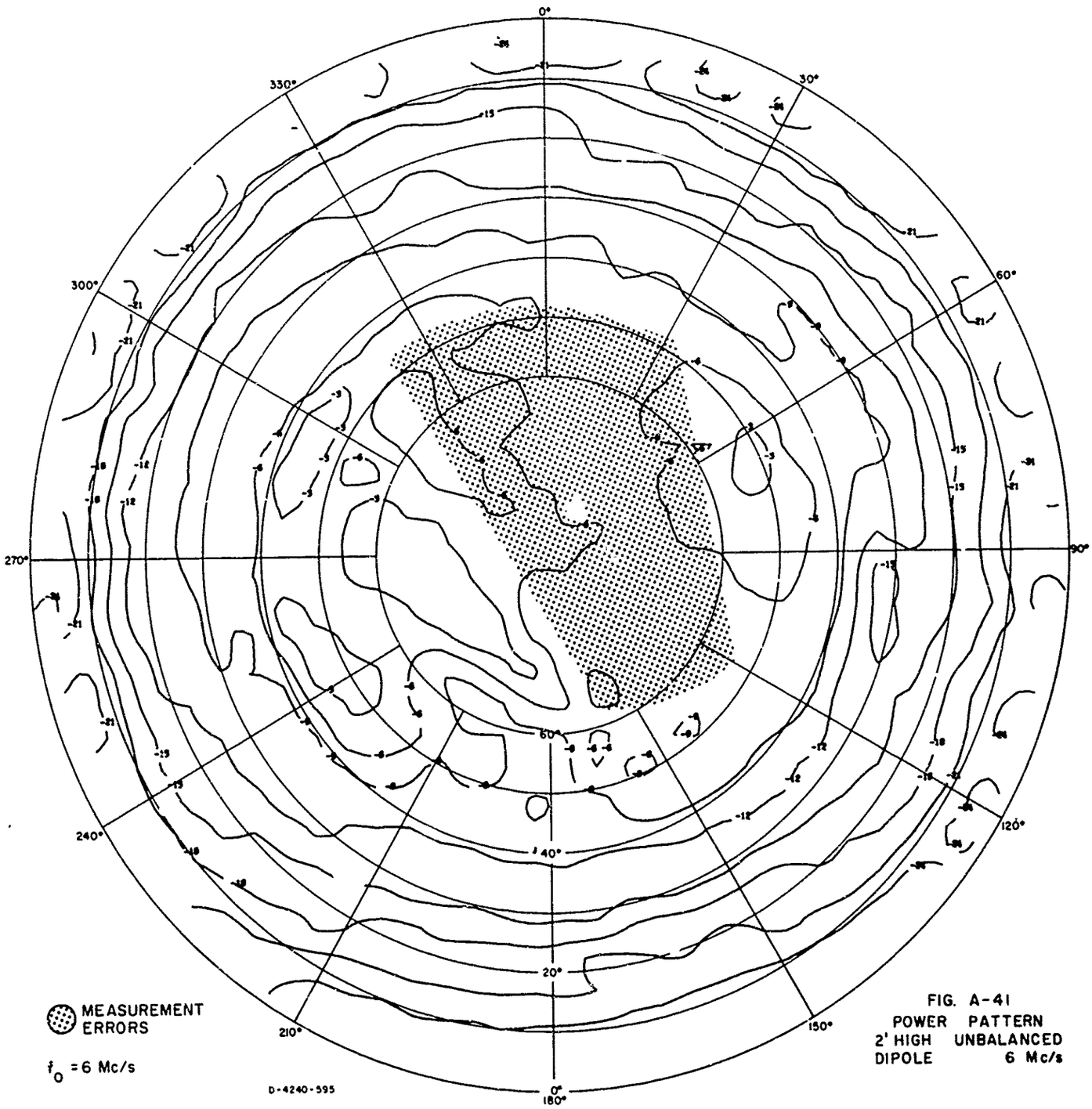

FIG. A-41
POWER PATTERN
2' HIGH UNBALANCED
DIPOLE 6 Mc/s

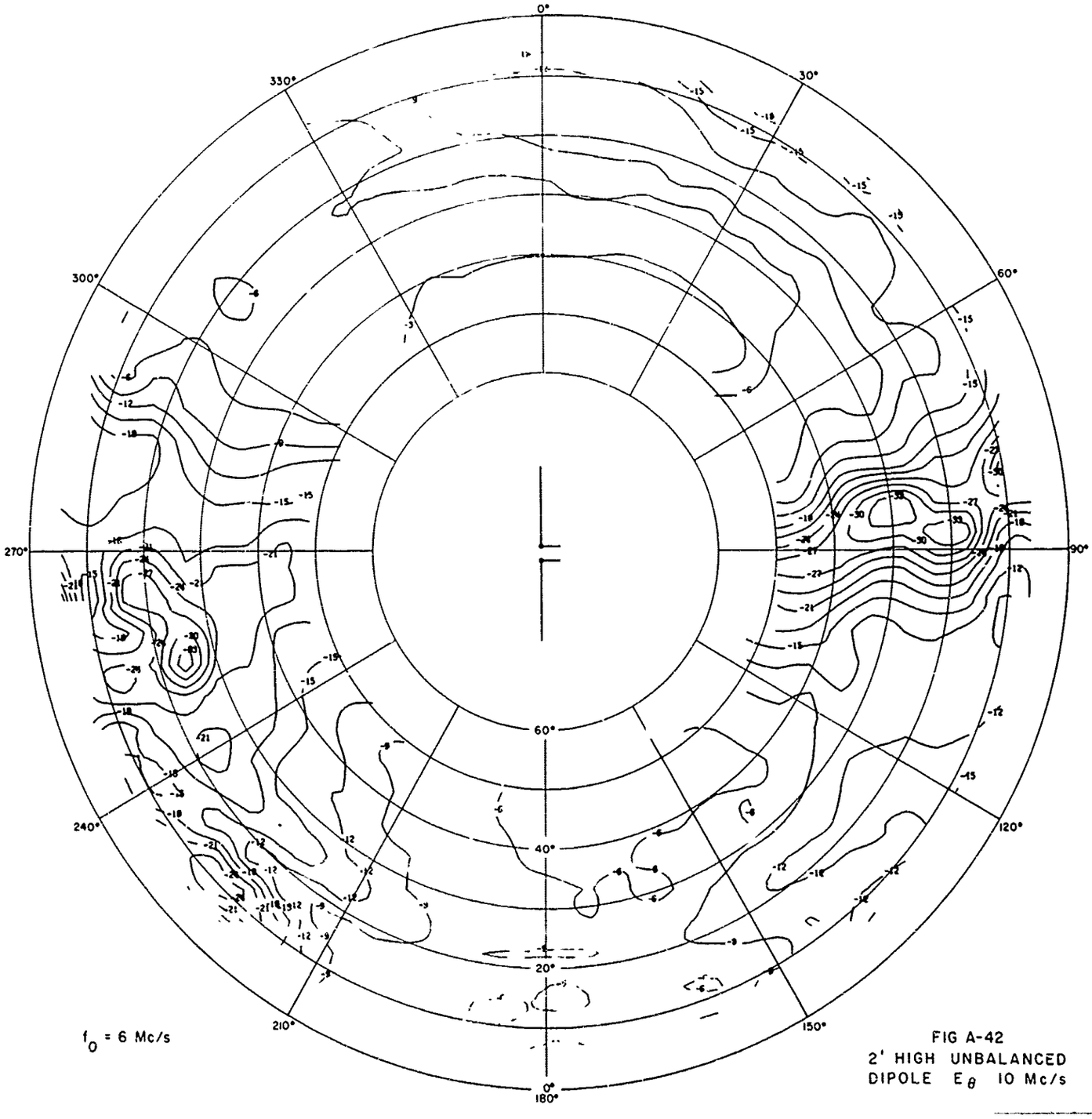

f_0 = 6 Mc/s

FIG A-42
2' HIGH UNBALANCED
DIPOLE E_θ 10 Mc/s

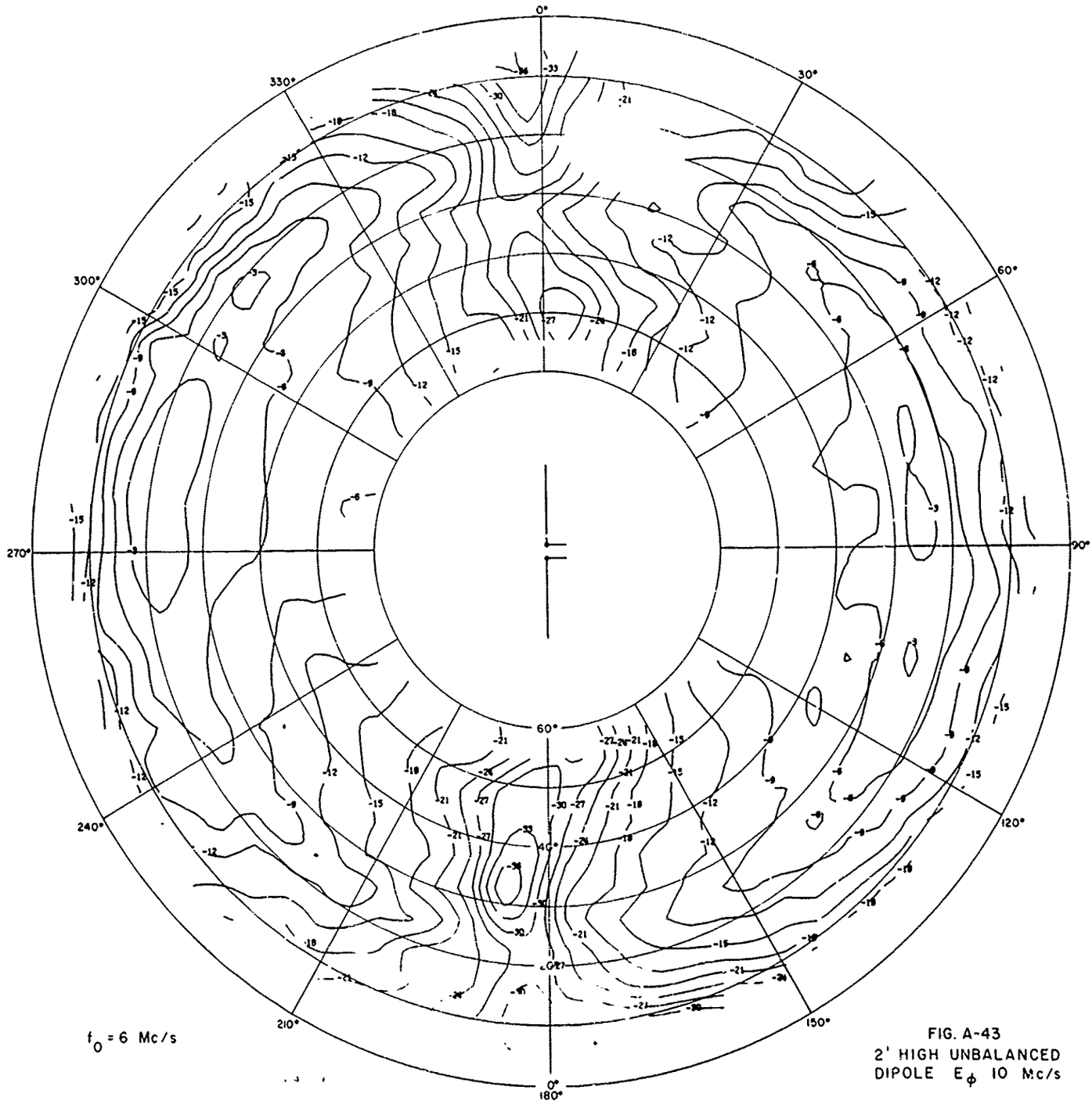

$f_0 = 6$ Mc/s

FIG. A-43
2' HIGH UNBALANCED
DIPOLE E_ϕ 10 Mc/s

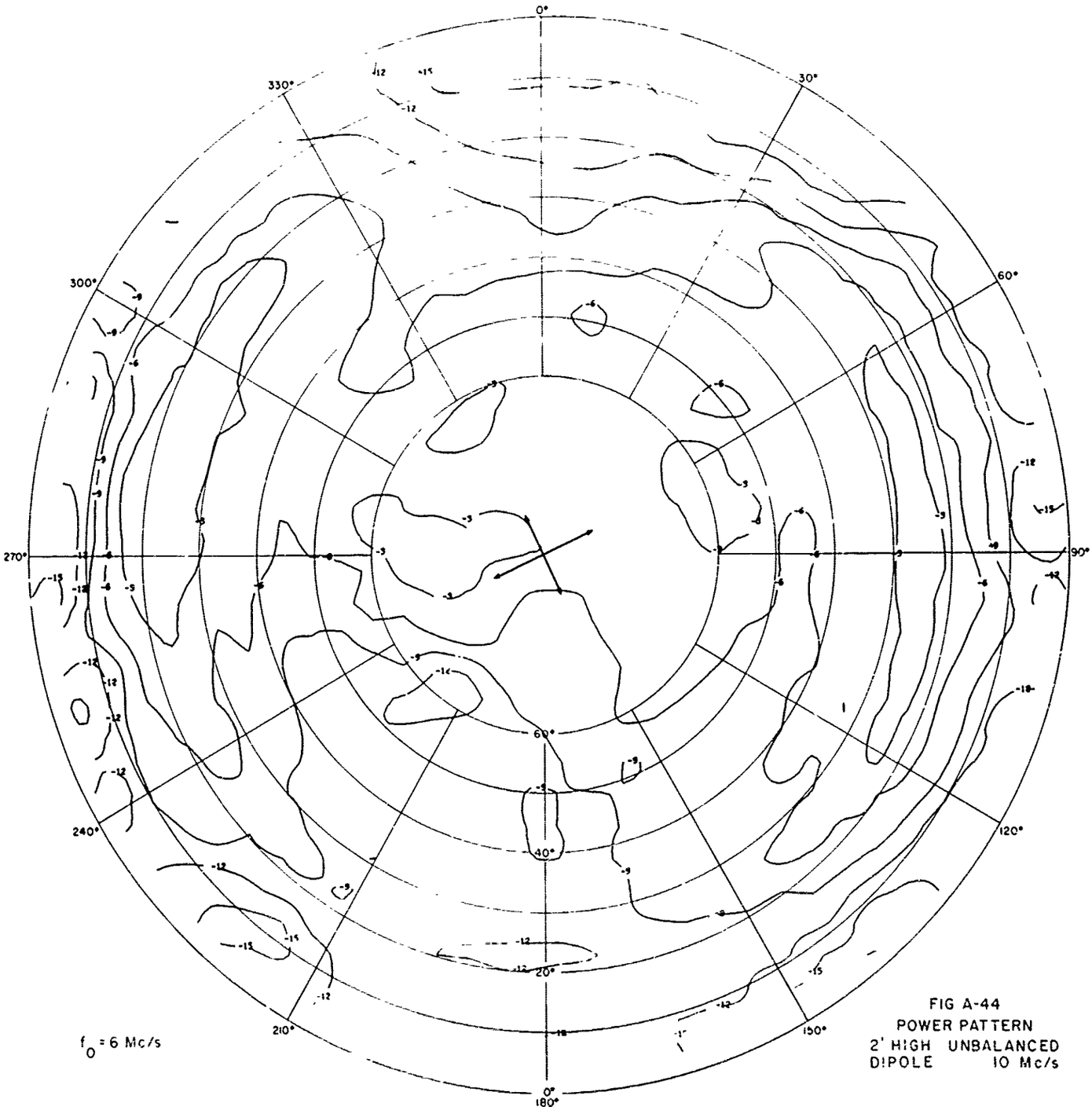

f_0 = 6 Mc/s

FIG A-44
POWER PATTERN
2' HIGH UNBALANCED
DIPOLE 10 Mc/s

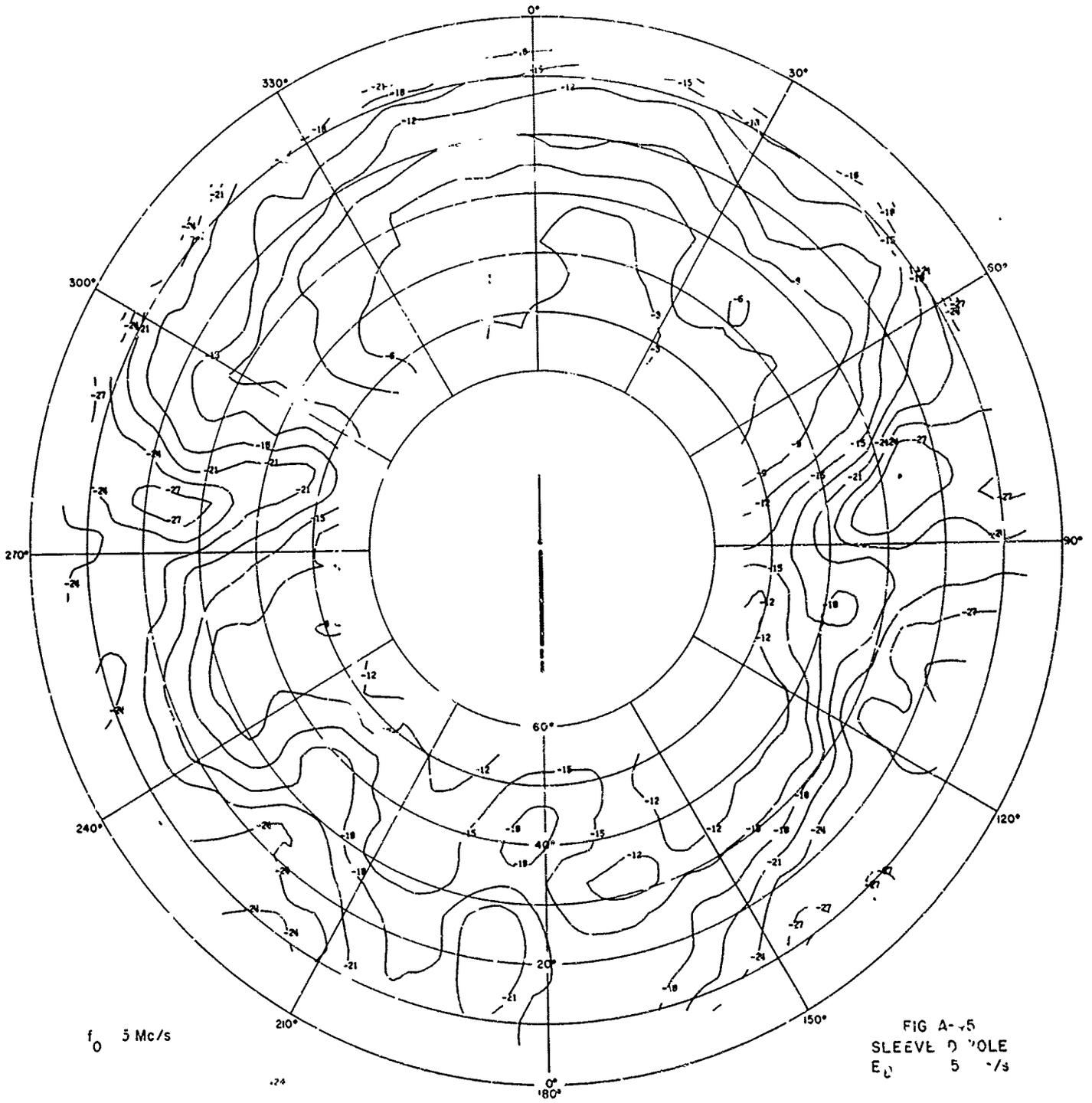

f_0 5 Mc/s

FIG A-45
SLEEVE DIPOLE
E_0 5 v/s

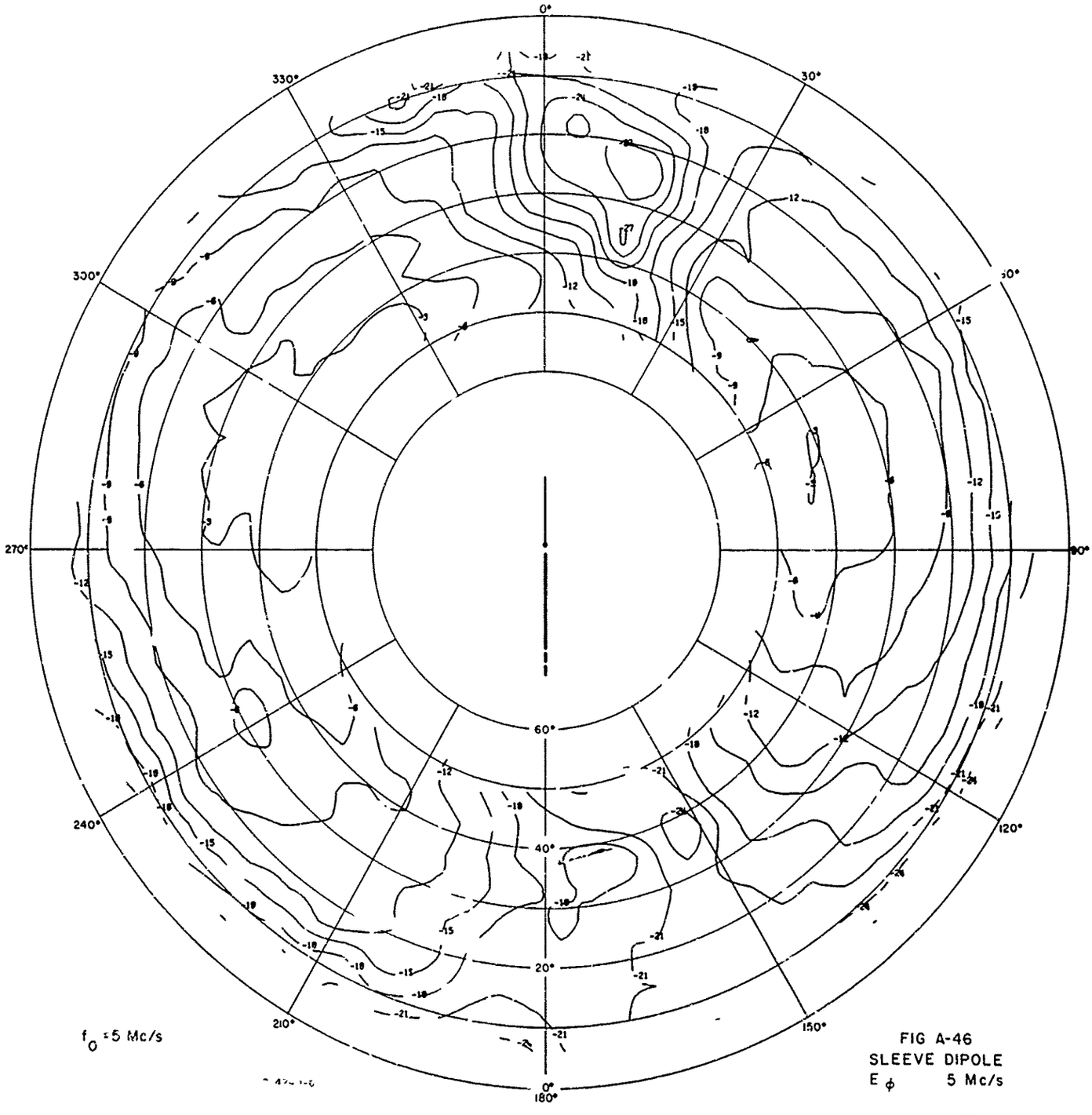

f_0 = 5 Mc/s

FIG A-46
SLEEVE DIPOLE
E_ϕ 5 Mc/s

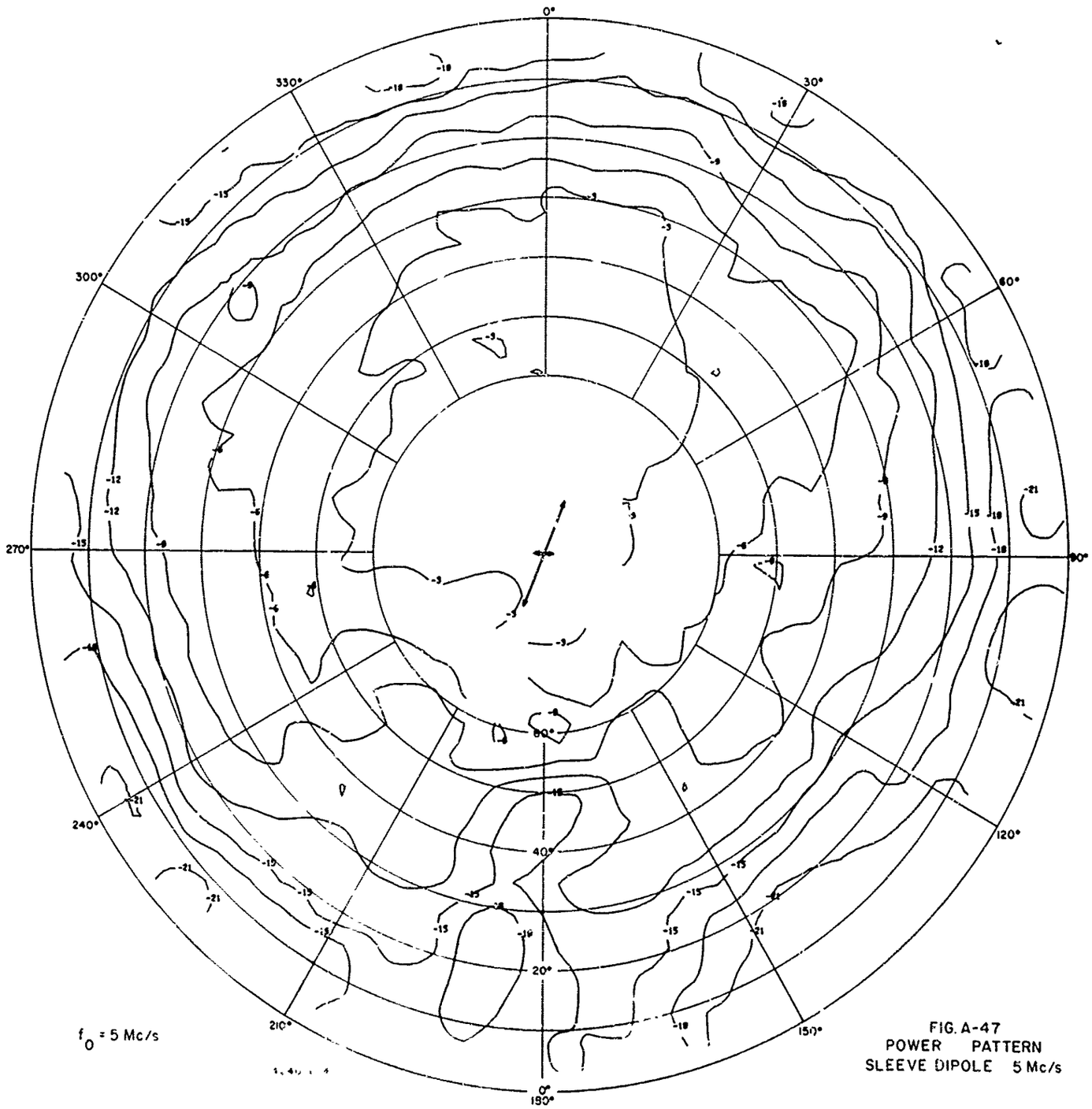

FIG. A-47
POWER PATTERN
SLEEVE DIPOLE 5 Mc/s

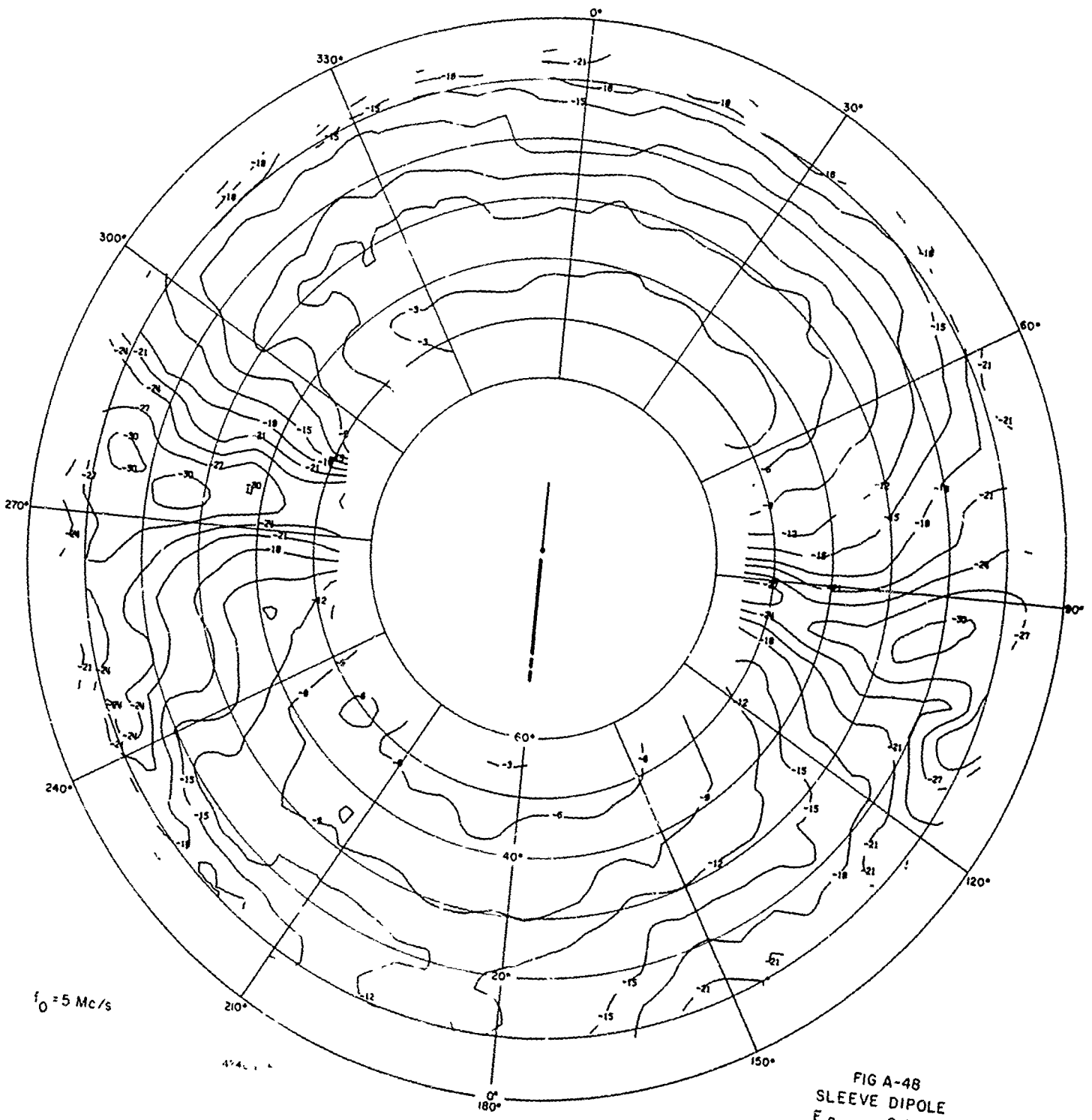

FIG A-48
SLEEVE DIPOLE
E_θ 8 Mc/s

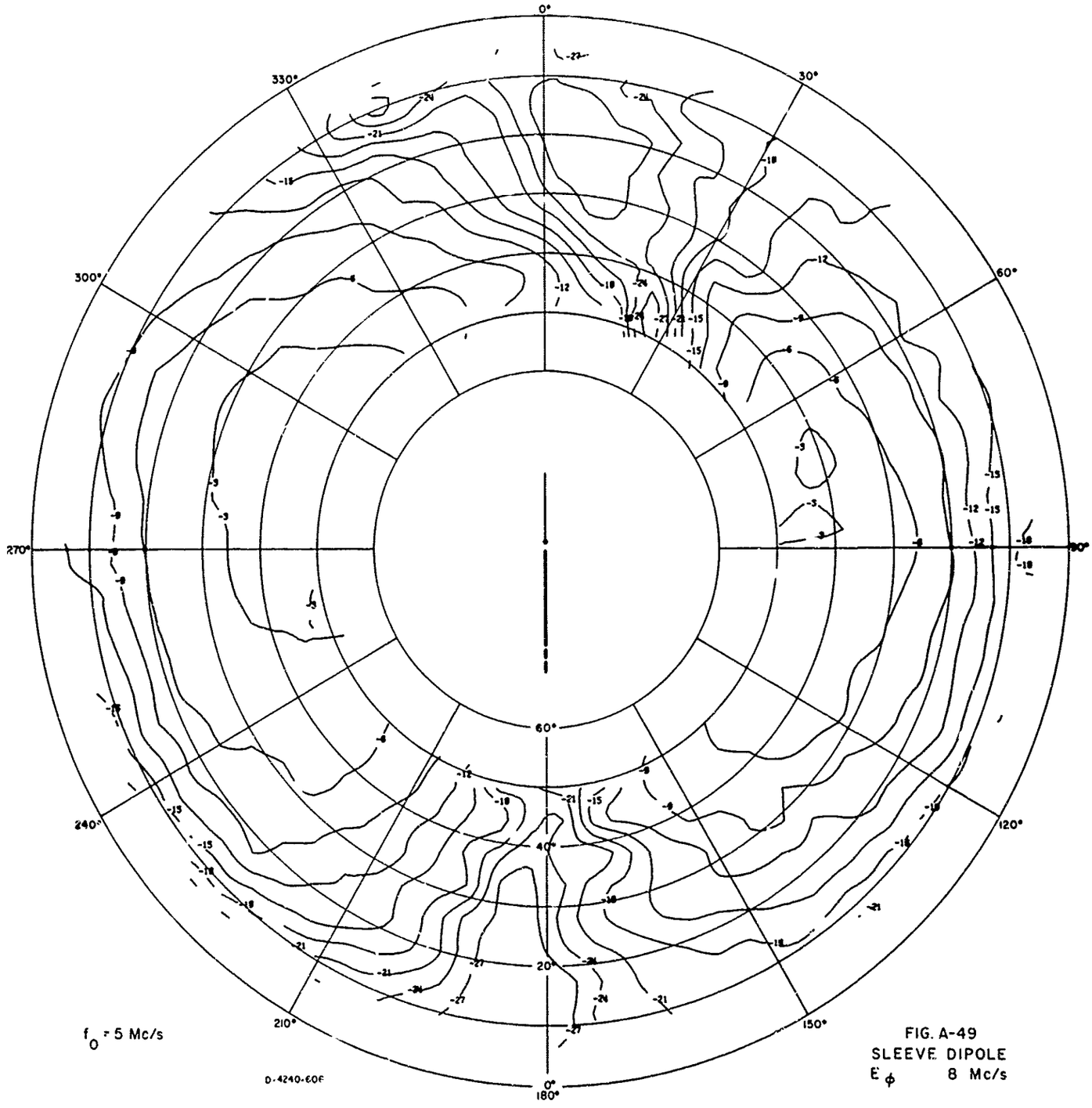

FIG. A-49
SLEEVE DIPOLE
E_ϕ 8 Mc/s

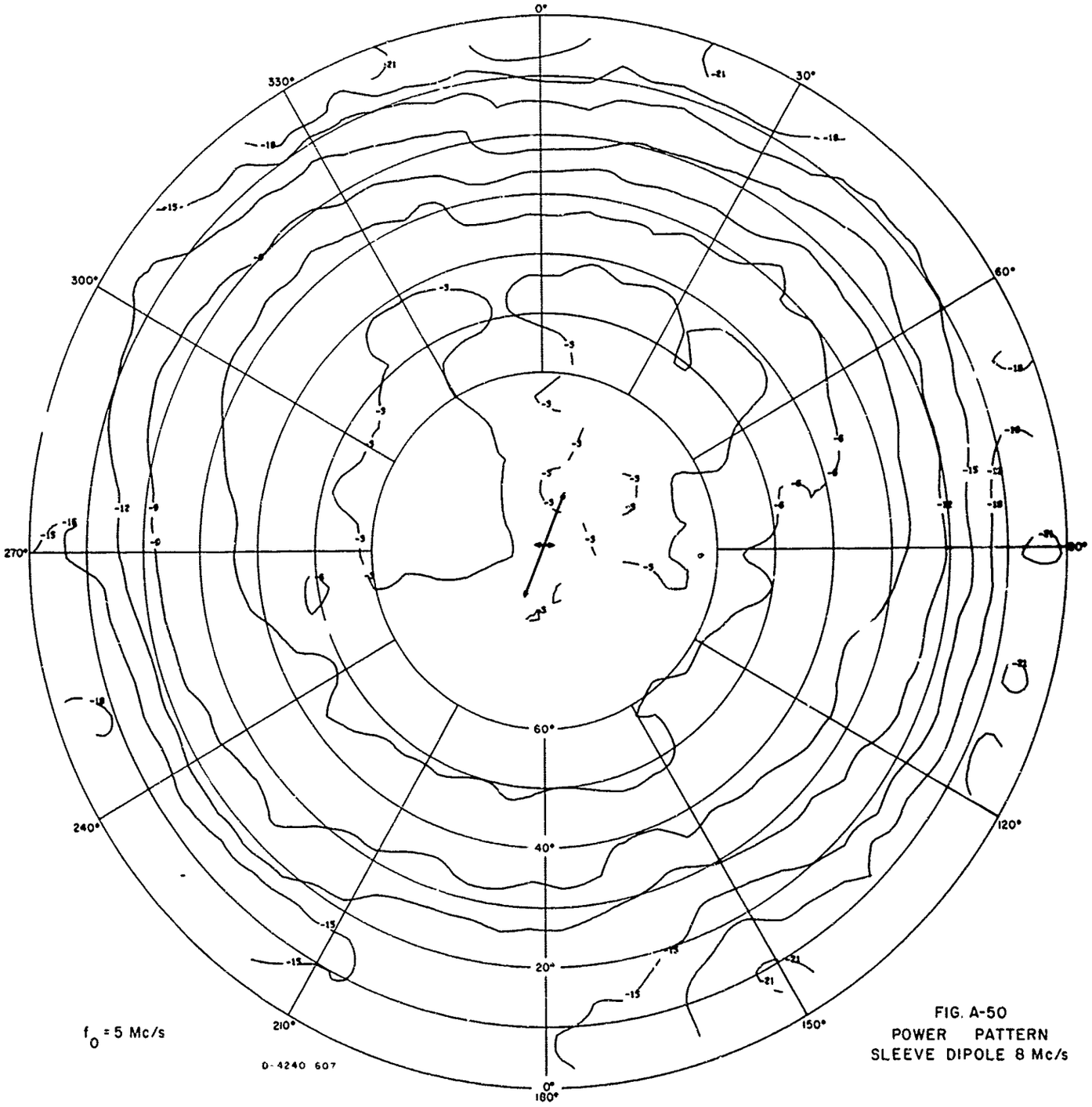

FIG. A-50
POWER PATTERN
SLEEVE DIPOLE 8 Mc/s

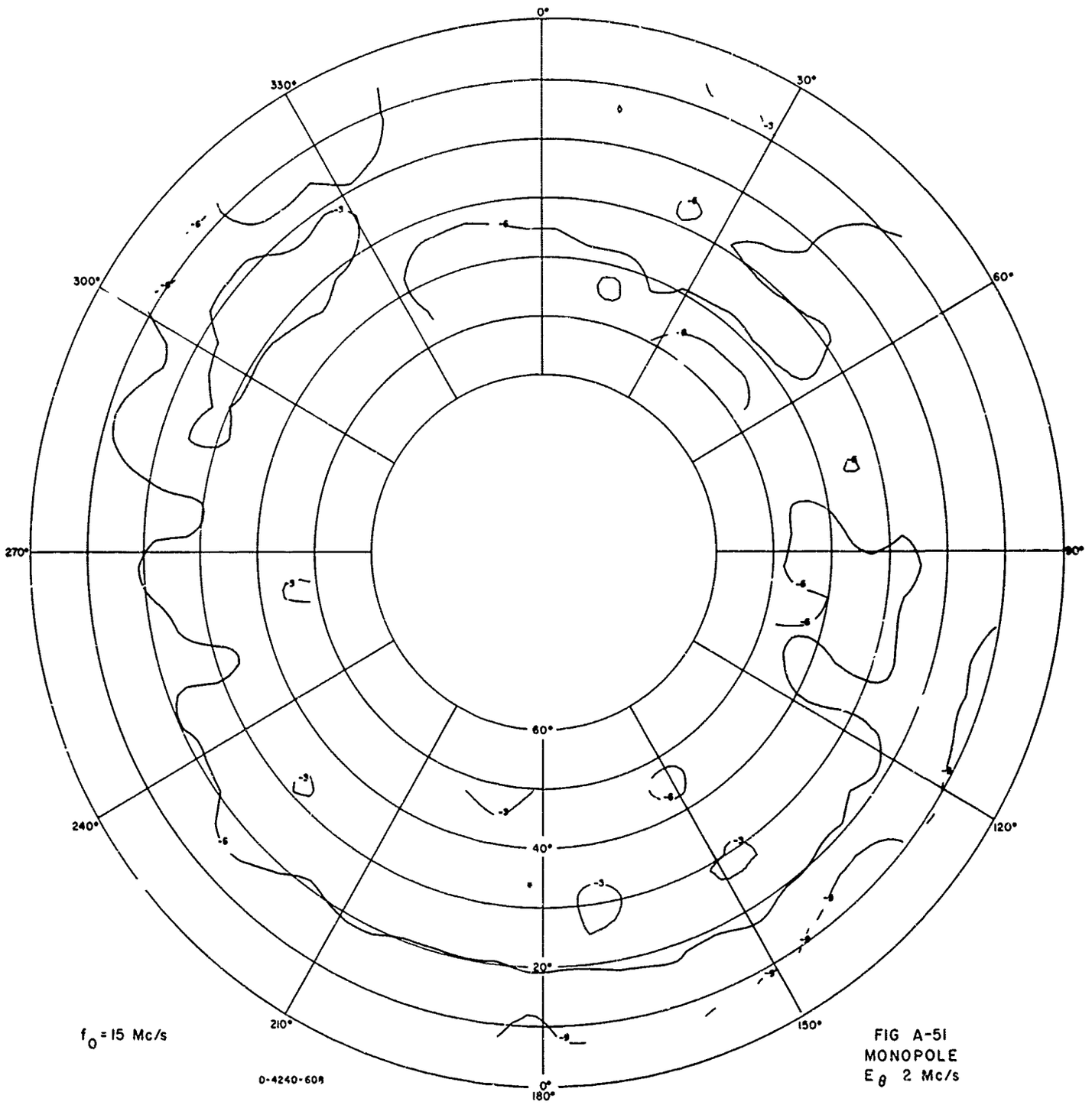

f_0 = 15 Mc/s

0-4240-609

FIG A-51
MONOPOLE
E_θ 2 Mc/s

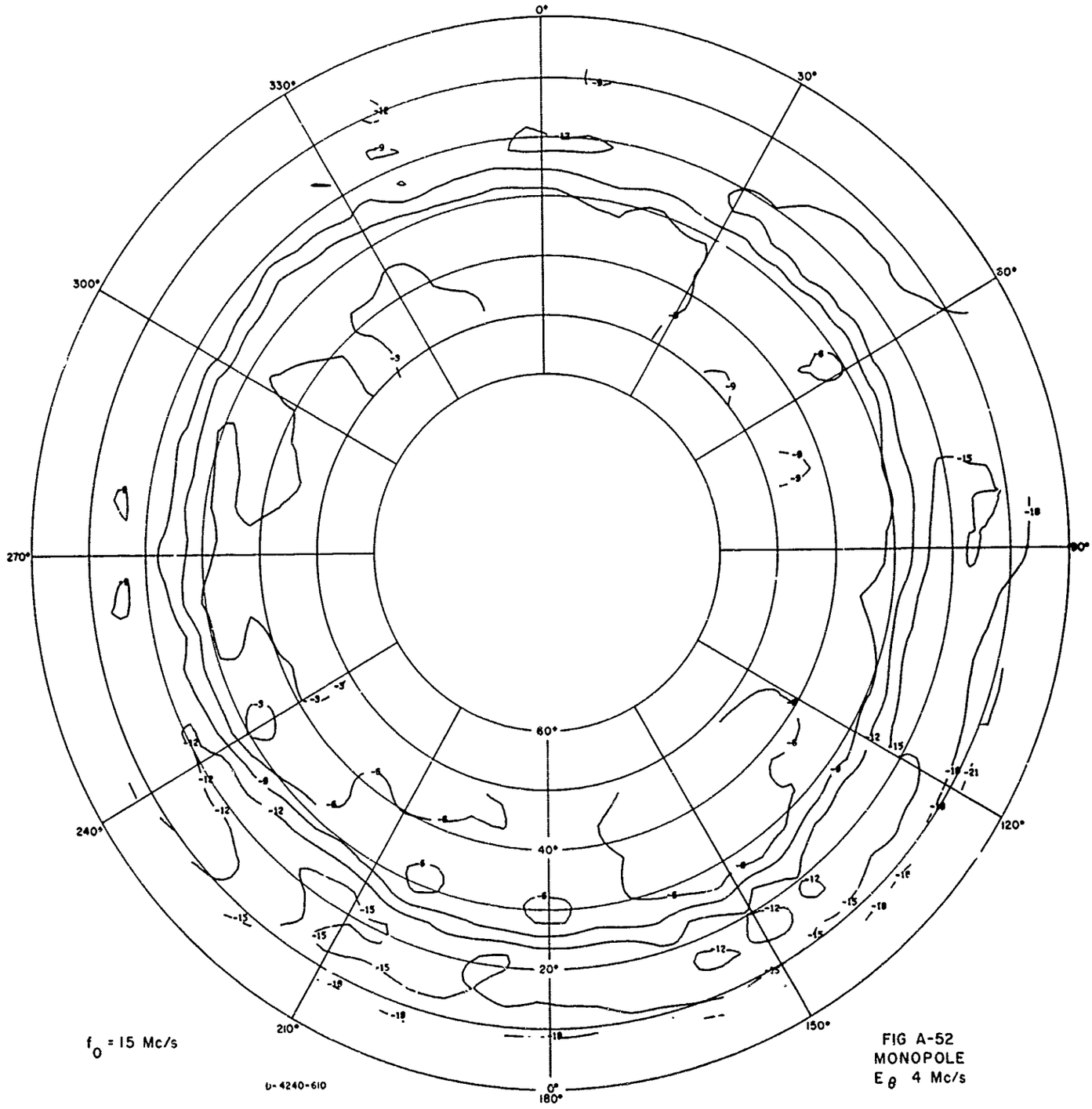

f_0 = 15 Mc/s

b-4240-610

FIG A-52
MONOPOLE
E_θ 4 Mc/s

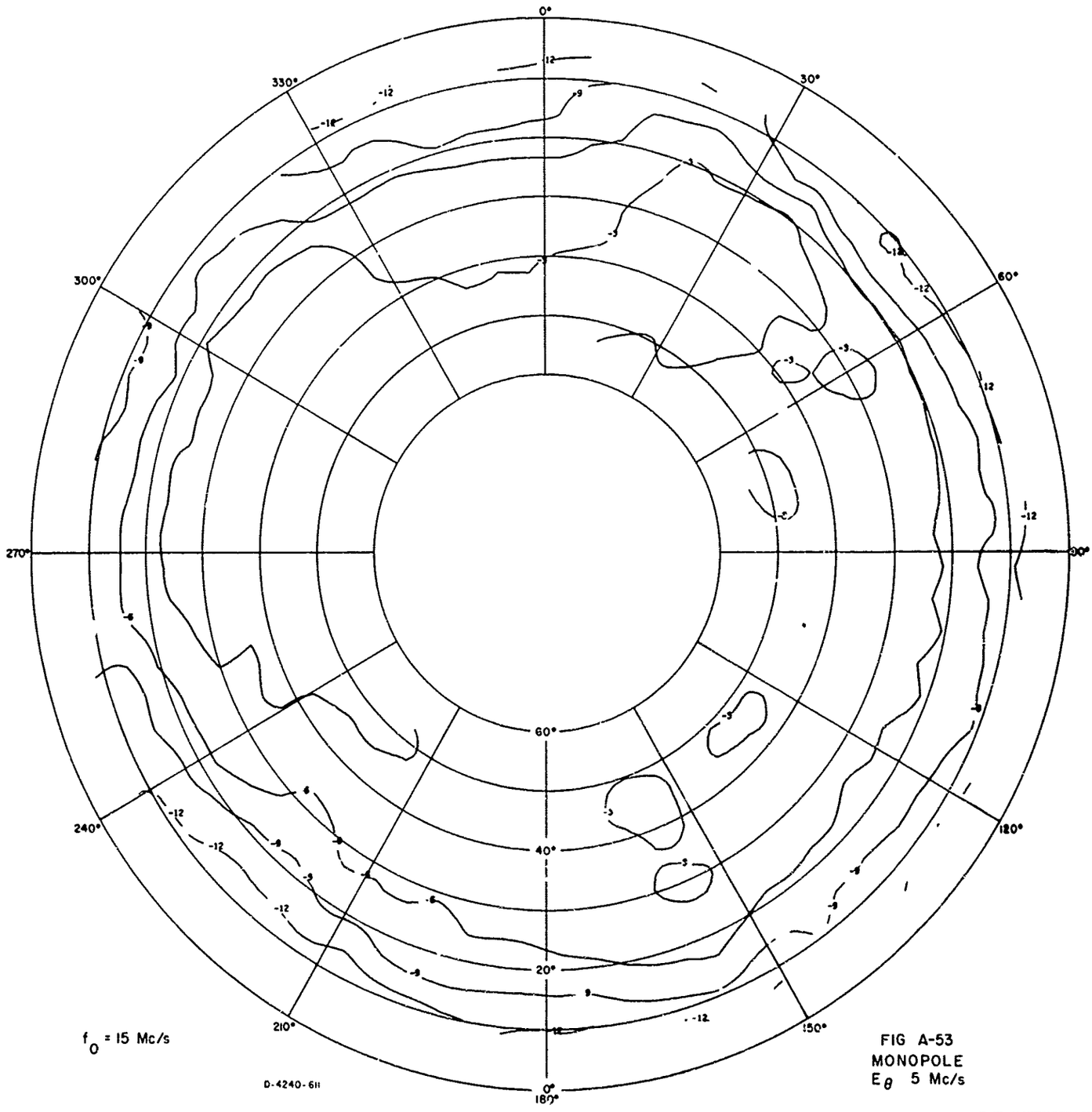

f_0 = 15 Mc/s

D-4240-611

FIG A-53
MONOPOLE
E_θ 5 Mc/s

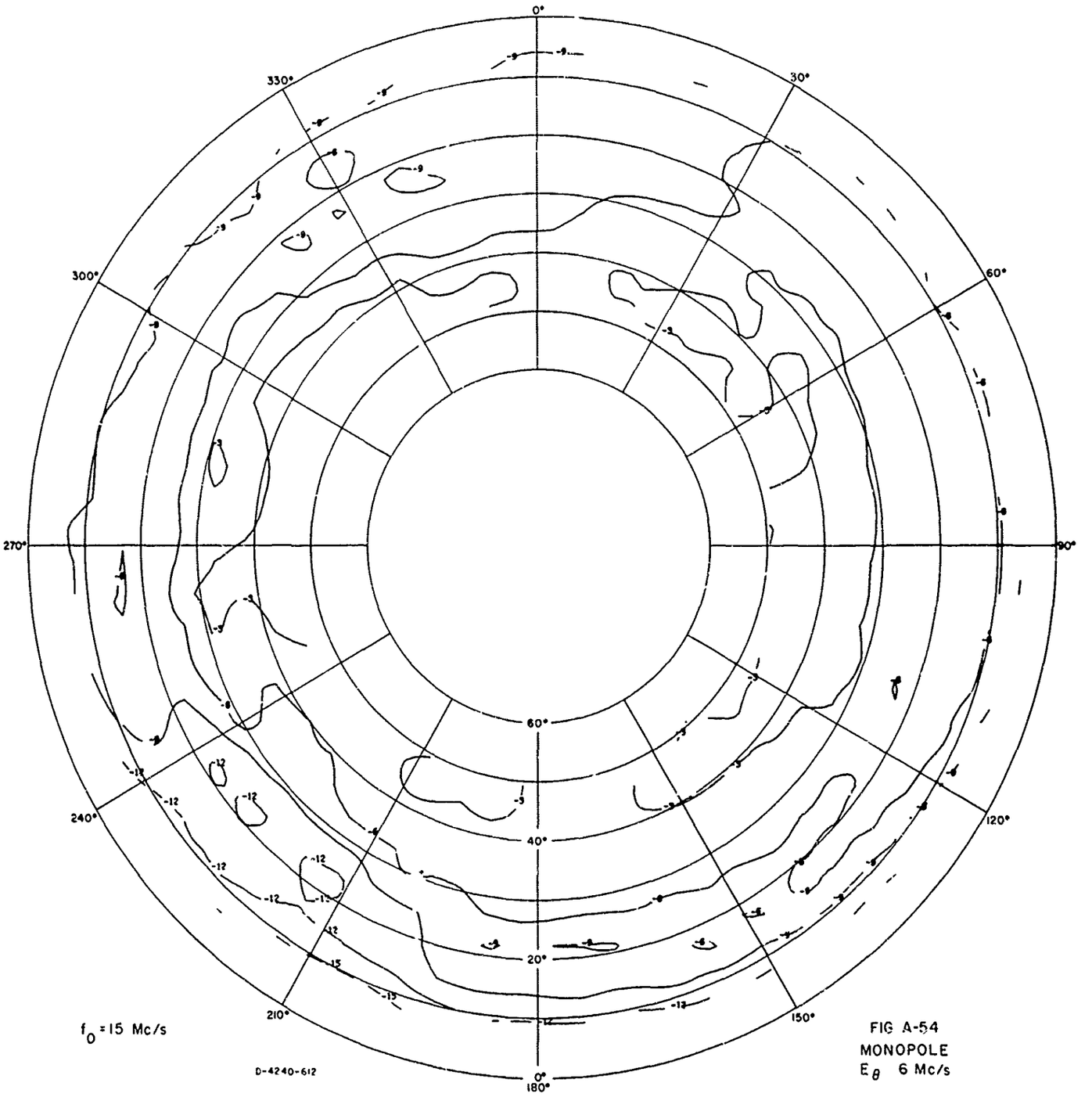

f_0 = 15 Mc/s

D-4240-612

FIG A-54
MONOPOLE
E_θ 6 Mc/s

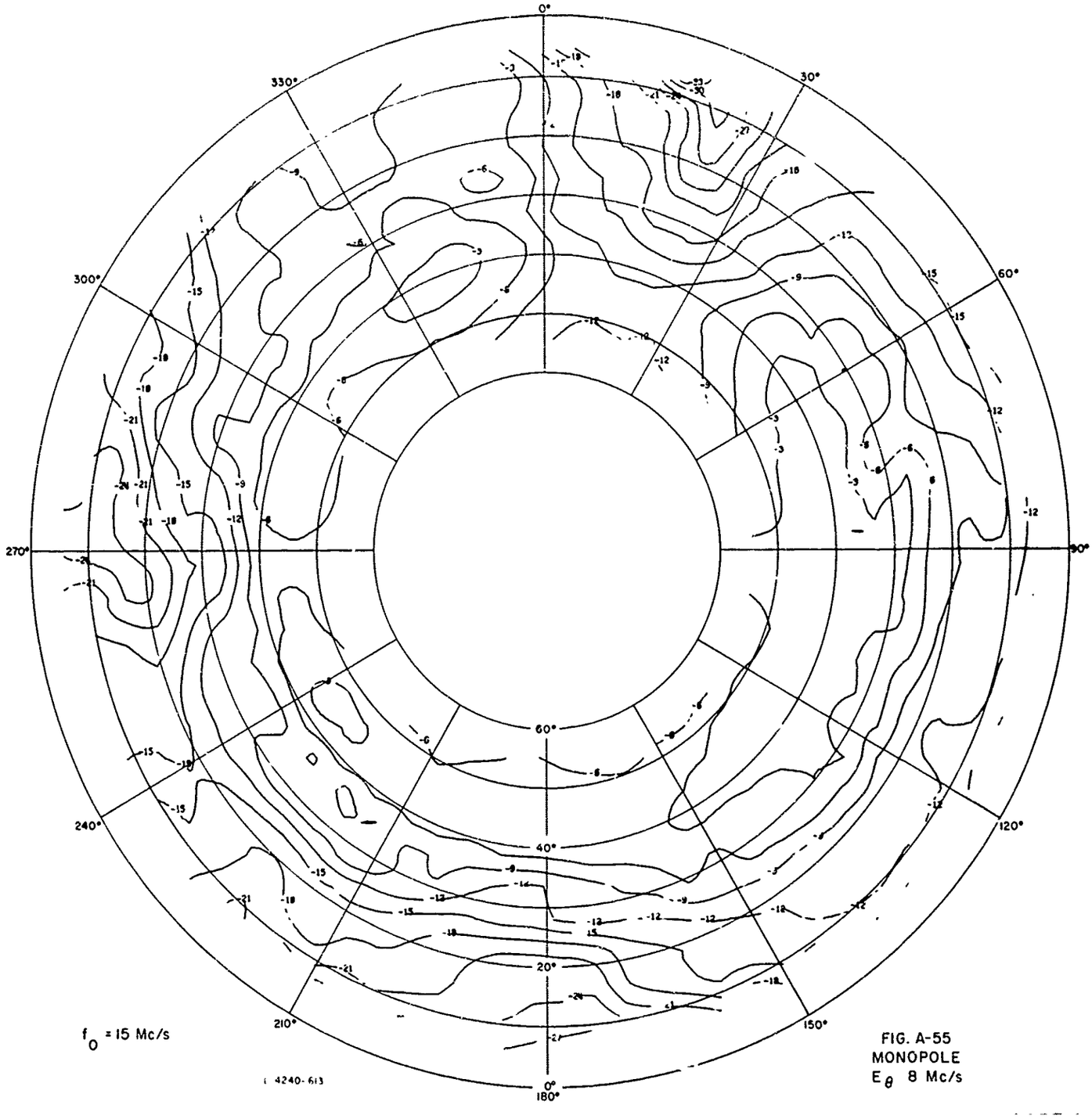

FIG. A-55
MONOPOLE
E_θ 8 Mc/s

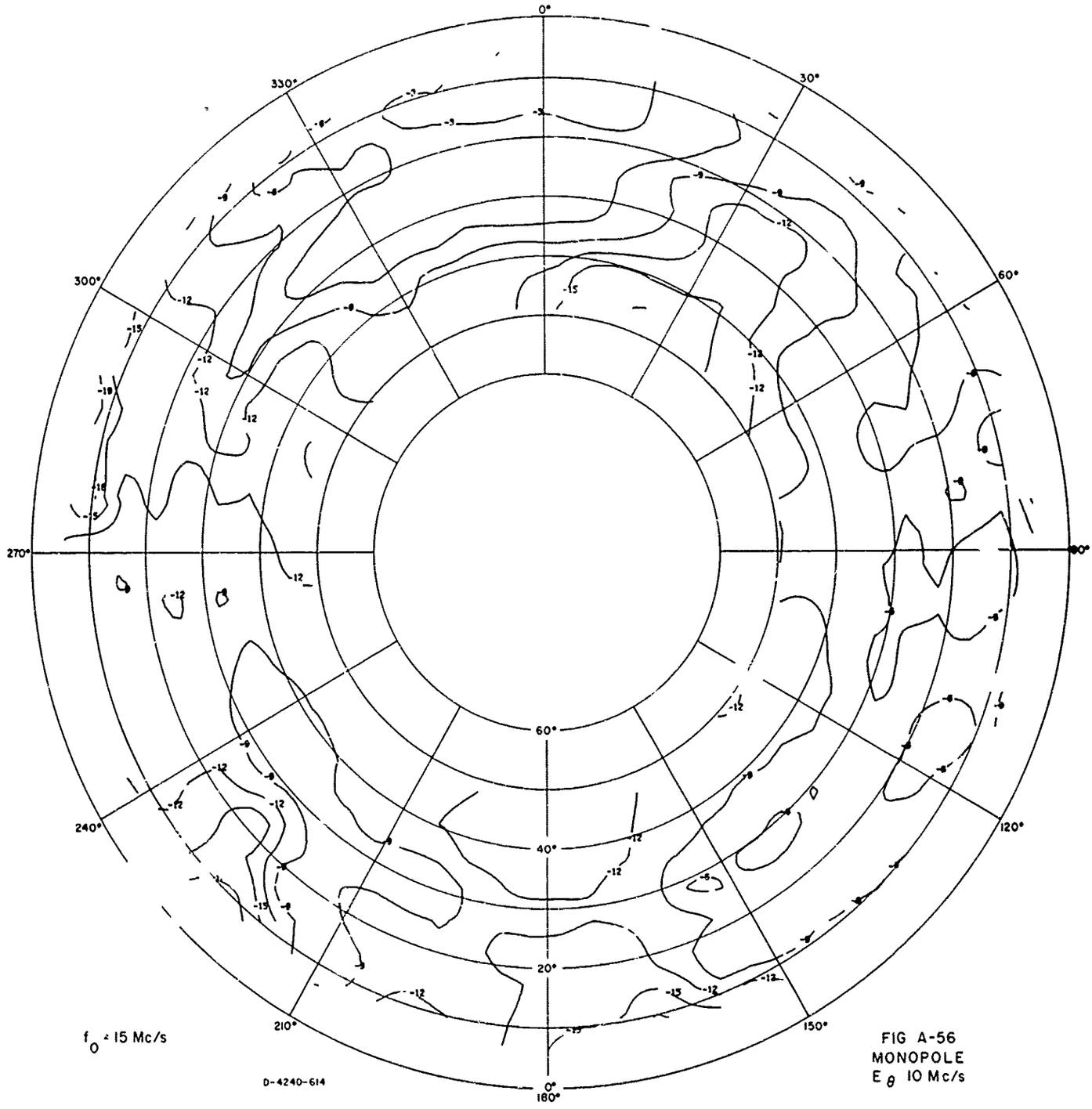

f_0 = 15 Mc/s

D-4240-614

FIG A-56
MONOPOLE
E_θ 10 Mc/s

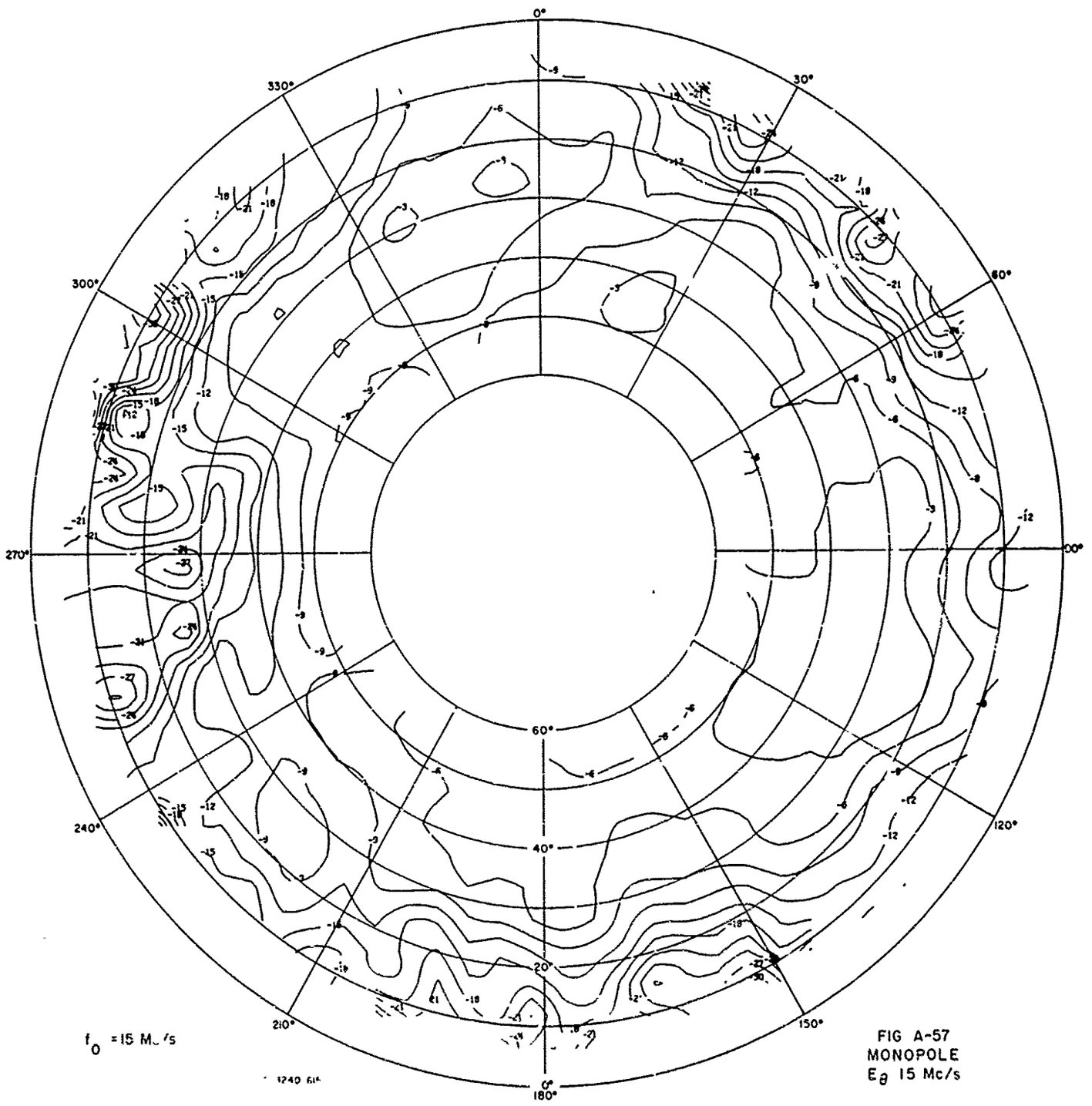

f_0 = 15 Mc/s

1240 61A

FIG A-57
MONOPOLE
E_θ 15 Mc/s

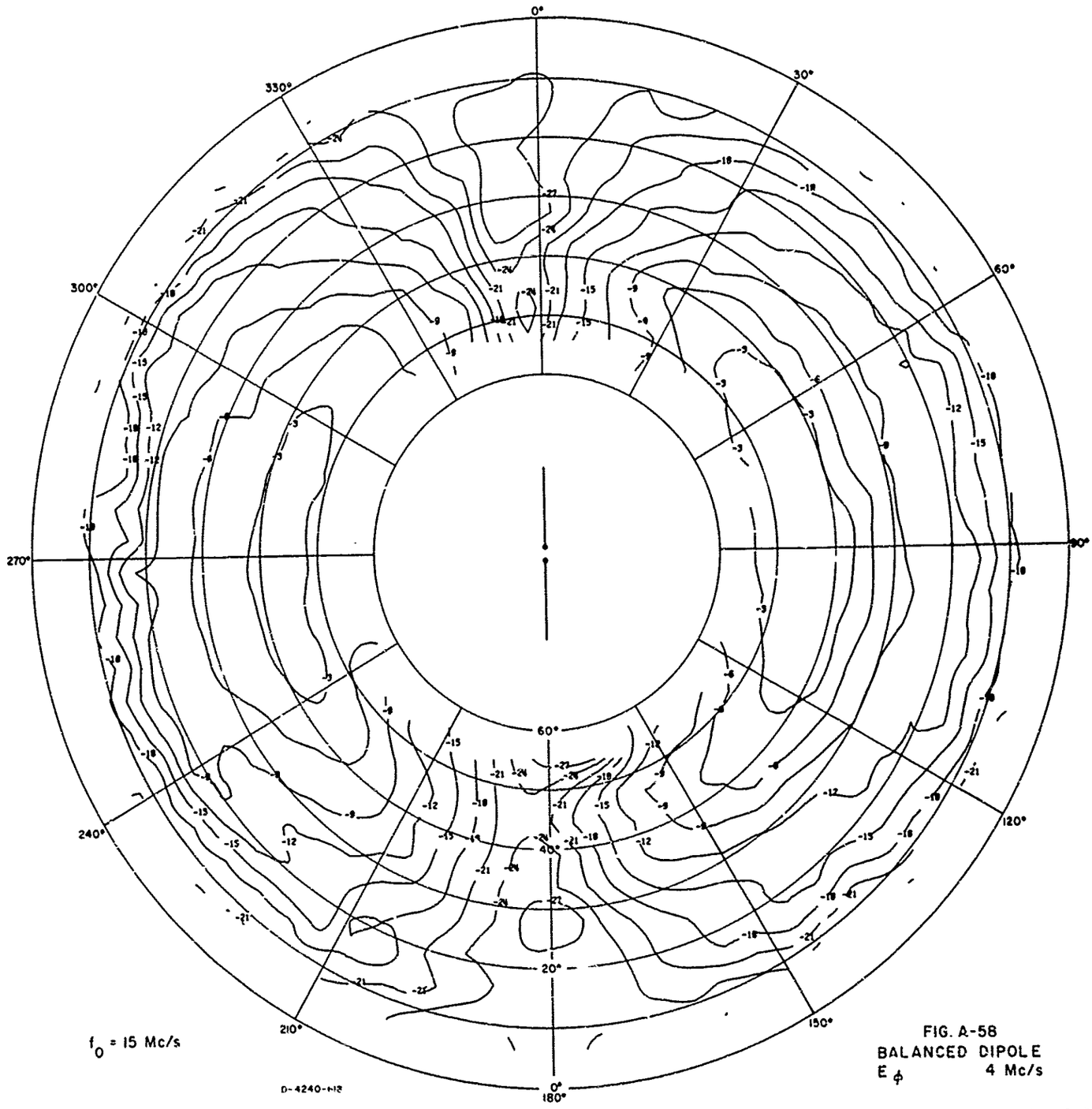

f_0 = 15 Mc/s

FIG. A-58
BALANCED DIPOLE
E_ϕ 4 Mc/s

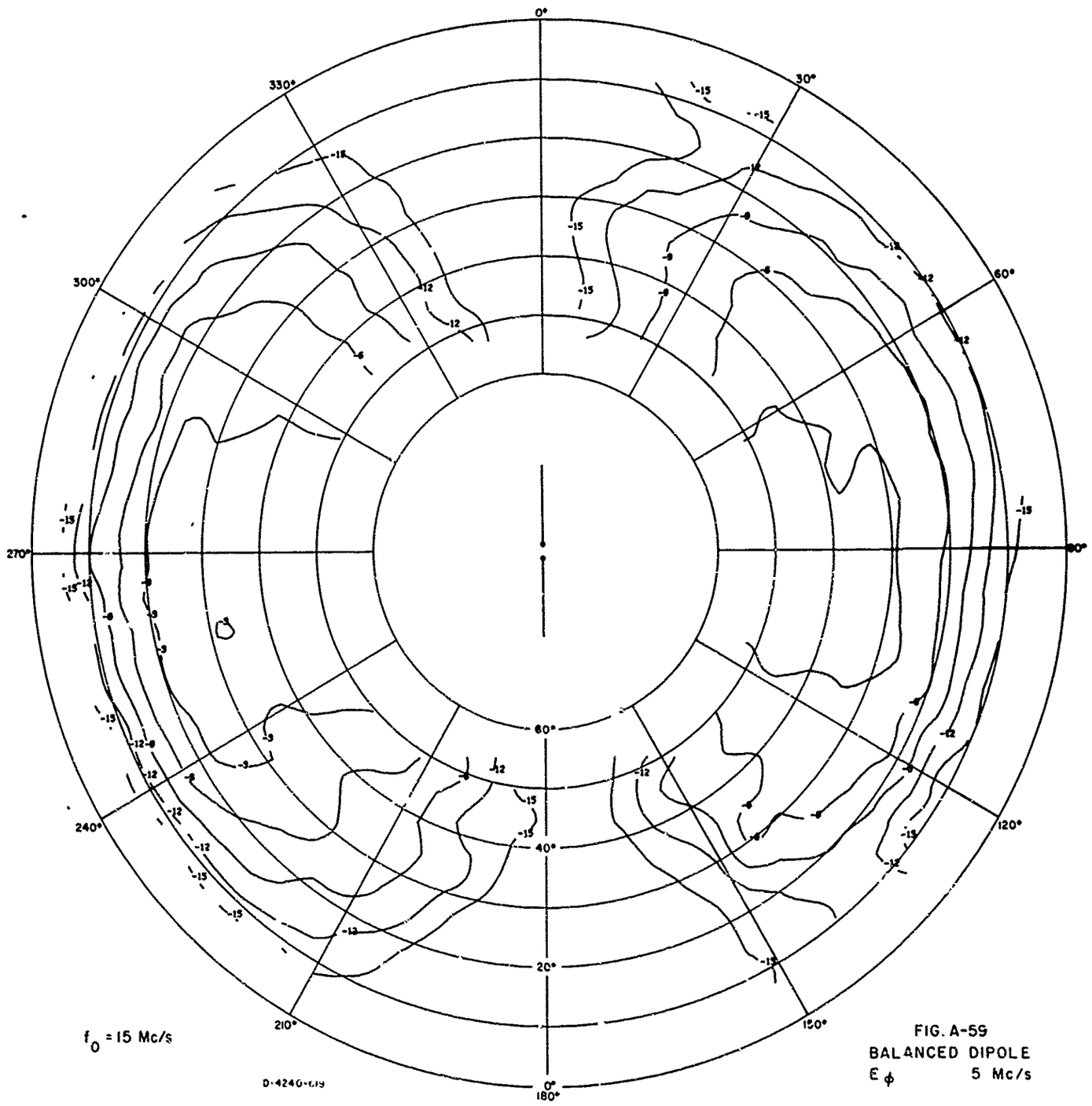

f_0 = 15 Mc/s

D-4240-619

FIG. A-59
BALANCED DIPOLE
E_ϕ 5 Mc/s

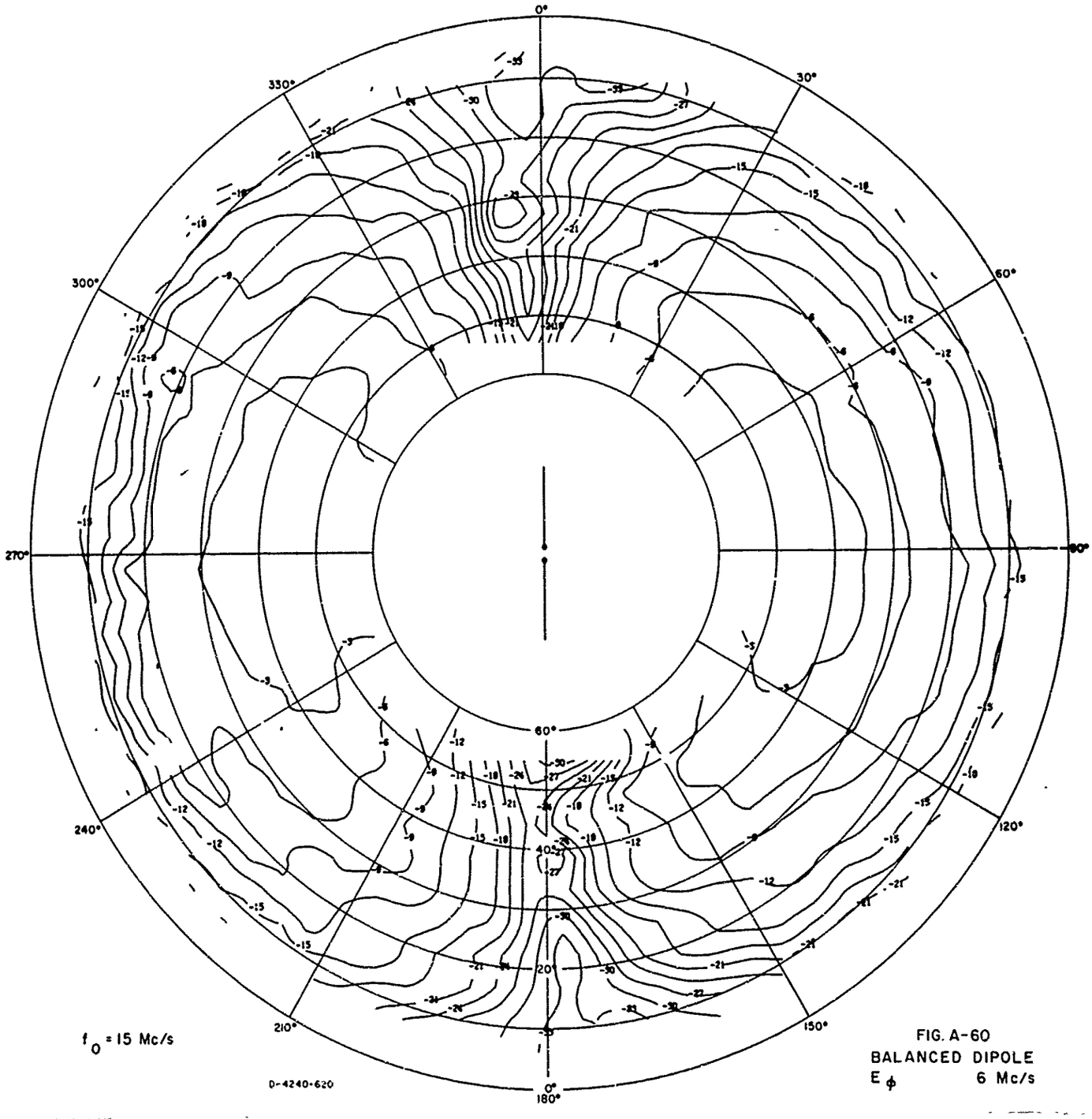

f_0 = 15 Mc/s

D-4240-620

FIG. A-60
BALANCED DIPOLE
E_ϕ 6 Mc/s

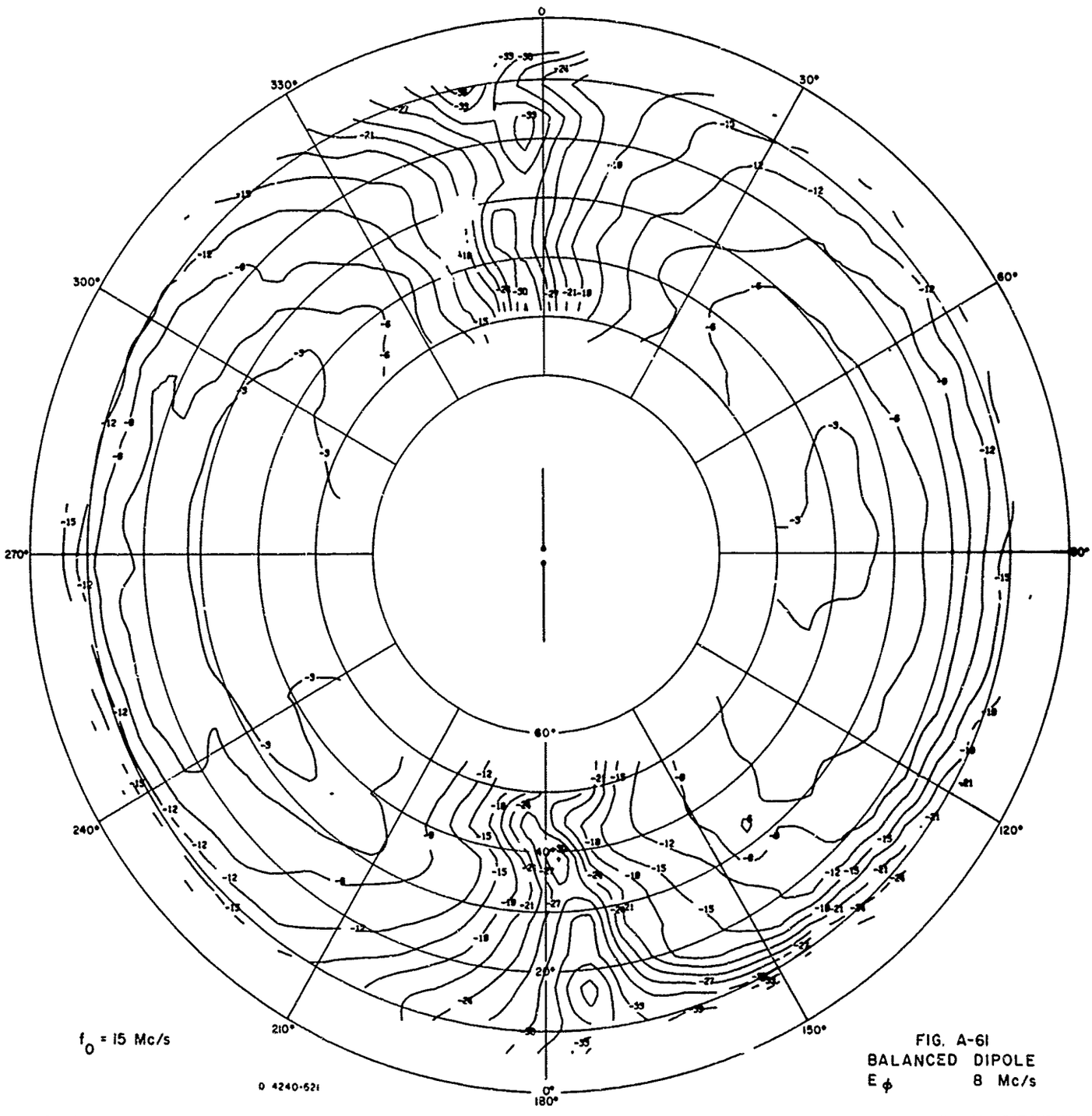

f_0 = 15 Mc/s

0 4240-521

FIG. A-61
BALANCED DIPOLE
E_ϕ 8 Mc/s

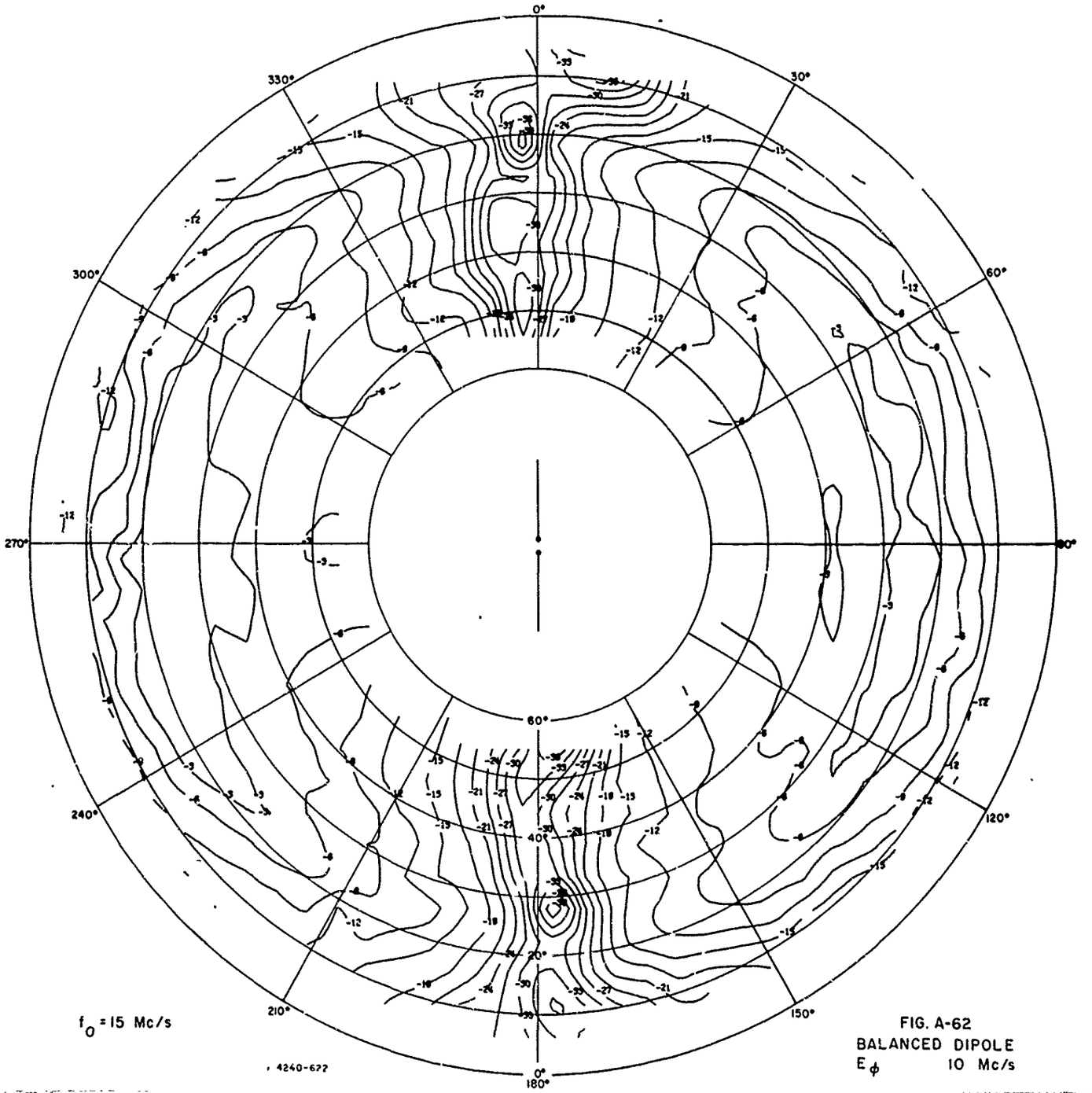

f_0 = 15 Mc/s

4240-622

FIG. A-62
BALANCED DIPOLE
E_ϕ 10 Mc/s

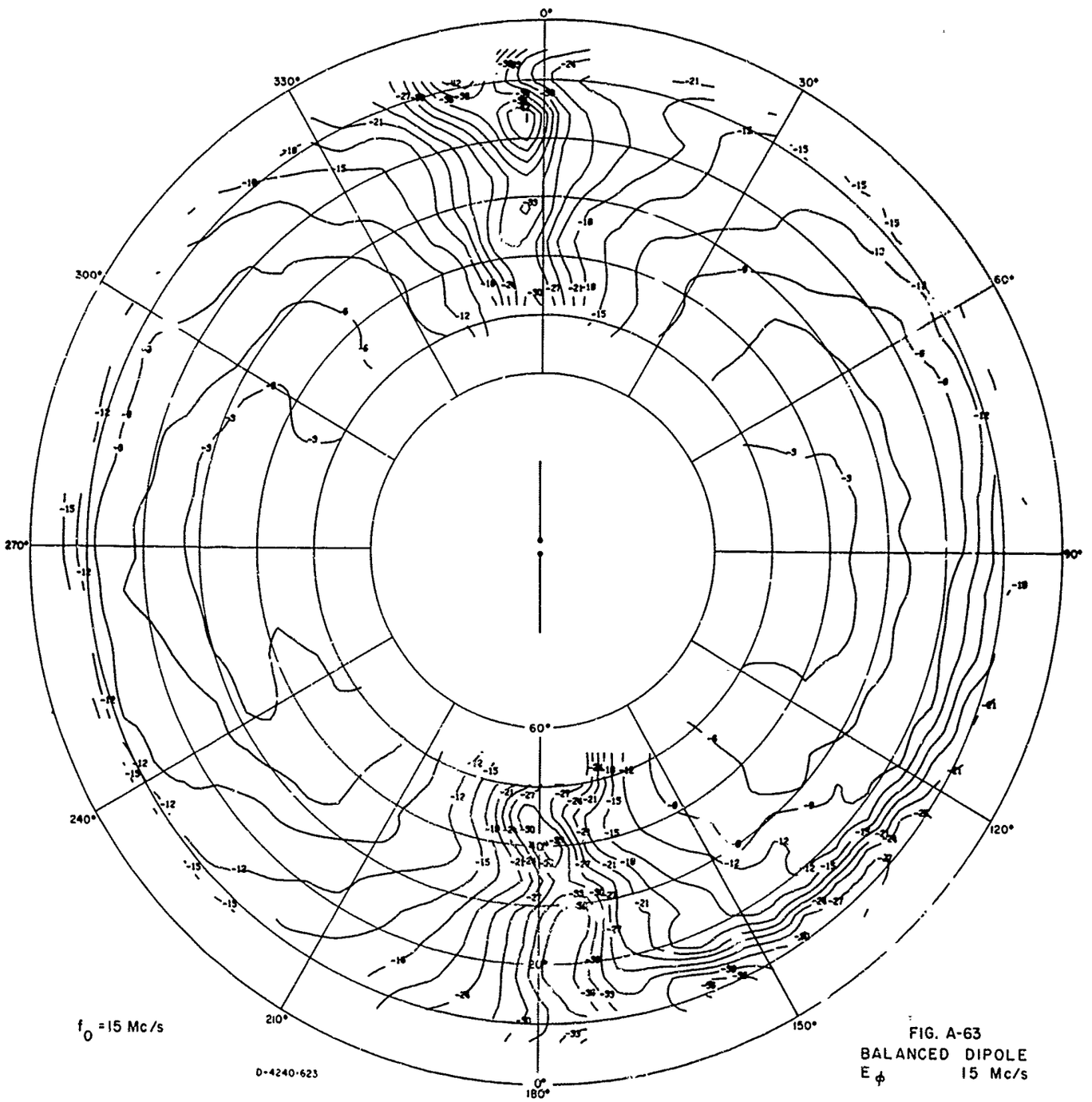

FIG. A-63
BALANCED DIPOLE
E_ϕ 15 Mc/s

UNCLASSIFIED

Security Classification

DOCUMENT CONTROL DATA - R & D

Security classification of title, body of abstract and indexing annotation must be entered when the overall report is classified

1 ORIGINATING ACTIVITY (Corporate author)	2a. REPORT SECURITY CLASSIFICATION
Stanford Research Institute 333 Ravenswood Avenue Menlo Park, California 94025	Unclassified 2b. GROUP N/A

3 REPORT TITLE

FULL-SCALE PATTERN MEASUREMENTS OF SIMPLE HF FIELD ANTENNAS IN A US CONIFER FOREST

4 DESCRIPTIVE NOTES (Type of report and inclusive dates)

Special Technical Report 25

5 AUTHOR(S) (First name, middle initial, last name)

Ray A. William; Gary E. Barker; Sandra S. Martensen

6 REPORT DATE	7a. TOTAL NO OF PAGES	7b. NO OF REFS
February 1967	105	4

8a. CONTRACT OR GRANT NO	9a. ORIGINATOR'S REPORT NUMBER(S)
DA 36-039 AMC-00040(E) b. PROJECT NO Order No. 5384-PM-63-91 c. ARPA Order No. 371 d.	Special Technical Report 25 SRI Project 4240 9b. OTHER REPORT NO(S) (Any other numbers that may be assigned this report)

10. DISTRIBUTION STATEMENT

Distribution of this document is unlimited.

11. SUPPLEMENTARY NOTES	12. SPONSORING MILITARY ACTIVITY
Report on communications research in tropical vegetated environments.	Advanced Research Projects Agency Washington, D.C.

13 ABSTRACT

During May and June of 1965, measurements of field-expedient antenna impedance and radiation patterns were conducted in a conifer forest. The antennas measured included dipoles, slant wires, and inverted L's.

The pattern measurements were conducted with an aircraft-towed transmitter. The results are presented on contour maps showing individual polarization response for elevation angles from 5 to 60° from the horizon and power response from 5° above the horizon to the zenith for several frequencies between 2 and 15 Mc/s.

Input impedances are presented on Smith charts for each antenna over the frequency range that the above pattern data are presented. In addition, curves of resonant frequency and input impedance as a function of antenna height are presented for selected dipoles.

The results demonstrate that the trees surrounding the antennas begin to cause perturbations to the vertical polarization response of antennas at approximately 8 Mc/s.

DD FORM 1 NOV 65 1473 (PAGE 1)

S/N 0101-807-6801

UNCLASSIFIED

Security Classification

14 KEY WORDS	LINK A		LINK B		LINK C	
	ROLE	WT	ROLE	WT	ROLE	WT
Field Expedient Antennas						
Pattern Measurements						
Impedance Measurements						
Xeledop						
Slant-Wire Antenna						
Inverted L Antenna						
Unbalanced Dipole Antenna						
Balanced Dipole Antenna						
Monopole Antenna						